Molecular Design of Polymer Combs and Living Gels

A Dissertation Presented

by

Adrian A. Lorenzana

Submitted to the Graduate School of the
University of Massachusetts Amherst in partial fulfillment
of the requirements for the degree of

Doctorate of Philosophy in Chemical Engineering

February 2025

Graduate Program in Chemical Engineering

Molecular Design of Polymer Combs and Living Gels

A Dissertation Presented

By

Adrian A. Lorenzana

Approved as to style and content by:

_____

Shelly R. Peyton, Co-Chair

_____

John Klier, Co-Chair

_____

Sarah Perry, Member

_____

Todd Emrick, Member

_____

Cathal Kearney, Member

_____

Dimitrios Maroudas, Department Head

Chemical Engineering

Dedication

To Meg. To my family.

"Perhaps Gonzalo can encourage us to take another look at where we stand and who we are. What are the forces that shape us, and how will we respond when a storm throws us up against an unfamiliar shore?"

—Joachim I. Krueger[1]

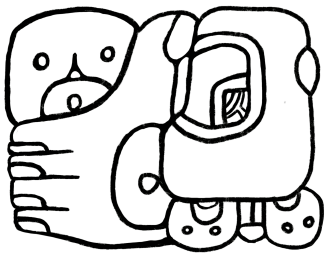

Acknowledgements

I'm thankful for Professor Shelly Peyton and Professor John Klier for giving me a chance and choosing me to work on their at the time new strain sensitive materials grant. You two encouraged me to be creative and explore research, provided me with valuable insight and perspective, and put things into perspective when I was down. I couldn't have asked for anything more. You're both inspirations to me.

I'm thankful for Professor Yingxi Zhu for taking a chance on me and taking me on to do undergraduate research, reminding me how much I missed experiments. Thanks to Dr. Manuela Ferreira for being a great mentor in undergrad and a true friend.

I'm thankful for my committee members, Professor Sarah Perry, Professor Todd Emrick, and Professor Cathal Kearney for supporting me in my research, being valuable sources of inspiration and knowledge, and being there when I needed them.

I'm grateful to have Dr. Megan Wancura as my partner through all of this. I couldn't have gotten through this without her supporting me both with my work and outside of it. I can't wait to start the next chapter of our lives together.

I'd like to thank my friends who kept me company during graduate school. Thanks to Dr. Anne Le and Becca Huber for always being down to go for drinks and food or shopping. Thanks to Dr. Ning-Hsuan Tseng, Becky Gordon, and David Pingree for being awesome outdoors buddies, always down for weekend trip to the mountains.

Thanks to Dr. Carey Dougan, Dr. Sonu Kizhakkepura, Dr. Katherine Bittner, Dr. Akaansha Rampal, Ninette Irakoze, and Auggie Wirasaputra for making the lab a lovely

place to work and excellent company at lab events. Special thanks to Dr. Nathan Richbourg for dragging me to a bowling event at SFB and introducing Meg and I.

Thanks to University of Massachusetts Amherst, NSF, NIH, and the Army Research Office for funding my work.

I'd like to thank Dr. Cedric Bobst for collecting and analyzing MALDI-ToF data that was crucial for my work with xanthogen disulfides. I'd like to thank Dr. Jessica Schiffman and Jichao Song for collecting and interpreting DSC data for my first, first author paper. I'd like to thank Hsu Shwe Yee Naing for conducting and analyzing nanoindentation data. I'd like to thank Professor Henning Winter for allowing me access to his and Jessica's rheometer, as well as always being excited about my research and willing to offer his wisdom. Thanks to Emrick Lab members Dr. Le Zhou, Grace Leon, Kyoungwon Lee, Krishnamurthy Munusamy, and Carla Stefan for helping me with access to equipment that dramatically sped up my work. Thanks to Gwen Tillinghast for chatting with me about rheology and research.

Thanks to the mystery mesoamerican who discovered thermosetting rubbers all those years ago.

Abstract

Molecular Design of Polymer Combs and Living Gels

February 2025

Adrian A. Lorenzana, B.S., Wayne State University

Ph.D., University of Massachusetts Amherst

Directed by: Professors Shelly R. Peyton and John Klier

Thermosetting resins are materials that undergo crosslinking by forming interchain linkages to create robust 3D networks that impart creep, thermomechanical, and solvent resistance. These materials are critical for a number of high-performance applications, such as aerospace and automotives, and biomedical crosslinked hydrogels. Thermosetting materials can be cured chemically or thermally, or by using ultraviolet (UV) light or electron beams. However, these methods are not always possible, accessible, and they can be harsh to embedded cells. Taking inspiration from natural materials such as fibronectin, a protein that contains hidden or cryptic sites that become exposed under tension, this dissertation first presents a new class of synthetic force-responsive materials that exhibit force-responsive behavior by exposing cryptic sites and forming new crosslinks. Long pendant poly(ethylene glycol) (PEG) chains along the polymer backbone create a significant steric barrier and prevent reactive moieties from spontaneously crosslinking, which is overcome by mechanical force. In this dissertation, I extended this approach to densely grafted comb polymers with reactive side chains, which resulted in highly crosslinked comb copolymers with minimal intramolecular crosslinking. Finally, I harnessed xanthogen disulfides to

produce telechelic acrylic polymers and hydrogels responsive to visible light. Overall, I successfully designed and produced methods of easily implementing mechanosensitivity in synthetic polymers, strategies for producing high molecular weight crosslinkable resins, and fast techniques for synthesizing biocompatible gels. Importantly, the design principles laid out in this work provide a blueprint for developing next-generation stimuli responsive materials.

Table of contents

Page

Acknowledgements v

Abstract vii

List of tables xiv

List of figures xv

Chapter

1 Thermosetting materials and their limitations 24

1.1 Introduction 24

1.2 Mechanoresponsive Thermosetting Materials 27

1.2.1 Introduction 27

1.2.2 Sonication as a tool for applying targeted force 30

1.2.3 Mechanophores 32

1.2.4 Limitations 33

1.3 Polymer architecture and bulk properties 35

1.3.1 Introduction 35

1.3.2 Comb polymers 36

1.3.3 Bottlebrush polymers 37

1.3.4 Highly crosslinked combs 40

1.4 Hydrogel preparation 40

1.4.1 Introduction 40

1.4.2 Mixing and light 42

1.4.3 Reversible deactivation radical polymerizations 42

1.5 Hypothesis 43

1.6 Objectives 44

1.7 Significance 44

2 Molecularly shielded, on-demand, ultrasound-cured polymer networks ... 46

2.1 Abstract 46

2.2 Introduction 46

2.3 Materials and methods 49

2.3.1 Chemical and polymer sourcing 49

2.3.2 Representative polymer synthesis 49

2.3.3 Polymer characterization 50

2.3.4 Copolymer solution preparation 50

2.3.5 Parallel plate rheology 56

2.3.6 Sonication-induced gelation of shielded polymers 57

2.3.7 Differential scanning calorimetry 57

2.3.8 Needle induced cavitation 58

2.4 Results and discussion 58

2.4.1 Gelation kinetics of polymers under static conditions 58

2.4.2 Controlling gel time through shield graft density 64

2.4.3 Force-induced gelation of shielded polymers 67

2.4.4 Ultrahard materials from shielded copolymers 71

2.5 Conclusion 73

3 Highly crosslinked, ultra-hard networks from polymer combs 75

3.1 Abstract 75

3.2 Introduction 75

3.3 Materials and methods 77

3.3.1 Chemical sourcing 77

3.3.2 2-(2-Bromoisobutyryloxy)ethyl methacrylate (BIEM) synthesis 78

3.3.3 Copper activation and stirbar cleaning 78

3.3.4 CuBr purification 79

3.3.5 PolyGMA synthesis 79

3.3.6 pGMA-*b*-BMA and pGMA-*co*-BMA synthesis 79

3.3.7 PolyBIEM (pBIEM) synthesis 80

3.3.8 Comb polymer synthesis 81

3.3.9 Polymer characterization 83

3.3.10 Sample preparation 83

3.3.11 DMA 83

3.3.12 Swelling ratio 83

3.3.13 Toughness measurements 84

3.4 Results and discussion 84

3.4.1 Controlled synthesis of reactive combs 84

3.4.2 Crosslinking and storage modulus of reactive comb polymers 87
3.4.3 Network architecture effects on material properties 90
3.5 Conclusion 94
4 Fast, oxygen-tolerant RAFT polymerization of hydrogels 96
4.1 Abstract 96
4.2 Introduction 96
4.3 Materials and methods 99
4.3.1 Reagents used 99
4.3.2 Instrumentation 99
4.3.3 Polymerization kinetics 100
4.3.4 Synthesis of O,O-diethyl 1,2-disulfanedicarbothioate (bis(xan)) 102
4.3.5 Photopolymerization 103
4.3.6 Hydrogel preparation 105
4.3.7 Rheological characterization of hydrogels 106
4.3.8 MALDI-ToF 107
4.4 Results and discussion 107
4.4.1 Kinetics and livingness 107
4.4.2 End group fidelity of polymers 112
4.4.3 Rapid hydrogel fabrication 115
4.5 Conclusion 116
5 Conclusions, limitations, and future directions 118

5.1 Conclusions 118

5.2 Materials and methods 119

5.2.1 Chemical sourcing 119

5.2.2 Synthesis of polyinitiator and vitrimers containing GMA 120

5.2.3 Representative PEG shielded and control polymer synthesis 120

5.2.4 Copolymer solution preparation 121

5.2.5 Parallel plate rheology 121

5.2.6 Time-temperature superposition measurements 122

5.3 Limitations 122

5.3.1 PEG-shielded polymers require high strain and/or strain rates to induce crosslinking 123

5.3.2 Steric shielding by PEG is not generalizable to all crosslinking chemistries 123

5.3.3 Grafting-from produces unstable brushes 126

5.3.4 GMA is not suitable for transesterification based vitrimers 128

5.4 Future directions 130

5.4.1 Improving elastic modulus of thermoset bottlebrushes 130

5.4.2 Mechanosensitive nanocapsule thermosets 133

5.4.3 Xanthogen disulfide optimization and hydrogel stereolithography 136

Bibliography 139

List of tables

Table Page

1 Polymers used in each experiment, their target DP, comonomer feed ratio, actual DP, and actual comonomer ratio as determined by ^{1}H NMR. 60

2 Synthetic setup for comb polymerizations. 83

3 Tabulated properties of polymers used in this study. 83

4 Characterization of xanthate polymerizations for a range of monomers. Polymerization conditions (temperature, atmosphere, targeted DP) and characterization (measured DP, molecular weight (M_n), dispersity (Đ), and conversion are detailed. 108

5 Impact of temperature on xanthate polymerization of pMA. 111

6 GPC characterization of polymerizations of MA and block polymers built from living PMA. 112

List of figures

Figure Page

1 Mesoamerican people were the first polymer scientists. An image of a rubber ball preserved in soil, from El Manatí, 1600 BC.[2] 24

2 Dynamic overstretched chain model. Overstretched segments of polymer (red) propagate and grow along the backbone in response to cavitations caused by ultrasound. 30

3 Cartoon depiction of the predicted reaction pathways of 1,2-diacetoxybenzocyclobutene. Reproduced from Hickenboth et al.[3] 33

4 Phase diagram for methacrylic bottlebrush polymers. Depending on n_{sc}, n_{bb}, and n_g polymers with grafted sidechains can be categorized either as combs, bottlebrushes with rigid sidechains (RSC), stretched sidechains (SSC), or stretched backbones (SBB). 38

5 ^{1}H NMR spectra of poly(GMA-*co*-MEMA) targeting 50 DP and 1:1 comonomer ratio. Spectra recorded at 500 MHz in $CDCl_3$. 50

6 ^{1}H NMR spectra of poly(GMA-*co*-PEGMA500) targeting 50 DP and 1:1 comonomer ratio. Spectra recorded at 500 MHz in $CDCl_3$. 50

7 ^{1}H NMR spectra of poly(GMA-*co*-PEGMA950) targeting 50 DP and 1:1 comonomer ratio. Spectra recorded at 500 MHz in $CDCl_3$. 50

8 ^{1}H NMR spectra of poly(GMA-*co*-PEGMA950) targeting 50 DP and 60:40 comonomer ratio. Spectra recorded at 500 MHz in $CDCl_3$. 50

9 ^{1}H NMR spectra of poly(GMA-*co*-PEGMA950) targeting 50 DP and 70:30 comonomer ratio. Spectra recorded at 500 MHz in $CDCl_3$. 50

10 ^{1}H NMR spectra of poly(GMA-*co*-PEGMA500) targeting 50 DP and 60:40 comonomer ratio. Spectra recorded at 500 MHz in $CDCl_3$. 50

11 ^{1}H NMR spectra of poly(GMA-*co*-PEGMA500) targeting 50 DP and 70:30 comonomer ratio. Spectra recorded at 500 MHz in $CDCl_3$. 50

12 ^{1}H NMR spectra of poly(GMA-*co*-PEGMA500) targeting 50 DP and 30:70 comonomer ratio. Spectra recorded at 500 MHz in $CDCl_3$. 50

13 ^{1}H NMR spectra of poly(GMA-*co*-MEMA) targeting 50 DP and 60:40 comonomer ratio. Spectra recorded at 500 MHz in $CDCl_3$. 50

14 ^{1}H NMR spectra of poly(GMA-*co*-MEMA) targeting 50 DP and 70:30 comonomer ratio. Spectra recorded at 500 MHz in $CDCl_3$. 50

15 Large molecular shields inhibit or delay crosslinking. (a) Illustrations of polymer components used throughout the paper. (b) Effect of shielding group functionality on storage modulus (G') over time with amine crosslinks at constant 50 wt % polymer, reacting with EDA. Inset depicts high density poly(GMA-*co*-MEMA) with many epoxy groups. (c) Effect of shielding group functionality on storage modulus over time with amine crosslinks at constant 1 M concentration epoxy, reacting with EDA. Inset depicts low density poly(GMA-*co*-MEMA) with a fixed amount of epoxy groups. (d) Effect of shielding group functionality on storage modulus over time with thiol crosslinks at constant 1 M concentration epoxy, reacting with EDT. Inset

depicts poly(GMA-*co*-PEGMA950) with a fixed amount of epoxy groups and large shielding groups preventing crosslinking. For all experiments, a 1:1 ratio of GMA:MEMA, PEGMA500, or PEGMA950 was used. Error bars show the standard deviation of G' at each timepoint (n = 3). For all conditions, including the enhanced kinetics provided by the thiol-epoxy reaction, a latency period before gelation at static conditions is present. 61

16 Ratio of pendent shields to reactive groups controls gelation time. (a) Illustrations of polymers at different GMA:PEGMA molar ratios, showing the change in backbone flexibility and exposed reactive sites. b-e. Storage modulus evolution over time for: (b-c) varying mole percentage of PEGMA950 with a diamine (b) or dithiol (c) crosslinker; (d) varying mole percentage of PEGMA500 and (e) MEMA with a diamine crosslinker. Arrows represent trends in shielding resulting from increased ratio of shielding monomer. 64

17 Sonication induces shielded polymer crosslinking. (a) Gel time of poly(GMA-*co*-PEGMA950) under static and sonicated conditions at varying DP with 1:1 molar ratio. Samples at 25 and 50 DP did not form a gel. Insets show a liquid polymer solution during a bubble test and a polymer cured through sonication, still attached to the sonicator probe. (b) Elastic modulus of poly(GMA-*co*-PEGMA950) cured with sonication as measured *via* NIC. Samples were crosslinked with a 1:1 molar ratio of thiol to epoxy and at a DP of 100, 150, or 200 and measured 60 s post sonication and after two weeks. 68

18 Evolution of G' for poly(GMA-*co*-PEGMA950) at a 1:1 molar ratio of comonomers and 25 DP during parallel plate rheology. Frequency sweeps were run from 1 to 100 rad/s over 17.5 hrs using a 20 mm top plate. Data plotted at 1 Hz and 1% strain. At 25 °C the sample increases in modulus rapidly after a 2.5 hr latency period. At 40 °C the same shows a small uptick in modulus after 12.5 hrs and never fully gels during the measurement period. 69

19 Shielded copolymers create ultrahard and durable materials. (a) Compression modulus of a fully cured poly(GMA-*co*-PEGMA2000) with 1:1 molar ratio of monomers. Elastic modulus is calculated by taking the slope during the linear portion of the stress-strain curve. Red line shows the linear best fit through four points. (b) Fully cured poly(GMA-*co*-PEGMA2000) gels immersed into acetone, ethanol, water, acetonitrile, and dichloromethane. 73

20 Differential scanning calorimetry thermogram of 1:1 GMA:PEGMA2000 crosslinked with EDT with all acetonitrile solvent evaporated off. ΔH_m of the sample was calculated to be 97.9 J/g with T_m at 49.29 °C. 73

21 ^{1}H NMR and GPC of pGMA-*co*-BMA. Spectra recorded at 500 MHz in $CDCl_3$. THF used as eluent. 80

22 ^{1}H NMR and GPC of pGMA and pGMA-*b*-BMA. Spectra recorded at 500 MHz in $CDCl_3$. THF used as eluent. 80

23 SARA-ATRP produces narrowly dispersed, well defined comb polymers. (a) Illustrations of the monomers used in this paper. (b) GPC chromatogram showing

the shifting of precursor polymer to earlier elution times, demonstrating the successful chain extension with GMA-*co*-BMA. (c) GPC chromatogram showing successful chain extensions of pBIEM with first GMA and then BMA to create block copolymer side chains. (d) GPC chromatogram showing successful chain extensions of pBIEM with first BMA and then GMA to create block copolymer side chains. For (b-d), insets depict the idealized structure of the initial and final polymer. 85

24 ^{1}H NMR of pBIEM-*g*-(GMA-*co*-BMA) after successive polymerizations. Spectra recorded at 500 MHz in $CDCl_3$. 87

25 ^{1}H NMR of pBIEM-*g*-(GMA-*b*-BMA) after successive polymerizations. Spectra recorded at 500 MHz in $CDCl_3$. 87

26 ^{1}H NMR of pBIEM-*g*-(BMA-*b*-GMA) after successive polymerizations. Spectra recorded at 500 MHz in $CDCl_3$. 87

27 Comb polymers crosslink to form high modulus materials. (a) Schematic of the crosslinking reaction between glycidyl esters and succinic acid, catalyzed by TBD. (b) Storage modulus of block polymers crosslinked with succinic acid, as measured by DMA. (c) Storage modulus of homopolymers crosslinked with succinic acid, as measured by DMA. (d) Storage modulus of random copolymers crosslinked with succinic acid, as measured by DMA. 88

28 Swelling of thermosetting polymers. (a) Swelling ratios of crosslinked polymers in mixed xylenes. n = 3 (b) Cartoon depiction of comb copolymers with random (left) and block (right) sidechains. 91

29 pBIEM-*g*-(BMA-*b*-GMA), pBIEM-*g*-(GMA-*co*-BMA), and pGMA-*b*-BMA swelling in xylenes. 91

30 Random comb sidechains suppress intermolecular crosslinking and create tougher materials. Tensile toughness of comb and linear polymers. n = 3 93

31 GPC traces of polymers studied, synthesized in air or nitrogen. 100

32 ^{1}H NMR of bis(xan). Spectra recorded at 300 MHz in $CDCl_3$. 100

33 ^{1}H NMR of pnBA. Spectra recorded at 300 MHz in $CDCl_3$. 100

34 ^{1}H NMR of pMA. Spectra recorded at 300 MHz in $CDCl_3$. 100

35 ^{1}H NMR of pMA-*b*-EA. Spectra recorded at 300 MHz in $CDCl_3$. 100

36 ^{1}H NMR of piDA. Spectra recorded at 300 MHz in $CDCl_3$. 100

37 ^{1}H NMR of pEA. Spectra recorded at 300 MHz in $CDCl_3$. 100

38 ^{1}H NMR of bis(xan) and MA evolution over time under 405 nm light in nitrogen. 102

39 ^{1}H NMR of bis(xan) and MA evolution over time under 405 nm light in air. 102

40 Schematic of photoiniferter polymerization of vinyl monomers. PI polymerization proceeds through a SUMI step to yield a better initiating R group capable of initiating the propagation step, followed by conventional RAFT kinetics. 108

41 Bis(xanthates) mediate ultra-fast polymerizations of acrylates and produce living polymers. (a) Conversion over time of xanthate-mediated PI polymerization of 50 wt% MA under air and nitrogen atmosphere. (b) GPC chromatogram showing

degree of polymerization of pMA and pMA-*b*-EA synthesized in air and under nitrogen. 111

42 Structural characterization of pMA synthesized with bis(xanthates) in air and nitrogen. (a) MALDI-ToF spectra of pMA synthesized in nitrogen (Mn = 4310 g/mol). (b) MALDI-ToF spectra of pMA synthesized in air (Mn = 4396.2 g/mol). (c) GPC (DMF) chromatogram of pMA polymers with a targeted DP of 25 (d) ^{1}H NMR spectra showing characteristic xanthate peaks. 113

43 Linear MALDI-ToF of pMA synthesized under nitrogen. 113

44 Linear MALDI-ToF of pMA synthesized under air. 113

45 Structural characterization of pMA synthesized with bis(xanthates) in air and nitrogen. (a) MALDI-ToF spectra of pMA synthesized in nitrogen (Mn = 4310 g/mol). (b) MALDI-ToF spectra of pMA synthesized in air (Mn = 4396.2 g/mol). (c) GPC (DMF) chromatogram of pMA polymers with a targeted DP of 25 (d) ^{1}H NMR spectra showing characteristic xanthate peaks. 115

46 PEG shielded polymers are not activated by parallel plate shear. G' evolution over time of pGMA-*co*-PEGMA950 at 1 % and 30 % strain. 123

47 PEG shielding completely prevents gelation with Jeffamine. G' evolution over time of pGMA-*co*-PEGMA950 in the presence of Jeffamine ED-900. 124

48 pAAEM-*co*-PEGMA950 rapidly gels in the presence of primary amines. G' evolution over time of pAAEM-*co*-PEGMA950 in in the presence of pAPMA-*co*-MEMA. 126

49 Characterization of pAAEM produced by SARA ATRP. (a) GPC chromatogram of pAAEM. (b) ^{1}H NMR of pAAEM. Spectra recorded at 500 MHz in $CDCl_3$. THF used as eluent. 126

50 Characterization of pBIEM-*g*-(AAEM-*b*-EHMA) prepared by SARA ATRP. (a) GPC chromatogram of pBIEM-*g*-(AAEM-*b*-EHMA). (b) ^{1}H NMR of pBIEM-*g*-(AAEM-*b*-EHMA). Spectra recorded at 500 MHz in $CDCl_3$. THF used as eluent. 127

51 pGMA-*b*-BMA performs well as a reprocessible adhesive. (a) Fragments of crosslinked pGMA-*b*-BMA are melt pressed into a homogeneous solid. (b) An image of a rheometer stage showing that the epoxy adhesive securing sandpaper to the bottom plate has failed, while pGMA-*b*-BMA is still adhering the bottom sandpaper and top plate. 129

52 Time-temperature superposition of pGMA-*b*-BMA. (a) Time-temperature superposition of the elastic modulus of pGMA-*b*-BMA. (b) Time-temperature superposition of the loss factor of pGMA-*b*-BMA. 130

53 Proposed route to reactive bottlebrush polymers with labile side chains. 132

54 Proposed routes to aldehyde functionalized styrenic monomer for improved reactive bottlebrush polymers. 133

55 Mechanosensitive nanocapsule thermosets expose a reactive core in response to shear forces. 135

56 Proposed polymerization and chain-end chlorination of amine functional styrenes. 136

57 Proposed xanthate structures. 137

Chapter 1

Thermosetting materials and their limitations

1.1 Introduction

The crosslinking of polymers to create thermosets was a crucial innovation in human history. The first polymer scientists, the ancient Olmec, were known to extract latex from *Castilla elastica* trees and mix it with juice from the *Ipomoea alba* vine to convert the latex into rubber as early as 1600 B.C.E. In fact, the name Olmec means "rubber people" in Nahuatl. Olmec derives from the Nahuatl Ōlmēcatl (singular) or Ōlmēcah (plural), which in turn is derived from ōlli, meaning "natural rubber", and mēcatl, meaning "people."[4] Archaeologists applied this name to the ancient culture before it was understood that the rubber people the Nahuas referred to were their contemporary neighbors in the Gulf Lowlands since the time of the Aztecs (more properly the Mēxihcah), not the ancient Olmecs of 2000 years prior. The name stuck, and it wonderfully illustrates the ingenuity of the Olmecs.[5]

The Olmec used this rubber to fashion elastic balls as heavy as 9 lbs for use in the mesoamerican ballgame. By varying the ratio of latex to juice, rubbers of varying elasticity could be produced suited to different needs. In addition to making game balls (Figure 1), they would also make rubber soled sandals, watertight containers, and waterproof fabrics by impregnating fabric with the latex/juice mixture.[6–9] This technology would spread to later mesoamericans, and eventually be noted by colonists.

Figure 1: Mesoamerican people were the first polymer scientists. An image of a rubber ball preserved in soil, from El Manatí, 1600 BC.[2]

While this rubber was initially viewed as a curiosity by Europeans, some three and a half millennia later, this class of materials and its characteristic liquid to solid transition would come to underpin many developments in polymer science. Charles de la Condamine sent a sample of rubber to the Académie Royale des Sciences from Ecuador in 1736. La Condamine described rubber as originating from the milk, or as he called it "latex," a term still in use today, of Hévé trees. Joseph Priestley coined the term "indiarubber" in 1770 after coming across a sample in an artist supply shop being sold to rub off pencil markings, eventually being shortened to just rubber.[10] In 1844 Charles Goodyear rediscovered and received a patent for the process of vulcanization of natural rubber.[11,12] In 1907 Leo Baekeland introduced the first commercial synthetic plastic, phenol-formaldehyde resin

Bakelite, "the material with a thousand uses."[13] The molecular underpinnings of these materials was put forward by the "father of polymer chemistry" Hermann Staudinger in his groundbreaking paper "On polymerization" in 1920.[14] Staundinger himself unintentionally supported his macromolecular hypothesis with cyclopentadiene crosslinked by Diels-Alder reactions, which would not be understood until 1928.[15–17] The concept of gelation, the point at which polymers are crosslinked into a single molecule that spans a given volume element, was then first quantitatively described by Paul Flory in 1941,[18] as well as a statistical mechanical treatment of crosslinked polymers in 1943.[19,20]

The years since have seen momentous developments in the field of polymer chemistry enabling the synthesis of polymers, and by extension thermosets, by radical polymerizations with predictable molecular weights, low dispersity, and diverse functionality. Prior, free-radical polymerizations would produce "dead" polymers, those that cannot participate in further monomer addition, with heterogeneous degrees of polymerization. In 1956, Szwarc introduced the concept of a "living" polymerization,[21] in which the propagating carbanion remains active even after all monomer is consumed. However, carbanions are easily destroyed by impurities and cannot be regenerated after their destruction. In 1993, Georges *et al.* demonstrated a "living" free-radical polymerization with a narrow dispersity using nitroxide-mediated polymerization (NMP).[22] In 1995, Wang & Matyjaszewski and Kato *et al.* independently introduced atom transfer radical polymerization (ATRP).[23,24] In 1997, the third of the three major reversible deactivation radical polymerizations (RDRP), reversible addition-fragmentation chain transfer (RAFT) polymerization, was

introduced by Chiefari *et al.*[25] All three methods produce polymers with stable, dormant end groups that can subsequently be reinitiated. Suddenly chemists and engineers had several techniques at their disposal for easily preparing well defined polymers with low dispersity, a variety of functional groups, and with controlled architectures, enabling the production of ever more sophisticated thermosets.

Polymer thermosets have since come a long way, rising to dominate much of our world. By adjusting the crosslink density, as the ancient Olmecs discovered, and chemical structure the properties of the final material can be tuned to suit a whole host of applications. Additionally, the crosslinked nature of thermosetting polymers impart solvent resistance, thermo-mechanical resistance, and chemical, wear, and creep resistance.[26] The combination of these properties, as well as their light weight, have made them irreplaceable in high performance environments such as aerospace[27] and renewable energy.[28] With applications further ranging the gamut from soft materials like touch sensors,[29] tissue mimicking hydrogels for cell culture,[30] re-processable pressure sensitive adhesives,[31] to high-modulus materials like printed circuit boards,[32] protective coatings,[33] structural composite materials,[34] and many more too numerous to list, crosslinked materials have become completely irreplaceable.

1.2 Mechanoresponsive Thermosetting Materials

1.2.1 Introduction

Until recently, virtually all thermosetting materials have been crosslinked, a.k.a. cured, by either temperature, radiation, or simply spontaneous reactions upon mixing. These

techniques generally induce the formation of covalent bonds between polymer chains or the polymerization of small multifunctional molecules to form a three-dimensional network structure. Each approach to crosslinking has distinct advantages and disadvantages. Thermal curing involves using high temperatures to drive forward crosslinking reactions that either occur very slowly at room temperature or not at all.[35] Thermal curing is well suited for large samples, but is very energy intensive and requires an understanding of the thermal properties of the substrate to drive full conversion.[36] Spontaneously thermosetting materials are cured by mixing, often by step polymerization, however this relinquishes spatiotemporal control over gelation and can make applying the mixture difficult. Radiation-based curing, often achieved through free radical polymerization (FRP) with photosensitive radical initiators, can be very fast and energy efficient, but the penetration depth of light or electrons is limiting and the byproducts of radical initiators can be toxic. Reaching full cure is often not possible, and further thermal curing is required in addition to radiation exposure.[37] Additionally, radiation curing cannot be conducted through opaque materials, limiting their application space. As such, there is a need to develop new methods of curing thermosets that can be conducted through opaque materials, with lower energy cost, and with spatiotemporal control.

Nature has had eons to develop and refine exquisite molecular machinery that puts even the very best of modern chemistry and engineering to shame. Looking across the natural world, one will find it replete with stimuli responsiveness. Retinal based photosynthesis captures and stores the energy of light through cis-trans isomerization

coupled to ion pumps,[38] and chlorophyll based photosynthesis stores the energy of light through electron transfer.[39] It's worth noting that chlorophylls have been harnessed by polymer chemists to induce polymerization with light.[40] Methods of sensing oxygen content, temperature, and pH just to name a few more, are crucial for survival.[41–43] More rare in synthetic materials, but common in nature, is constructive responsive to mechanical forces.[44]

Natural materials can respond to mechanical force constructively by polymerizing under deformation, as is the case for fibronectin.[45–48] Under stain, the tertiary structure of fibronectin partially unravels, exposing cryptic binding sites that then participate in mechanically-induced polymerization and fibril formation. Mechanical force can also change gene expression. Extracellular mechanical forces can be propagated from focal adhesions through the cytoskeleton and LINC complex directly to chromatin, causing chromatin stretching and mechanosensitive gene expression.[49] Taking mechanically-induced unfolding of proteins and protein complexes as inspiration, our lab and others have developed gels that stiffen in response to applied cyclic compression by forming interchain disulfide bonds and thioethers.[50–52] However, these gels are not currently well suited for adhesives or coatings due to the difficulties of applying solid materials to substrates. The development of liquid pre-cursor solutions that can crosslink via mechanical perturbation for easy solution spread across a chosen substrate would transform a range of industries where reliance on thermal, UV, and electron beam curing makes on-demand curing of adhesives and post-crosslinking strengthening of coatings difficult.

1.2.2 Sonication as a tool for applying targeted force

Imparting force onto polymer chains is commonly achieved when the polymer is in a fluid state, either as a melt, a glassy liquid, or a solution. When studying polymers, shear is most often applied, and shear is applied through the oscillations of parallel plates, extrusion, or ultrasonic waves. In solution, linear polymers exist in a solvent dependent coiled state (a Gaussian coil) in which the end-to-end distance is much smaller than the contour length of the polymer (the length of the polymer at maximum extension).[53] When polymer solutions flow rapidly near a surface (as in the case of parallel plate rheology or extrusion through a narrow opening)[54,55] or are sonicated,[56] the shear forces cause this coiled structure to be disrupted. Commonly, and perhaps intuitively, it is thought that tension along the polymer backbone reaches a maximum at the chain center, at which point enough force is accumulated along the backbone such that mechanochemistry can occur. Models have been proposed based on this, one suggesting polymers fully stretch, with the end-to-end distance reaching the contour length (overstretched chain), or there is only partial unfolding of the polymer coil based around the chain center (overstretched segment, Figure 2).[57] More recent work has suggested instead that polymer unfolding in response to shear force may instead be a dynamic process in which chain unfolding begins at the polymer ends, with the overstretched segment propagating and growing along the backbone until it is sufficiently strained to react mechanochemically.[58]

In the case of polymers flowing near a surface, the shear forces are driven by physically pushing a solution through an opening or moving a surface rapidly parallel to the liquid. In

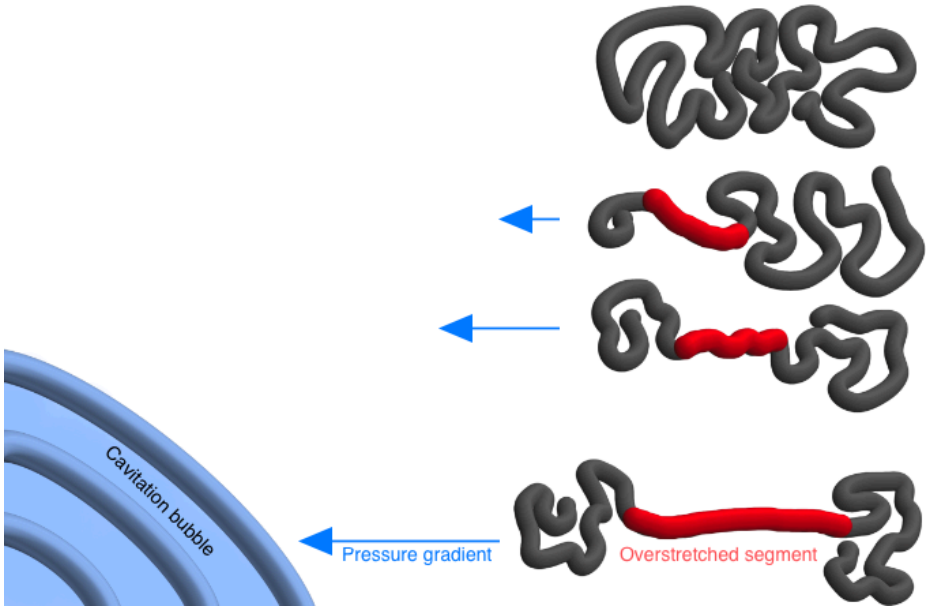

Figure 2: Dynamic overstretched chain model. Overstretched segments of polymer (red) propagate and grow along the backbone in response to cavitations caused by ultrasound.

the case of sonication, force is generated through the application of ultrasound, which has been known to degrade polymer chains since 1939.[59] Ultrasound consists of high frequency sound waves, with the 20 kHz to 2 MHz regime being "destructive" ultrasound necessary for for sonochemical and mechanochemical transformations. Sound waves compress and expand liquids as they are ultrasonicated, in places causing distances that are large enough to "break" the liquid and form cavitation bubbles. These bubbles expand over several cycles of compression and rarefaction until they grow large enough to become unstable, at which point it collapses. The collapse generates strong pressure gradients, causing a shear force as the surrounding area is pulled towards the center of the implosion, affecting an area on a micrometer scale.[60] These pressure gradients and resultant shear forces are commonly cited as the source of mechanochemical transformations of polymers in

response to sonication. Sonication as a means to drive chemical changes offers advantages over radiation and thermal curing. For one, sonication can be focused through opaque materials.[61] Additionally, sonication consumes up to 25,000 times less energy than thermal curing processes.[62] However, sonication also generates heat, and the strong shear forces generated can cause chain scission events.

1.2.3 Mechanophores

The field of polymer mechanochemistry has its origins in papers published by none other than Staudinger himself in the 1930s describing the reduction in molecular weight of polystyrene samples after ball milling.[63–65] The idea that this decrease in molecular weight was a direct result of shear forces causing homolytic C–C bond cleavage was put forward by Kauzmann and Eyring in 1940,[66] and then confirmed by Tabata *et al.* by studying ultrasonicated polymers with electron paramagnetic resonance in 1980.[67] That same year, Encina *et al.* demonstrated that polymers containing randomly distributed peroxide linkages preferentially undergo scission at O–O bonds over C–C bonds.[68] In 2005, Berkowski *et al.* took the field a step further from random cleavages to targeted cleavages by demonstrating the preferential cleavage of chain-centered azo linkages.[69] Around this time at an Army Research Office workshop on polymer mechanochemistry, Caster suggested the name "mechanophore" for functional groups that undergo chemical transformations in response to mechanical force.[70]

The field grew after Hickenboth *et al.* published on biasing reaction pathways with mechanical force,[3] and while Woodward and Hoffman may have been certain there would

never and could never be exceptions to their pericyclic selection rules,[71] exceptions would indeed arise. In this case, Hickenboth et al. conclusively showed that both cis and trans isomers of polymer chain centered 1,2-diacetoxybenzocyclobutene undergo a disrotary and conrotary, respectively, electrocyclic ring opening to form the E,E isomer of ortho-quinodimethide in response to mechanical force, in direct violation of the Woodward-Hoffman rules (Figure 3). This of course caused an explosion of interest in polymer mechanochemistry, and mechanophores have since been developed for several applications including strain sensing,[72] catalysis,[73] and of course, crosslinking.[74–76] Whereas previously mechanochemical reactions resulted in the breaking and weakening of polymer chains, now there are ways to link chains together to form crosslinked solids through mechanical force.[77,78]

1.2.4 Limitations

A popular route to achieve mechanochemical transformation of polymeric materials is to employ mechanophores. These motifs are specially tailored weak bonds that can be incorporated into polymer chains that transform into predictable products upon application of force.[79–82] However, mechanophore-mediated strengthening of polymeric materials remains a challenging approach for mechanical force curing of polymers for several reasons. First, these moieties typically are restrained by limited incorporation in polymer chains resulting in low crosslinking densities upon activation. Further, conversion of mechanophores is often low, resulting in poor activation even with good incorporation.[83] The chemistry necessary to implement mechanophores is complex in its design and

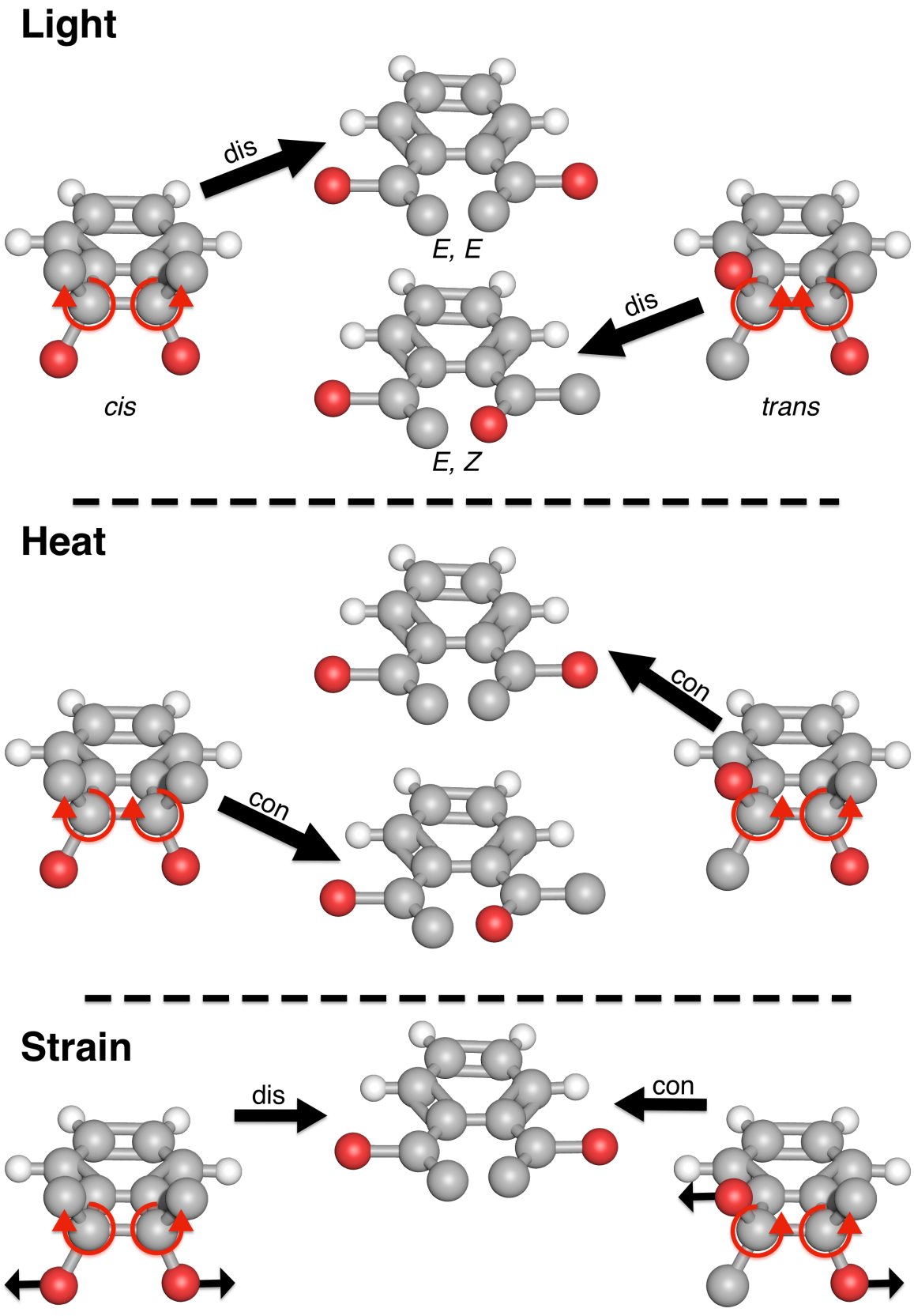

Figure 3: Cartoon depiction of the predicted reaction pathways of 1,2-diacetoxybenzocyclobutene. Reproduced from Hickenboth et al.[3]

execution, making the approach inaccessible. These moieties are not commercially available. Typical means of mechanochemical activation tend to introduce significant and destructive bond scission, which one must be careful to avoid by selecting appropriate force regimes.[84,85] Chapter 2 describes my approach using off the shelf chemistries to produce materials that are constructively sensitive to mechanical force with high conversions.

1.3 Polymer architecture and bulk properties

1.3.1 Introduction

Likely the first report of controlled polymer architecture and the first report of comb polymers arrived in the 1944 when Rehberg and Fisher prepared high *n*-alkyl polyacrylates.[86] This was followed by Kaufman *et al.* 1948 who observed that higher *n*-alkyl polyacrylates show sidechain crystallization.[87] These comb-like polymers were defined as polymers where each monomer bears its own polymer sidechain[88], though in modern polymer science they can be defined as polymers were only some monomers bear their own polymer sidechains.

Another early example of controlled polymer architecture, block polymers, arrived in 1951 when Vaughn et al. published a study of new nonionic surfactants, including block copolymers of poly(ethylene oxide) (a.k.a. poly(ethylene glycol) (PEG)) or poly(propylene oxide).[89,90] Known commercially as poloxamers, this particular class of polymers remains highly studied and useful examples of molecular design to this day.[91] Living polymerizations would be described just a few years later in 1956,[21] which would subsequently enable

the facile preparation of whole new classes of block polymers as well as far more exotic examples of molecular architecture.

Living polymerizations would enable far more exotic examples of polymer architecture compared to linear polymers.[92] In the absence of impurities, the carbanion active site remains intact even at full monomer conversion, meaning a wealth of facile chain end modifications were now within reach. In 1984, Rempp et al. published the first synthesis of macromonomers by modification of the carbanion.[93,94] This would soon be followed up by the first publications on what are now called bottlebrush polymers by Tsukahara et al. in 1989[95] through a combination of living anionic polymerization and FRP, and then a more detailed investigation into their physical properties in 1994.[96] At this point however, the preparation of bottlebrush polymers was still quite difficult. The free radical homopolymerization of ω-methacryloyl functionalized polymers has several limitations, chiefly among them the dilute nature of the methacrylate functional group.[97] It would take further progress in polymer synthesis to unlock new routes to bottlebrush polymers, with ring opening metathesis polymerization and RDRPs in particular enabling the routine synthesis of cylindrical molecular brushes with a huge array of monomers.

1.3.2 Comb polymers

Polymer thermosets have several advantages over their small molecule counterparts, including shortened gelation time due to less reactions needing to take place to achieve a volume spanning element, tunable architecture and phase behavior inherited from the polymer architecture, and the formation of stable one-pot latexes. Properties of the final

crosslinked material are often inherited from the properties of the constituent linked polymers. For example, the fibrillar structure of collagen I results in strain stiffening behavior,[98] and synthetic block copolymers exhibit microphase separation affecting vitrimer processing,[99] allowing for additional handles to control the properties of these crosslinked networks.

Comb polymers are no exception to this, and the vast design space of these branched polymers allows for the preparation of polymers with interesting phase behavior and conformation. For example, synthesizing reactive comb polymers with easily crystallizable sidechains allows for the preparation of crosslinked thermosets containing crystalline domains in the cured product,[100,101] increasing it's toughness and modulus. Their high molecular weight allows for quick gelation times,[29] consequently requiring less energy to cure. The low viscosity of comb polymer solutions and melts further reduces the energy needed to process polymer combs,[102] and can be used to modify the viscosity of polymer blends.[103] Moreover, by adjusting the composition and stiffness of the backbone, combs can be used as next-generation compatibilizers between immiscible polymer phases[104] as well as tough networks and adhesives on their own.[105,106]

1.3.3 Bottlebrush polymers

Formally defined as a subset of comb polymers, bottlebrush polymers are a class of polymers characterized by the presence of densely grafted side chains along a main backbone. These polymers can be described using three variables: the degree of polymerization between each graft $\left(n_g\right)$, the degree of polymerization of the main backbone (n_{bb}), and

the degree of polymerization of the side chains (n_{sc}). The crowding parameter (ϕ) is defined by n_g and n_{sc}, and provides a mathematical definition for the transition from loosely grafted comb to densely grafted bottlebrush polymer (Figure 4). Above a threshold ϕ, the intense sterics of the densely grafted side chains increase the rigidity of and creates tension along[107] the main backbone, causing the brush to adopt a wormlike morphology, and preventing polymer chain entanglements.[29,108,109] This lack of polymer entanglements, evidenced by the zero shear viscosity deviating from $\eta_0 \sim N^{3.4}$,[110] is most often exploited to create super soft additive free elastomers.

Perhaps owing to their recent discovery, bottlebrush polymers as a class of materials are relatively unexplored, and as a consequence poorly understood. Models of describing the conformation of individual bottlebrushes[111] and their melt behavior[112] have been put

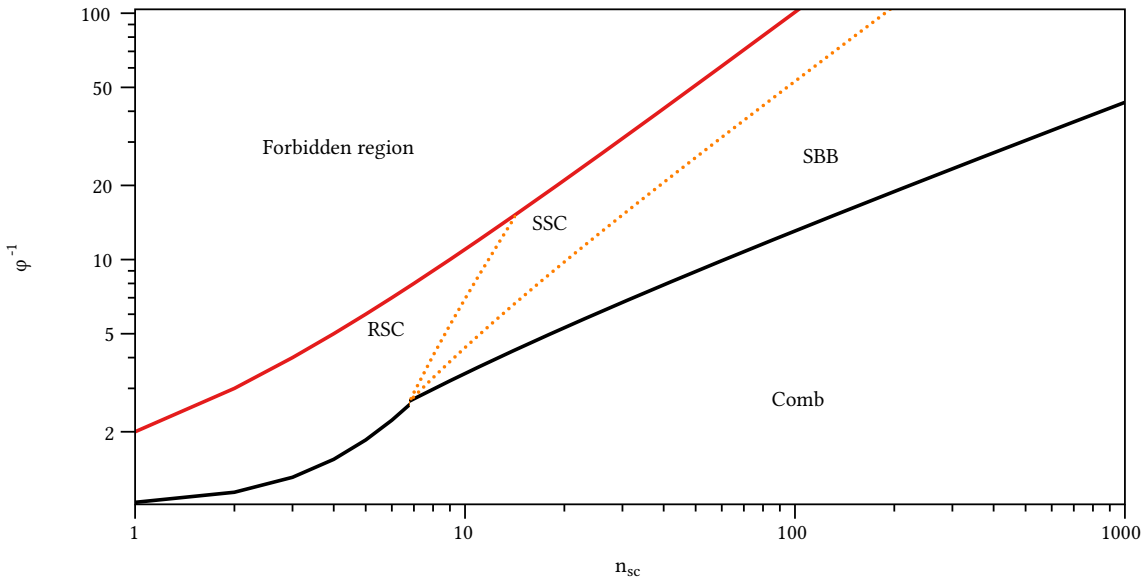

Figure 4: Phase diagram for methacrylic bottlebrush polymers. Depending on n_{sc}, n_{bb}, and n_g polymers with grafted sidechains can be categorized either as combs, bottlebrushes with rigid sidechains (RSC), stretched sidechains (SSC), or stretched backbones (SBB).

forward, but these almost always describe bottlebrush polymers with homopolymer side chains. Only recently has the self assembly of bottlebrush block polymers in melt[113] and solution[114] been described. Bottlebrush polymers with more complicated architecture, such as block polymer sidechains (core-shell architecture) are poorly described. Relatively well understood parameters of linear polymers such as the Flory-Huggins polymer-solvent interaction parameter, χ, are far less well modeled for bottlebrush architectures, and only grow more difficult to understand when secondary interactions like hydrogen bonding are taken into account.[115] Predicting the Kuhn lengths and persistence lengths of bottlebrush polymers as well remains a challenge, with experimental and theoretical studies offering contradicting conclusions.[116–120] Studies of bottlebrush polymers composed of reactive monomers capable of participating in crosslinking are almost completely absent, and only studied as additives to other thermosetting resins.[121] Some samples of bottlebrush mechanochemistry have been published, though these have very low functionality, only bearing mechanophores at the backbone-arm junction.[122,123] Given the unique morphology, lack of entanglements, large size, and potential for phase separation and microdomain formation, bottlebrush polymers present an opportunity to design high performance thermosetting materials. Already they have found applications in fields such as touch sensors,[29] pressure sensitive adhesives,[31,124] solvent free elastomers,[125] nanocapsules for drug delivery,[126] and antifouling coatings,[127] but highly crosslinked bottlebrushes have not been studied to date.

1.3.4 Highly crosslinked combs

Chapter 3 details my work preparing robust, highly crosslinked comb polymers. When designing these materials, I imagined a polymer of extremely high molecular weight with a high density of crosslinkable sites. The final crosslinked material should be a high modulus, insoluble solid. To achieve this, I selected GMA as the reactive monomer, which bears a pendent epoxide ring capable of participating in nucleophilic additions to create intermolecular crosslinks. To investigate the spatial effects of crosslinks on toughness of the final thermoset, I identified BMA as an attractive copolymer for GMA to act as a small spacer and internal plasticizer. My approach to identifying a highly crosslinkable, tough combs was to first synthesize a suite of polymers of different architectures: linear and comb, homopolymer and copolymer, and random and block. Then, I investigated crosslinking these polymers with succinic acid, a small di-carboxylic acid, to create a tightly crosslinked network. Finally, we investigated the toughness of the resultant materials. Comb polymers with random sidechains produced crosslinked materials with higher modulus and toughness than polymers with block or homopolymer sidechains.

1.4 Hydrogel preparation

1.4.1 Introduction

Whereas the previously discussed thermosets are designed to be dispersed in organic solvents or used neat, polymers can also be designed to be hydrophilic. When crosslinked, hydrophilic polymers form hydrogels that swell in the presence of water but do not dissolve. Mammalian, plant, and bacterial cells are known to synthesize, secrete, and

assemble a mix of proteins, proteoglycans, and sugars to create extracellular matrices (ECM).[128–130] The ECM in turn provides both chemical and mechanical cues to cells,[131] directing cell fate, morphology, and phenotype.[132–135] Hydrogels have for decades attracted researchers due to their 3D network structure closely mimicking that of natural ECM, with the first cell encapsulation being demonstrated in 1980.[136] Synthetic analogues in particular have been an area of intense focus as means to more precisely control the encapsulated cell environment compared to natural products, which often show large lot-to-lot variability.[137]

The first report of synthetic hydrogels as we currently know them appeared in 1958 in a publication by Danno in which poly(vinyl alcohol) in aqueous solution was crosslinked under gamma irradiation to form an insoluble gel.[138] This was soon followed up by Wichterle and Lím when they polymerized 2-hydroxyethyl methacrylate in the presence of ethylene glycol dimethacrylate to create water swollen gels for use as contact lenses,[139] which is still the basis for many contact lens formulations to this day.[140,141] In 1970 PEG hydrogels were prepared by irradiation with gamma and electron radiation,[142,143] and PEG gels started to attract attention due to their favorable biocompatibility and non-fouling properties.[144] The chain end alcohols of PEG have since been functionalized with methacrylates for the preparation of gels by FRP,[145] isocyanates[146] and succinimidyl esters,[147] and a variety of chemistries capable of participating in Michael-type additions.[148–150]

1.4.2 Mixing and light

Cell encapsulation techniques within hydrogels must be both rapid enough to prevent cell settling and cytocompatible.[151] Free radicals and high energy UV light are well known to cause cellular damage,[152] though UV photoinitiators and vinyl monomers are used to encapsulate cells. Michael-type reactions are commonly used as bio-orthoganol methods of crosslinking hydrogels, and are useful for their ability to incorporate bioactive peptides by exploiting Michael donors present in amino acids, such as the thiol in cysteine.[153,154] Additionally, the A–B type crosslinking by Michael-type reactions often produces highly homogenous gels.[147] However, the reaction kinetics vary amongst chemistries used, and tuning the kinetics within the framework of physiological conditions can be a challenge, not to mention relative difficulties of biology labs synthesizing functional PEG not commercially available.[155,156] Moreover, Michael-type reactions most often do not allow for spatiotemporal control, meaning the homogeneity of the network is dependent on the reaction kinetics.[157]

1.4.3 Reversible deactivation radical polymerizations

RDRPs, by contrast, are rarely used in biomedical applications. The reasons for this vary, though in general, RDRPs are slower than FRPs, are sensitive to trace oxygen and are traditionally thermally initiated. These aspects make them unsuitable for polymerization in the presence of living cells. ATRP most commonly requires cytotoxic metal halide salts among several other reactants, although there are efforts to replace them with powerful organic reducing agents capable of homolytically cleaving carbon-halogen

bonds.[158] NMP is traditionally extremely slow[159] and has serious challenges with monomer compatibility.[160] RAFT requires tuning of the chain transfer agent to match the desired monomers[161] and is expensive to source.

Despite all of this, RDRPs offer significant benefits over FRPs. FRPs produce gels with heterogeneous networks due to unavoidable termination, slow initiation relative to propagation, and slow segmental relaxation relative to chain growth in the gel phase.[162,163] FRPs commonly overcome inhibition from oxygen by overwhelming it with excess radical species, to the detriment of cytocompatibility. In contrast, RDRPs are able to produce highly homogenous gel networks due to their high initiation relative to propagation rates and low radical concentrations which minimize irreversible termination events as well as minimizing cellular damage. Furthermore, the reversible nature of RDRPs enable living gels[164] by postpolymerization modifications of gels.[165] Chapter 4 of this dissertation will harness RDRPs using the photoiniferter process to rapidly polymerize and crosslink biocompatible hydrophilic monomers.

1.5 Hypothesis

Current methods of curing thermosets are limited in their applications and cannot be applied in all circumstances. This is particularly true of biomedical applications, where conditions must be kept within the strict confines of physiological conditions. I hypothesize that grafting pendent PEG chains along the main polymer backbone will provide a facile way to install mechanosensitivity by sterically shielding reactive sites, enabling on demand gelation. Furthermore, I hypothesize densely grafted bottlebrush polymers with

reactive side chains can be prepared as high-modulus, tough thermosets by adjusting the sidechain architecture to favor intermolecular crosslinking. Finally, I hypothesize that rapid fragmentation of xanthogen disulfides in response to visible light will enable rapid preparation and crosslinking of biocompatible hydrogels. I predict that that this work will enable new methods of bottom up design of thermosetting materials.

1.6 Objectives

The following were the objectives for this dissertation:

1. Optimize a library of sparsely grafted copolymers carrying reactive pendent groups and methoxy poly(ethylene glycol) (PEG) grafts for use as mechanically activated crosslinkable materials;
2. Synthesize and characterize novel mechanically responsive core-shell bottlebrush polymers furnished with a high density of crosslinkable pendant groups;
3. Develop a method to rapidly crosslink hydrogels in response to light in the visible range.

1.7 Significance

I have identified a new path for easy installation of mechano-responsiveness into synthetic polymers using off-the-shelf chemistries and materials. Further, I have developed strategies to combat intramolecular crosslinking in densely grafted reactive polymers. Finally, I have designed a method of rapidly synthesizing and crosslinking biocompatible hydrogels. Overall, this dissertation presents easy and accessible approaches to designing strain sensitive polymers as well as preparing hydrogels by reversible deactivation radical polymerization that will enable more rapid translation of mechanosensitive polymers

and tailor-made hydrogels. Additionally, this dissertation provides new strategies for preparing tough thermosets from high molecular weight resins.

Chapter 2

Molecularly shielded, on-demand, ultrasound-cured polymer networks

Reprinted (adapted) with permission from Lorenzana, A. A. *et al.* Molecularly Shielded, On-Demand, Ultrasound-Cured Polymer Networks. *Macromolecules* **57**, 6465–6473 (2024).

2.1 Abstract

Networks formed from polymers can range from soft hydrogels to ultrahard protective coatings, making them useful for a wide range of applications from cell culture to highly bonded adhesives. Polymer networks are commonly crosslinked *via* heat or high energy light, and recently mechanical force has also been used to induce the formation of crosslinks in pre-existing networks. Here, I demonstrate a new strategy to use mechanical deformation and ultrasound to induce liquid-to-solid crosslinking. I synthesized graft copolymers with large poly(ethylene glycol) (PEG) side-chains acting as molecular shielding groups to protect otherwise highly reactive epoxide group. Solutions of highly shielded polymers could remain as a liquid solution when left undisturbed, and I could initiate gelation of these solutions with ultrasound in 20 seconds. These ultrasound-sensitive polymers are particularly useful in light and heat sensitive applications, and where precise control over the gelation time is required.

2.2 Introduction

Polymer networks can be crosslinked *via* permanent covalent bonds. Polymer networks can include super-soft hydrogels that mimic human tissue,[166] protective ultra-hard coatings,[167]

and highly bonded adhesives.[168] Highly crosslinked lightweight networks, such as those formed with epoxide, are crucial in industrial applications like transportation, where reducing vehicle weight improves passenger safety and reduces harmful greenhouse gas emissions. The process of crosslinking or "curing" polymers is typically accomplished via a) mixing, b) heat, c) high energy light, or d) electron beams.[169] Heat and light are popular routes, as they facilitate curing on-demand, allowing liquid application to a substrate. However, light and heat are not always feasible, as light cannot pass through opaque materials, and heat can damage delicate or flammable substrates. Electron beams are also popular industrially due to their high energy efficiency and excellent uniformity, however transmittance through metals can be challenging.

Alternatively, natural polymers (e.g. peptides, saccharides, nucleic acids), can form networks in response to temperature, light, and solvents by partially unfolding, thus exposing previously buried, or "cryptic", binding sites. Of particular interest to us, these cryptic binding sites can also be revealed in response to a mechanical stimulus.[170,171] For example, fibronectin will dynamically unfold and polymerize into fibrils in response to cell-generated forces.[45,172,173] In contrast, synthetic polymers commonly weaken or even rupture under force.[174]

Inspired by the unfolding triggered crosslinking of proteins like fibronectin, I sought to develop a new method of installing mechanosensitivity within synthetic polymer networks. Recently, we developed organogels[51] and hydrogels[52] with mechano-responsive properties, both based on preformed diacrylate crosslinks with reactive pendent thiols

for post-polymerization crosslinking. Both systems begin as a crosslinked network and respond to compression, strengthening several hundreds of kPa in elastic modulus over repeated cycles. The mechanosensitivity results from long PEG molecular shielding groups grafted to the polymer backbone, which prevent the reactive thiol groups from crosslinking until compression brings them together.

To date, the most successful method of creating synthetic mechanosensitive polymers that undergo liquid-to-solid transition is by inserting weak bonds, "mechanophores," within polymer chains that are converted to an active intermediate in response to force, capable of strengthening the material.[3,76,175] Still other approaches to designing force-sensitive materials involve the design of small molecules with several ways of participating in intermolecular interactions such as hydrogen bonding, π–π stacking, and van der Waals forces. Peptide-based isomers functionalized with cholesterol and napthalic groups have been shown to create micellar assemblies that undergo a gel-gel transition with the application of ultrasound.[176] This work, in contrast, uses the shielding group concept, starting with uncrosslinked, shielded polymers that can undergo a rapid liquid-to-solid transition upon application of force. To accomplish this, graft polymers bearing reactive epoxide[177] groups are mixed with small molecule amine/thiol crosslinkers. Ultrasonic irradiation is used to apply high strain rates to the shielded polymers. Straining of the graft polymers overcomes their steric barrier to interaction with the small molecule crosslinkers, facilitating a reaction, that rapidly strengthens the material. The resultant materials achieve elastic modulus values comparable to ultra hard commercial epoxy

coatings. I anticipate that these shielded polymers will be useful as extremely hard and solvent-resistant coatings and as adhesives that can be cured by focusing ultrasound through the surfaces the adhesive is bound to.

2.3 Materials and methods

2.3.1 Chemical and polymer sourcing

Materials were purchased from Sigma-Aldrich unless otherwise mentioned. (500 g/mol and 950 g/mol, PEGMA500 and respectively), glycidyl methacrylate (97%, GMA), and 2-methoxyethyl methacrylate (99%, MEMA) were passed through a column of neutral alumina to remove inhibitors before use. 2,2′-(Ethylenedioxy)diethanethiol (95%, EDT), ethylene diamine (99%, EDA), (99%, PPB), (98%, CPA), and 2-(azo(1-cyano-1-methylethyl))-2-methylpropane nitrile (98%, AIBN), 1-butanol (99.9%, BuOH), 1,4-dioxane (99%, dioxane), N,N-dimethylformamide (99.8%, DMF) were used as received. Diethyl ether (99%, ether), lithium hydroxide monohydrate (98.5%, LiOH), and acetonitrile (99%, MeCN) were purchased from Fisher Chemical and used as received. Basic alumina 60-325 mesh was purchased from Fisher Scientific and used as received.

2.3.2 Representative polymer synthesis

Poly(GMA-*co*-PEGMA) and poly(GMA-*co*-MEMA) of all molar ratios and degree of polymerization (DP) were synthesized by reversible addition-fragmentation chain transfer (RAFT) polymerization. The targeted monomer ratios and DP are described in Table 1. Each reaction was fed 0.01 moles of monomer total. For example, 0.71 g (0.005 mol) GMA, 0.72 g (0.005 mol) MEMA, 0.0559 g CPA (0.2 mmol), 6.6 mg AIBN (0.04 mmol) ([50]:[1]:

[0.2] [M]:[CTA]:[I], where [M]:[CTA] defines the DP), 4 mL of 1,4-dioxane, and a stir bar were added to a 20 mL scintillation vial. The vial was sealed with a rubber septum and the solution was purged with N2 (g) for ∼20-30 min in an ice bath to prevent solvent and monomer evaporation (PEGMA solutions were bubbled in cool water to prevent PEG crystallization). Subsequently, the vial was placed in a thermostated aluminum reaction block at 60 °C on top of a magnetic stir/hot plate. The reaction was left to stir overnight, yielding a viscous liquid. The solution was removed from heat and exposed to air to terminate the polymerization. The solution was precipitated into cold (-20 °C) ether, the solid washed twice more with cold ether, and dried at 0.01 mbar overnight.

2.3.3 Polymer characterization

Polymer DP and the comonomer incorporation ratio were determined through ^{1}H NMR on a Bruker Avance 500 at 500 MHz in $CDCl_3$ (Figure 5 - Figure 14).[178] The ratio of monomers was determined by integration of ^{1}H spectral resonances of the PEGMA/MEMA methoxy protons and the methanetriyl proton of the GMA glycidyl ring, normalized to the aromatic proton peak at the para position of the CPA phenyl ring, assuming there is one Z group[161] on every polymer chain.

2.3.4 Copolymer solution preparation

Polymer solutions were initially prepared to be 50 wt% polymer. For example, 0.3 g of polymer was dissolved in 0.3 g of solvent, and crosslinker was added such that the nucleophilic functional group was equimolar with the total epoxide concentration. To control for the concentration of crosslinking points in solution, polymers were subsequently

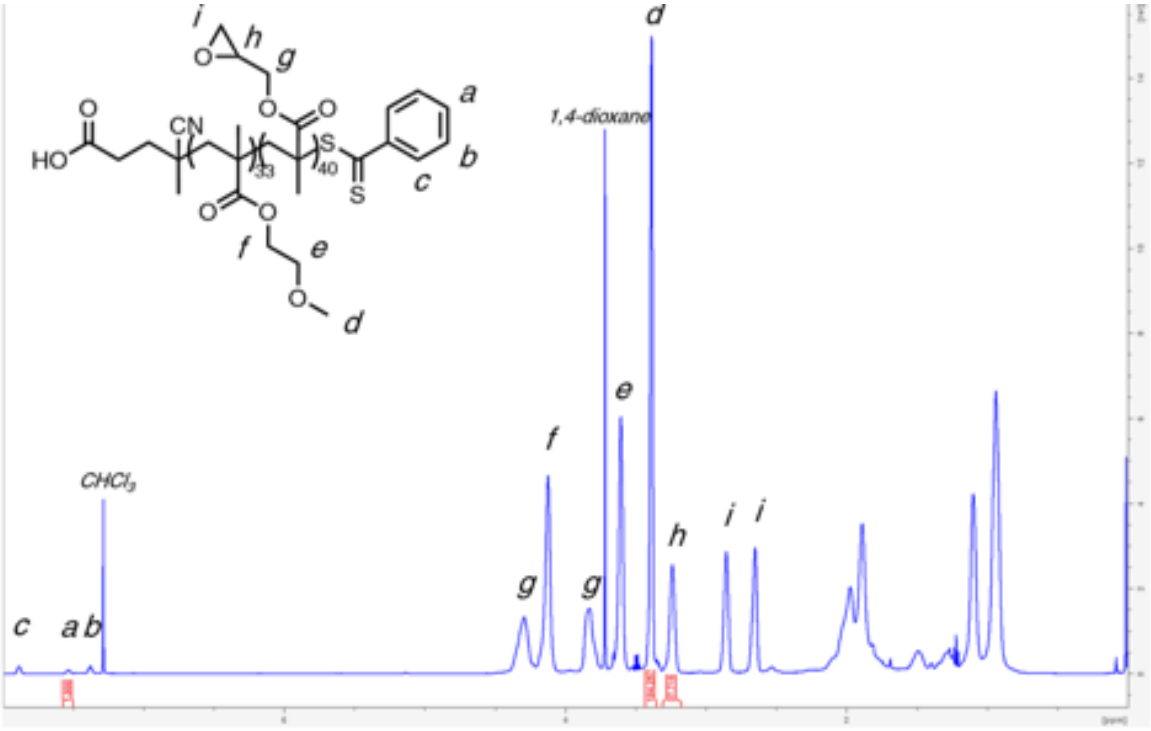

Figure 5: ^{1}H NMR spectra of poly(GMA-*co*-MEMA) targeting 50 DP and 1:1 comonomer ratio. Spectra recorded at 500 MHz in $CDCl_3$.

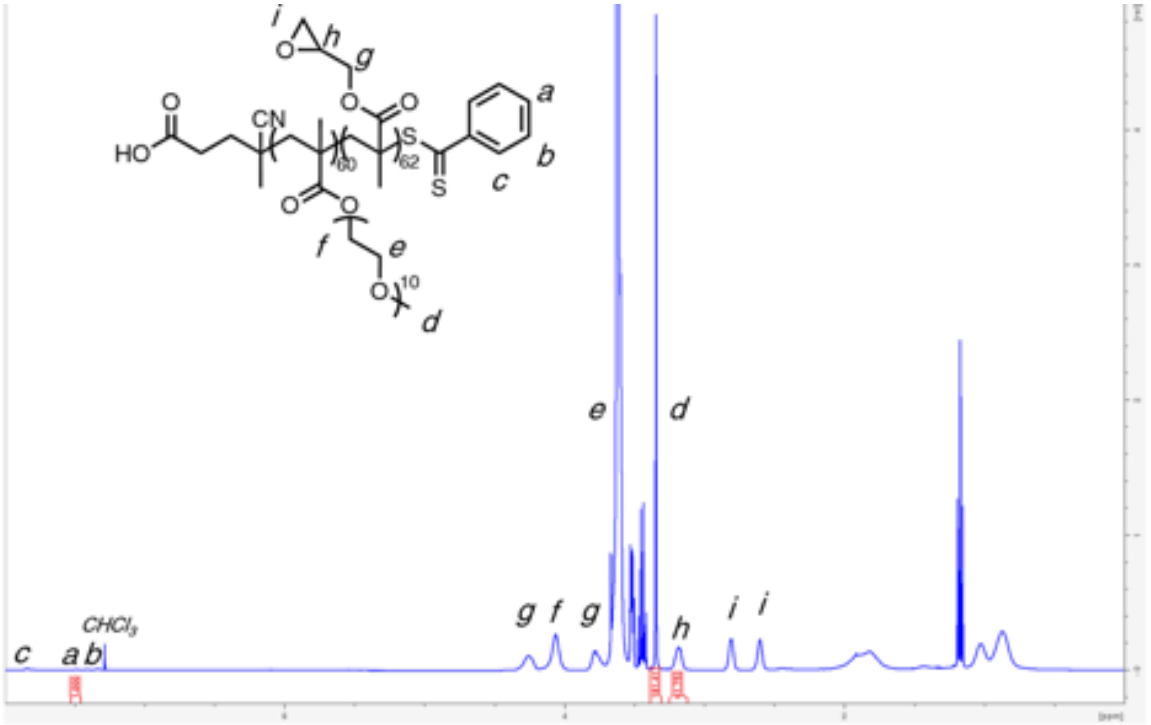

Figure 6: ^{1}H NMR spectra of poly(GMA-*co*-PEGMA500) targeting 50 DP and 1:1 comonomer ratio. Spectra recorded at 500 MHz in $CDCl_3$.

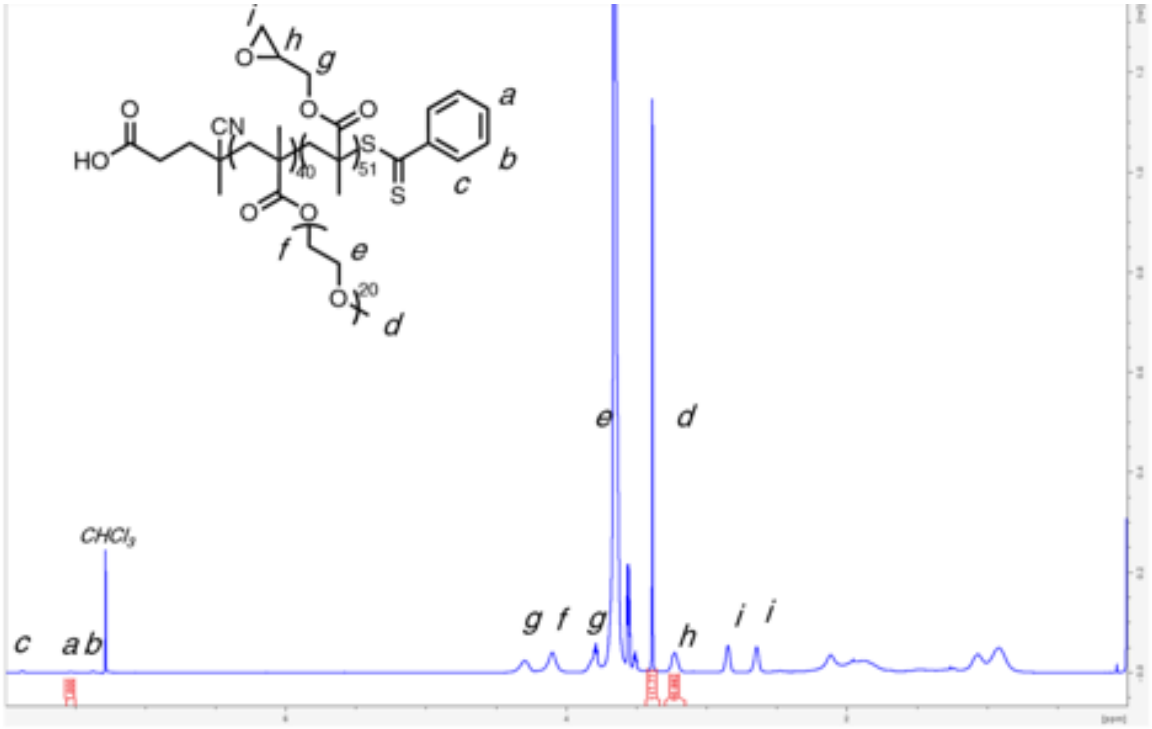

Figure 7: ^{1}H NMR spectra of poly(GMA-*co*-PEGMA950) targeting 50 DP and 1:1 comonomer ratio. Spectra recorded at 500 MHz in $CDCl_3$.

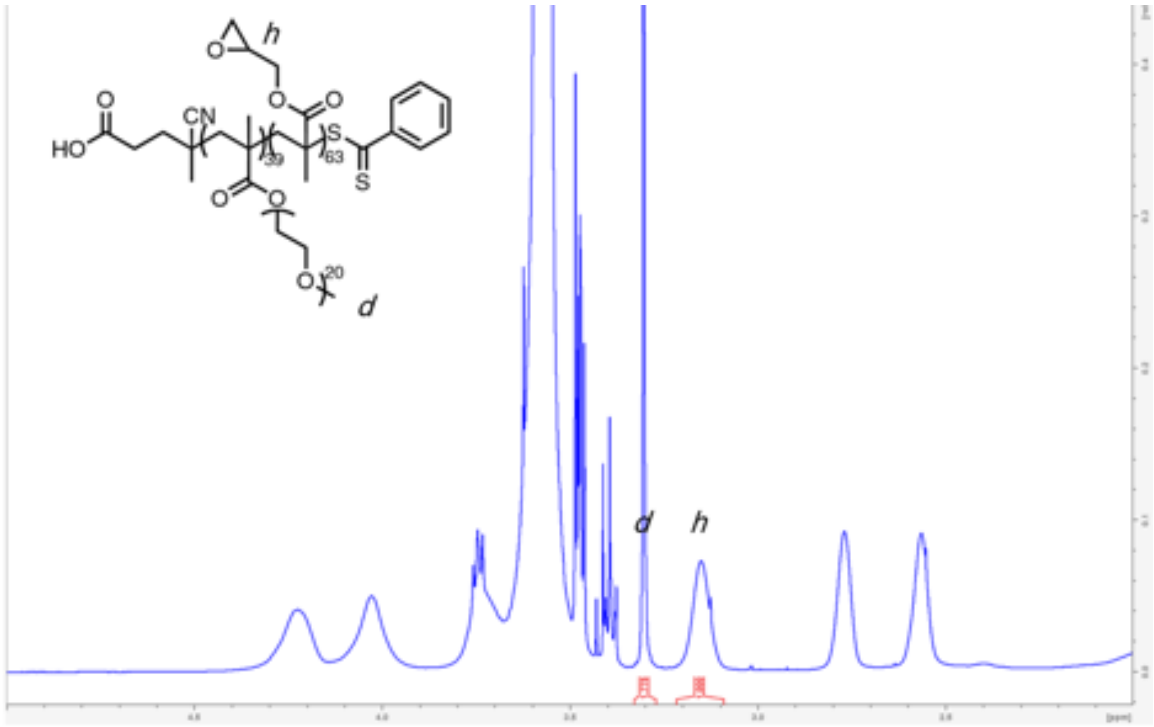

Figure 8: ^{1}H NMR spectra of poly(GMA-*co*-PEGMA950) targeting 50 DP and 60:40 comonomer ratio. Spectra recorded at 500 MHz in $CDCl_3$.

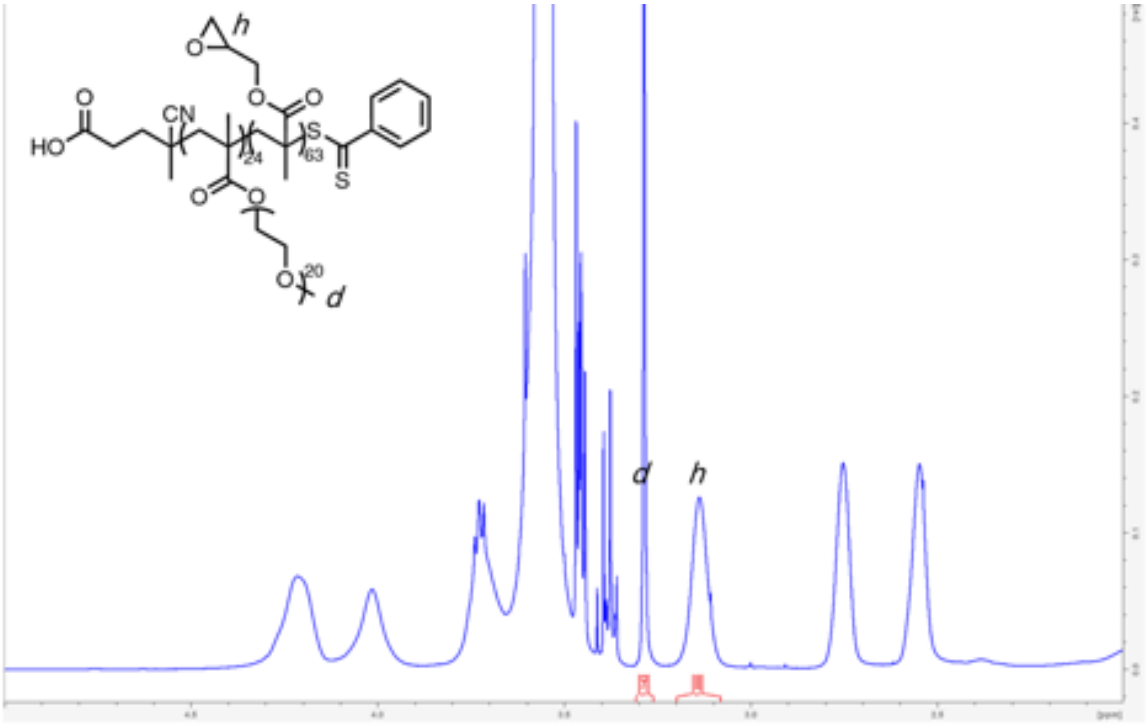

Figure 9: ^{1}H NMR spectra of poly(GMA-*co*-PEGMA950) targeting 50 DP and 70:30 comonomer ratio. Spectra recorded at 500 MHz in $CDCl_3$.

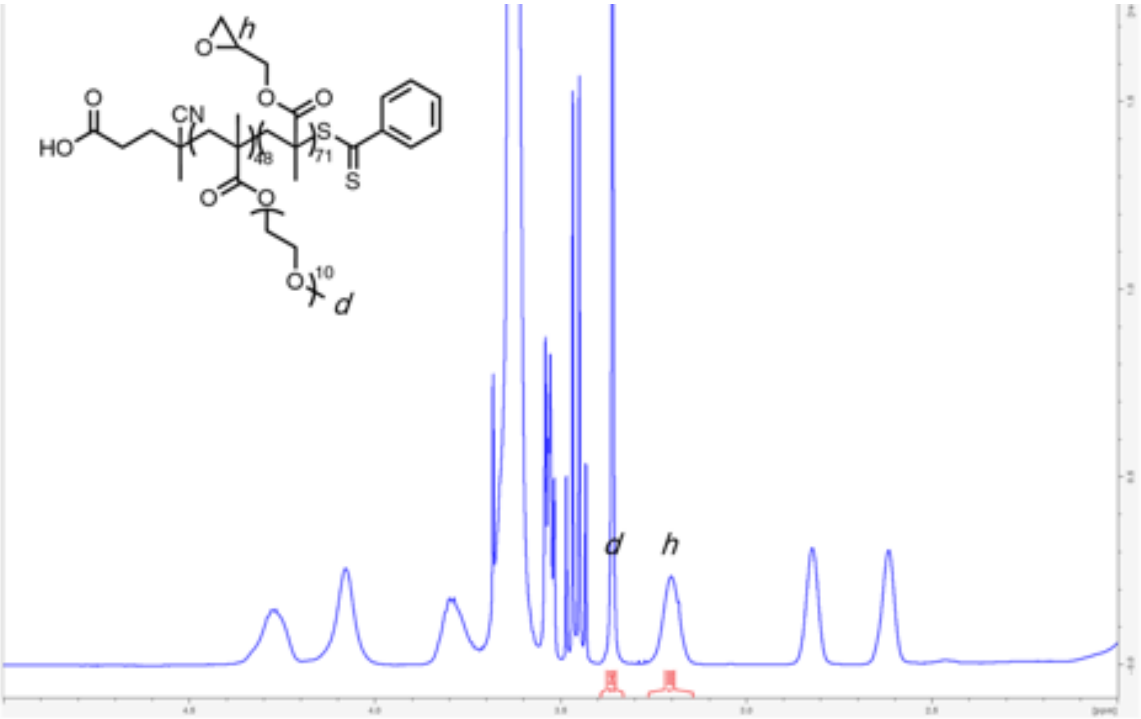

Figure 10: ^{1}H NMR spectra of poly(GMA-*co*-PEGMA500) targeting 50 DP and 60:40 comonomer ratio. Spectra recorded at 500 MHz in $CDCl_3$.

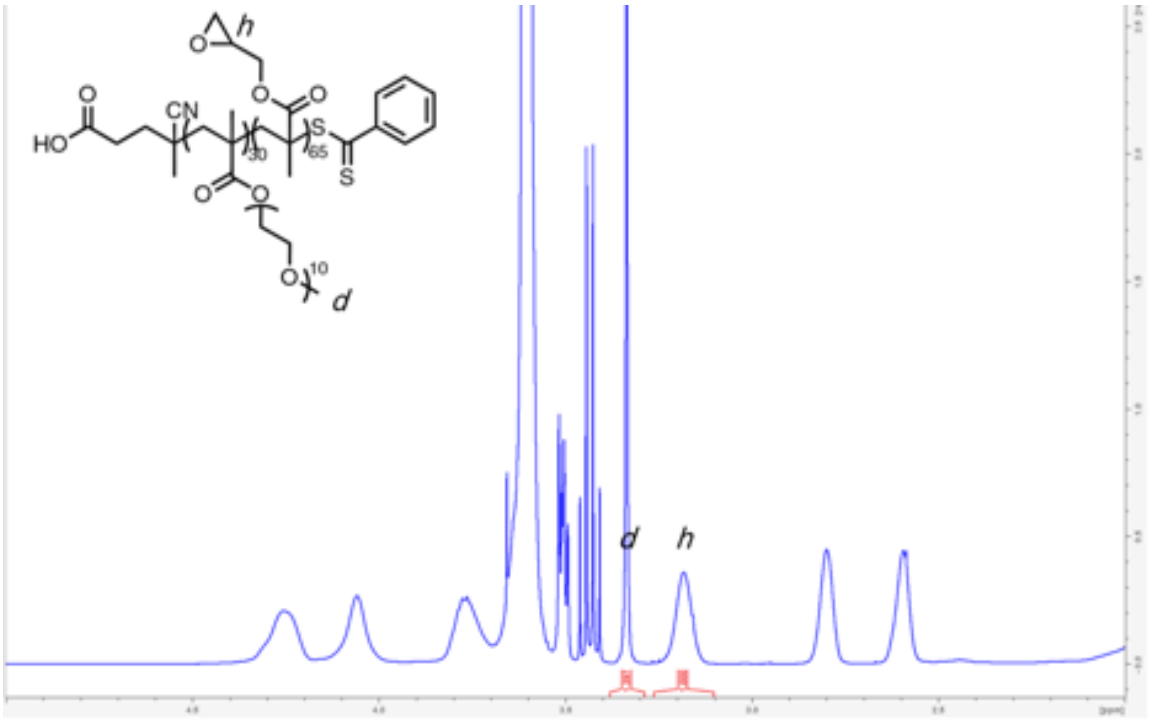

Figure 11: ^{1}H NMR spectra of poly(GMA-*co*-PEGMA500) targeting 50 DP and 70:30 comonomer ratio. Spectra recorded at 500 MHz in $CDCl_3$.

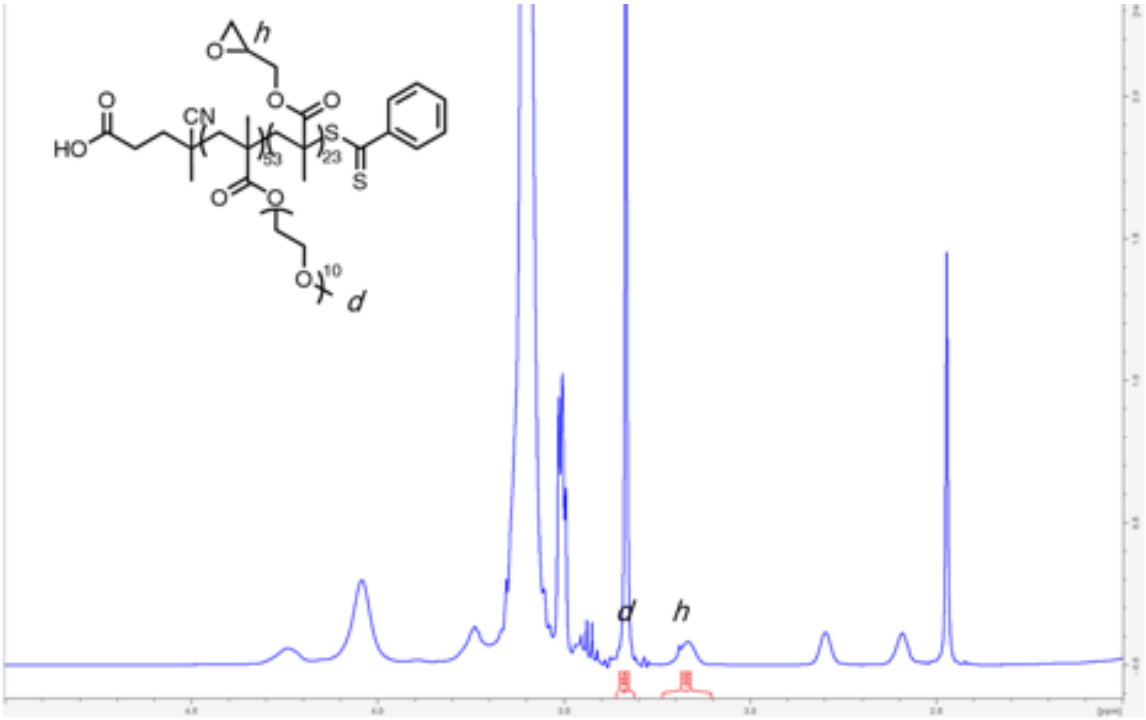

Figure 12: ^{1}H NMR spectra of poly(GMA-*co*-PEGMA500) targeting 50 DP and 30:70 comonomer ratio. Spectra recorded at 500 MHz in $CDCl_3$.

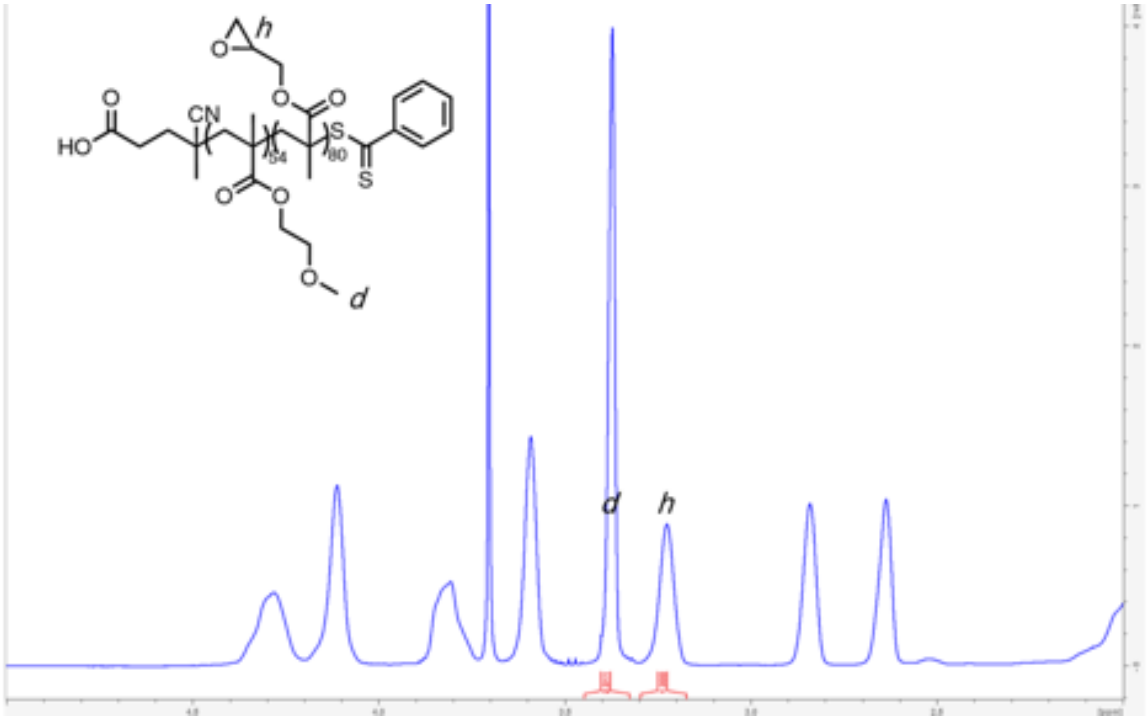

Figure 13: ^{1}H NMR spectra of poly(GMA-*co*-MEMA) targeting 50 DP and 60:40 comonomer ratio. Spectra recorded at 500 MHz in $CDCl_3$.

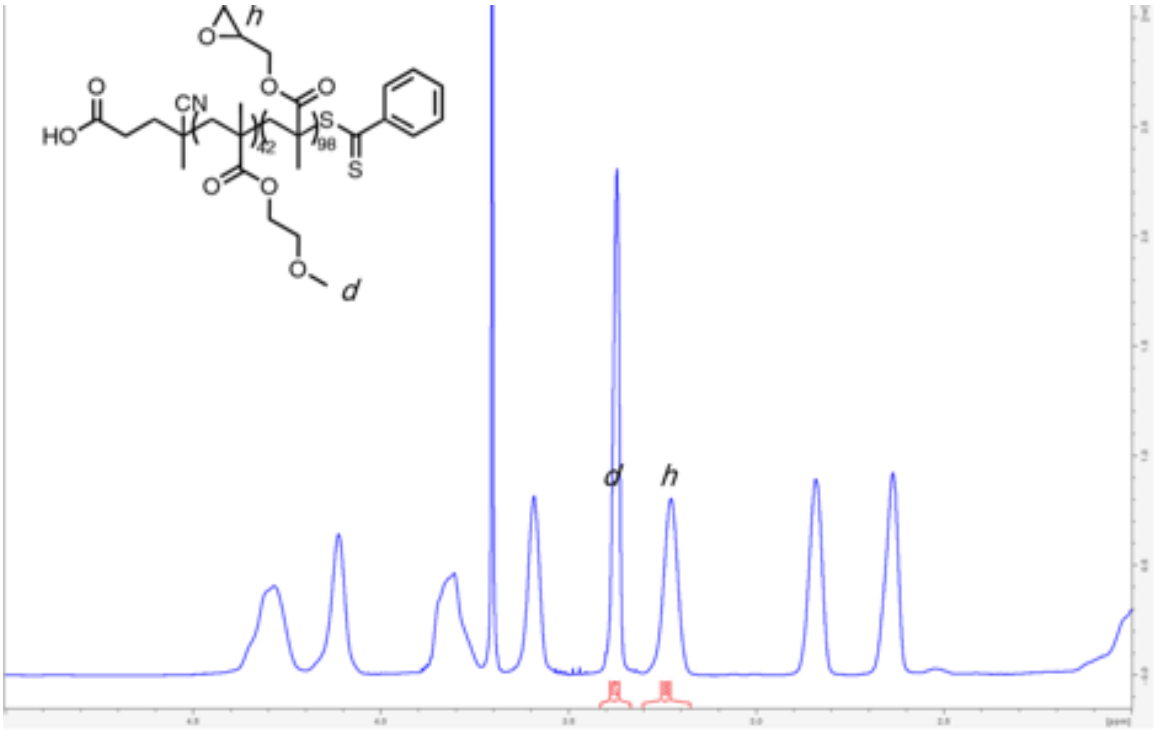

Figure 14: ^{1}H NMR spectra of poly(GMA-*co*-MEMA) targeting 50 DP and 70:30 comonomer ratio. Spectra recorded at 500 MHz in $CDCl_3$.

formulated to be 1 M of epoxide in solution. For copolymers containing PEGMA2000, solutions were formulated in MeCN at 0.5 M of epoxide functional units due to the large pendant chains dominating the overall mass of the sample and crosslinked with EDT catalyzed by LiOH. Each sample was vortexed for 5 sec to ensure complete mixing before proceeding with rheometry or sonication.

For all experiments crosslinked with amines, reactions were conducted in a solvent system of 1:1 BuOH:DMF. Alcohols are known to catalyze the reaction between amines and epoxides through the formation of a trimolecular complex.[179] Thiol-crosslinked reactions were conducted in MeCN with 10 μL of 2 M LiOH as a catalyst, necessary to deprotonate the thiols in order to perform a nucleophilic attack on the epoxide ring.[180]

2.3.5 Parallel plate rheology

Gelation times and storage moduli (G'), and $tan\delta$ of polymer solutions/gels were determined on a Kinexus Pro parallel plate rheometer (Netzsch, Selb, Bayern, Germany). Measurements were run on a 20 mm plate with a 1 mm gap at 1% strain and 1 – 100 rad s^{-1} frequency sweep. Each frequency sweep lasted approximately 5 min, and the entire measurement lasted approximately 15 hr. The gel point was defined using the Winter-Chambon criterion, for which the time of gelation is defined as the point at which $tan\delta$ becomes frequency independent at small frequencies.[181–183] For samples with very high modulus, the elastic modulus was determined using compressive rheology by taking the slope of the stress strain curve of cured gels with a 4 mm diameter. Rheological experiments were analyzed using IRIS Rheo-Hub (IRIS Development, Amherst, MA).[184]

2.3.6 Sonication-induced gelation of shielded polymers

Polymer solutions were sonicated using a QSonica Q500 with a microtip attachment. The microtip QSonica probe was immersed in a polymer solution in MeCN. Water was flowed across the outer surface of the tube using a custom-made jacketed beaker to control bulk temperature (University of Massachusetts Amherst Scientific Glassblowing Laboratory, Amherst, MA). Temperature was monitored with an IRT205 IR thermometer (General Tools, Secaucus, NJ) and confirmed with a mercury thermometer. This cooling setup was not sufficient to control temperature after 2 min and 40 s of sonication. Samples were sonicated at 10% amplitude and 20 kHz for 5 sec at a time, with 10 sec breaks in between pulses to avoid probe overheating. Gelation was determined by the point at which the power output would drop to ∼0 W and noise from vibrations would cease when the polymer had formed a solid gel. Samples were then immediately moved to the adjacent needle induced cavitation (NIC) setup to determine the elastic modulus immediately post sonication.

2.3.7 Differential scanning calorimetry

Differential scanning calorimetry (DSC, Q200, TA Instruments) was used for crystallization characterization. A sample of (3-5 mg) was sealed in a standard aluminum hermetic pan using TZERO press (TA Instruments) before being added to the calorimeter with an identical empty reference pan. The equipment was lowered to −90 °C and heated to 100 °C at a rate of 5 °C/min to remove the thermal history of the sample. The equipment was then lowered to −90 °C again and heated to 100 °C at the same rate, where enthalpy of

melting ($\Delta H\textsubscript{m}$) was obtained from the area of the melting curve divided by the sample weight.[185] Thermogravimetric analysis (TGA, Q50, TA Instruments) was used to determine the degradation of the samples before running DSC to meet the criteria of a maximum 1.5 wt% loss.

2.3.8 Needle induced cavitation

Characterization of elastic modulus of sonicated gels was done with needle induced cavitation (NIC) using a custom-made setup with water as the fluid, pressurized with a NE 1000 syringe pump (New Era, Farmingdale, NY), contained in a 6 mL disposable syringe with a 27-gauge stainless steel disposable needle, microstand, and Px409-015 GUSBH pressure gauge (Omega, Norwalk, CT). Data collected from NIC was recorded on a Surface Mini using a custom LabView program to interface with the pressure sensor and record the pressure values (Crosby Lab, University of Massachusetts Amherst, Amherst, MA). When calculating the elastic modulus of gels, the effects of surface tension were ignored and values were computed using Equation 1.[186,187] Each NIC experiment lasted on average from 30-90 sec.

$$E = \frac{6P_c}{5}$$

2.4 Results and discussion

2.4.1 Gelation kinetics of polymers under static conditions

My goal was to create a polymer network that was shelf-stable and would gel in response to force. First, I created a suite of polymers with varying crosslinker to comonomer

ratios. Shielded and control copolymers were synthesized using RAFT polymerization of PEGMA (molecular shielder, grafting-through process[188]) or MEMA (control) with GMA monomers. Poly(GMA-co-PEGMA) and poly(GMA-*co*-MEMA) were synthesized with varying monomer ratios (30:70 GMA:PEGMA/MEMA to 70:30 GMA:PEGMA/MEMA) and shield lengths (1, ∼10, and ∼20 PEG repeats for MEMA, PEGMA500, and PEGMA950, respectively) to determine their effect on gelation. Additionally, DP for each composition was varied to determine the effect of polymer length on force sensitivity.

When developing these materials, I imagined a polymer system that would be easily spreadable onto a substrate as a liquid that would then transition to a solid state after the introduction of mechanical stimuli. The final solid material should be bonded together permanently with covalent crosslinks. To achieve this goal, I selected the monomer GMA for its robust epoxide reactive group. Epoxides are known to undergo a ring-opening reaction in the presence of nucleophiles like amines and thiols. To introduce mechano-sensitivity, I sought to copolymerize my epoxide functional monomers with monomers functionalized with groups that could provide steric hindrance. Towards this goal, GMA was co-polymerized with PEGMA of varied molecular weights from 140 to 950 g/mol that I hypothesized could provide a steric hindrance to crosslinking *via* their ether side-chains.

Synthesis of this suite of polymers proceeded as expected, with final DPs and incorporation ratios closely matching the targeted DP and feed ratio when conducted in dioxane (Table 1). Successful incorporation and molar ratio of constituent monomers was confirmed using ^{1}H NMR spectroscopy (Figure 5 - Figure 14). DP and incorporation

Name	Target DP	Feed ratio	Actual DP	Actual ratio
50:50 GMA:MEMA	50	1:1	73	55:45
50:50 GMA:PEGMA500	50	1:1	122	51:49
50:50 GMA:PEGMA950	50	1:1	91	56:44
60:40 GMA:PEGMA950	50	60:40	102	62:38
70:30 GMA:PEGMA950	50	70:30	87	72:28
30:70 GMA:PEGMA500	50	30:70	76	30:70
60:40 GMA:PEGMA950	50	60:40	119	60:40
70:30 GMA:PEGMA500	50	70:30	95	68:32
60:40 GMA:MEMA	50	60:40	134	60:40
70:30 GMA:MEMA	50	70:30	140	70:30
50:50 GMA:PEGMA950 25DP	25	1:1	34	1:1
50:50 GMA:PEGMA950 50DP	50	1:1	61	54:46
50:50 GMA:PEGMA950 100DP	100	1:1	93	1:1
50:50 GMA:PEGMA950 150DP	150	1:1	130	52:48
50:50 GMA:PEGMA950 200DP	200	1:1	191	57:43

Table 1: Polymers used in each experiment, their target DP, comonomer feed ratio, actual DP, and actual comonomer ratio as determined by ^{1}H NMR.

ratios of poly(GMA-*co*-PEGMA) samples were less consistent compared to their MEMA counterparts, attributed to the inherent dispersity of PEGMA macromonomers skewing the actual molar amount added to reactions. After successfully synthesizing the desired copolymers, I moved on to assess their gelation kinetics.

For the crosslinkers, I chose EDT due to its non-volatile nature and reasonable stability in air, and EDA as it is commonly used to cure epoxy resins. Amines and thiols were chosen as two candidates both because they are frequently used in commercial epoxy formulations and to compare the effects of different reaction kinetics on the shielded copolymer system. I sought to determine a molecular weight of shielding groups that would facilitate delayed crosslinking of the epoxide groups in the presence of a

bifunctional nucleophile without preventing it entirely. In my experiments, I tested a range of effects including varying the DP of grafted chains from 1 to 20, varying the DP of the polymer backbone from 25 to 670, adjusting nucleophilic attack kinetics, and varying the ratio of comonomers from 30 to 70% GMA concentration. The monomers used to form the copolymers and the different crosslinkers in these experiments are represented in Figure 15 a.

First, the effect of pendent shield size on crosslinking was assessed at constant weight percent and static conditions (Figure 15 b). When solutions are formulated at 50 wt% of polymer with EDA, poly(GMA-*co*-MEMA) crosslinks very quickly (1 h) and reaches a final G' on the order of 106 Pa. Conversely, poly(GMA-*co*-PEGMA500) crosslinks more slowly (8 h) and reaches a final G' on the order of 104 Pa, and poly(GMA-*co*-PEGMA950) shows no change in modulus indicating no crosslinking occurred. At constant 50 wt% of polymer in solution, the concentration of epoxide for unshielded samples (MEMA) is very high compared to the shielded polymers (PEGMA). At this fixed concentration, the overall mass for the shielded polymer solutions is dominated by the presence of ether in the PEGMA side chains, skewing the sample in favor of unreactive ether and decreasing the number of possible crosslinks. The lack of increase in modulus with PEGMA950 may be due to this ether dominance preventing the formation of a volume-spanning network. Additionally, the relatively large mass of the ether side-chains decreases the amount of reactive epoxy in solution.

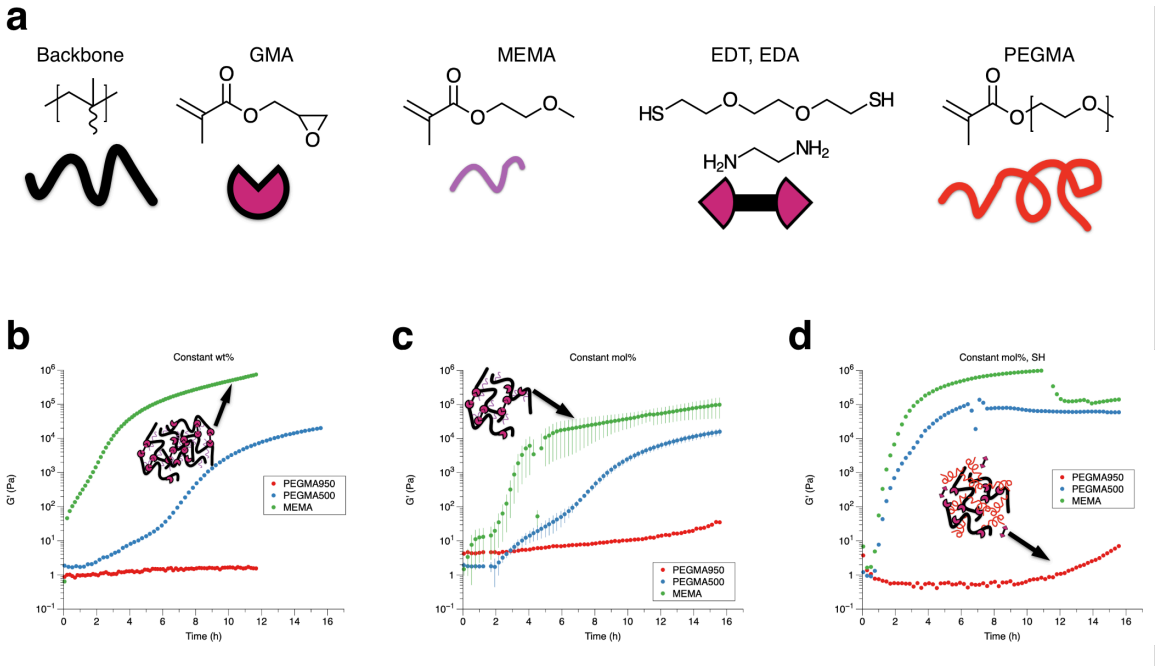

Figure 15: Large molecular shields inhibit or delay crosslinking. (a) Illustrations of polymer components used throughout the paper. (b) Effect of shielding group functionality on storage modulus (G') over time with amine crosslinks at constant 50 wt % polymer, reacting with EDA. Inset depicts high density poly(GMA-*co*-MEMA) with many epoxy groups. (c) Effect of shielding group functionality on storage modulus over time with amine crosslinks at constant 1 M concentration epoxy, reacting with EDA. Inset depicts low density poly(GMA-*co*-MEMA) with a fixed amount of epoxy groups. (d) Effect of shielding group functionality on storage modulus over time with thiol crosslinks at constant 1 M concentration epoxy, reacting with EDT. Inset depicts poly(GMA-*co*-PEGMA950) with a fixed amount of epoxy groups and large shielding groups preventing crosslinking. For all experiments, a 1:1 ratio of GMA:MEMA, PEGMA500, or PEGMA950 was used. Error bars show the standard deviation of G' at each timepoint (n = 3). For all conditions, including the enhanced kinetics provided by the thiol-epoxy reaction, a latency period before gelation at static conditions is present.

To control for the effect of variable epoxide concentration, samples were next formulated at a constant epoxide molar concentration (Figure 15 c). Epoxide concentration was set to 1 M, resulting in variable weight percent polymer in solution: control polymer samples with low (25%) and shielded samples with high (61%) weight percent. At 25 wt%,

poly(GMA-*co*-MEMA) crosslinks more slowly (2 h) than at 50 wt% and reaches a lower final G' on the order of 105 Pa. For poly(GMA-*co*-PEGMA950), wt% changes from 50 to 61 and expectedly shows only a small increase in G' of 35 Pa. For poly(GMA-*co*-PEGMA500 samples, 1 M epoxide concentration is equal to 50 wt% of polymer. Trends in the effect of shielding groups are the same at constant wt% polymer or mol% epoxides: as the shielding group MW increases, the time to gelation and the final modulus both decrease.

Finally, the effect of more reactive nucleophiles on crosslinking were investigated by replacing EDA with EDT and keeping the mol% epoxide constant (Figure 15 d). Thiols are known to be stronger nucleophiles than primary amines, and the ring opening reaction between thiols and epoxides proceeds orders of magnitude faster than between amines and epoxides.[189] At a constant 1 M epoxide concentration, poly(GMA-*co*-MEMA) with EDT crosslinked more rapidly (30 min) than the amine condition and attained a similar final G'. Poly(GMA-*co*-PEGMA500) samples crosslinked rapidly (42 min) with EDT, but more slowly than the MEMA copolymer and attained a final modulus on the order of 104 Pa. Poly(GMA-*co*-PEGMA950) samples still did not show any signs of gelation, increasing only to a final modulus of 10 Pa. Even with faster reaction kinetics, the PEGMA950 shielding groups suppress gelation.

For permanently crosslinked polymer networks, the equilibrium modulus of the cured material can be predicted by Flory's theory of rubber elasticity[18,190] and is proportional to the number of elastically effective chains in the network.[191,192] As the number of elastically effective chains increases, so does the equilibrium modulus; therefore, a low

equilibrium modulus implies the presence of unreacted crosslinks. With the same number of crosslinks possible in MEMA, PEGMA500, and PEGMA950 samples, and taking the equilibrium modulus of the MEMA polymer in Figure 15 c, PEGMA500 and PEGMA950 can be inferred to be have a lower crosslinking desntiy due to the protective effects of the polyether chains. This led us to believe that 950 g/mol shielding groups are most effective at creating a steric barrier to reaction, preventing crosslinking between adjacent polymers and resulting in lower final G' values.

2.4.2 Controlling gel time through shield graft density

We next aimed to determine the minimum molar ratio of shielding groups necessary to prevent spontaneous crosslinking by varying the ratio of GMA:PEGMA (Figure 16 a). I expected that high contents of shielding monomer would entirely inhibit gelation over the measurement time, eventually prohibiting crosslinking even under force. To assess the minimum molar ratio necessary for preventing gelation without applied mechanical stimulus, the mole percent of PEGMA950 ($\sim$20 repeat units) and PEGMA500 ($\sim$10 repeat units) shielding monomers within each polymer chain was varied from 30 to 50 mol%. Variations in mole percent of MEMA copolymers was assessed as a negative control. The total concentration of epoxides in solution remained constant at 1 M.

In the presence of EDA or EDT with shielding group concentrations at mol 50% (PEGMA950), a negligible increase in G' was seen; at 40%, a very slow increase in G' with a final value on the order of 103 Pa was demonstrated; and at 30%, a rapid increase in G' with a final G' of 104 Pa (Figure 16 b-c). At higher shielding monomer percentages, gelation

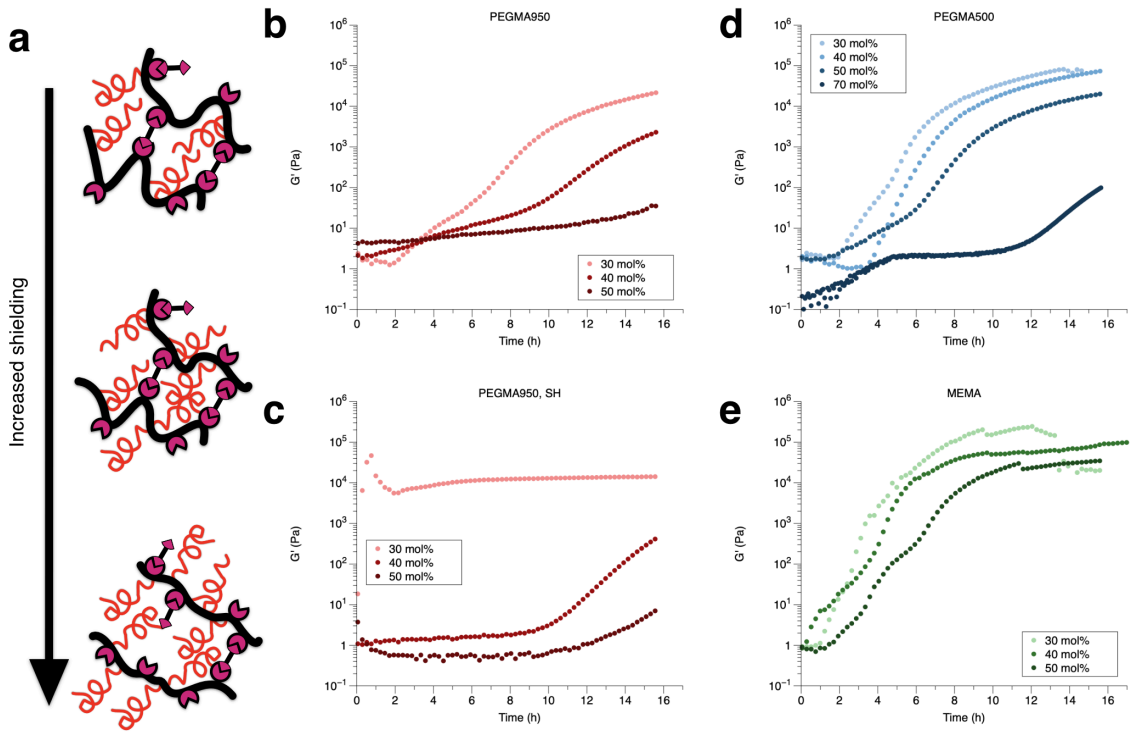

Figure 16: Ratio of pendent shields to reactive groups controls gelation time. (a) Illustrations of polymers at different GMA:PEGMA molar ratios, showing the change in backbone flexibility and exposed reactive sites. b-e. Storage modulus evolution over time for: (b-c) varying mole percentage of PEGMA950 with a diamine (b) or dithiol (c) crosslinker; (d) varying mole percentage of PEGMA500 and (e) MEMA with a diamine crosslinker. Arrows represent trends in shielding resulting from increased ratio of shielding monomer.

was entirely inhibited over the measurement time, even with the quick crosslinking EDT. In both the thiol and amine cases, the trend toward decreasing gel time with increasing PEGMA950 content is the same.

Next, polymers with PEGMA500 shielding units (∼10 repeat units) were varied from 30 to 70 mol% shielding monomer content while keeping the total epoxide group concentration in solution constant at 1 M (Figure 16 d) with EDA. When the shielding group concentration was 30 and 40 mol%, the material crosslinks rapidly and reaches final G' values on the order of 105 Pa. At 50% concentration of shielding groups, the material

reaches a lower final modulus on the order of 104 Pa. At the maximum tested 70% molar ratio of shielding group to reactive group, the shielded polymers still form a gel, but do not attain an equilibrium modulus during the experimental timeframe. The PEGMA500 shielding groups do not provide a sufficient steric barrier to reaction but do provide some hinderance to reaction evidenced by the decreased final modulus values compared to control samples.

Finally, polymers with one repeat unit pendent chains (MEMA) were varied between 30 and 50 mol% control monomer and reacted in the presence of EDA. Increasing the control monomer ratio from 30 to 50% slightly decreased to rate at which the material crosslinked and the final modulus, from 105 Pa at 30 and 40 mol% control monomer to just above 104 Pa at 50 mol% control monomer (Figure 16 e). As expected, the small size of the MEMA comonomer did not contribute significantly to suppressing the crosslinking kinetics of the crosslinking polymers.

At low ratios of shielding monomer to reactive monomer, there are statistically likely to be more stretches of reactive monomer with no steric effects to prevent them from crosslinking, as well as increased backbone flexibility. At high ratios of shielding monomer to reactive monomer, there are far fewer reactive monomer sequences as well as a straighter backbone due to pendent chains preventing backbone flexing. In summary, only the compositions achieved this with a high degree of shielding. Gelation was completely inhibited at a 1:1 ratio of reactive to shielding groups. This composition was selected as the most promising candidate for force-activated gelation.

2.4.3 Force-induced gelation of shielded polymers

We hypothesized sonication would be a facile method to mechanically induce gelation of shielded polymer. Sonication can achieve enormous strain rates approaching 10^8 s^{-1}.[193] This enormous strain rate arises from cavitations introduced during ultrasonic irradiation, nearly instantaneously creating and destroying microscopic bubbles that in turn create pressure gradients able to apply force through fast solvent flows to polymers of sufficient size. The force accumulated along the polymer backbone result in overstretched regions, which is what is generally accepted to drive conventional mechanochemical reactions.[58]

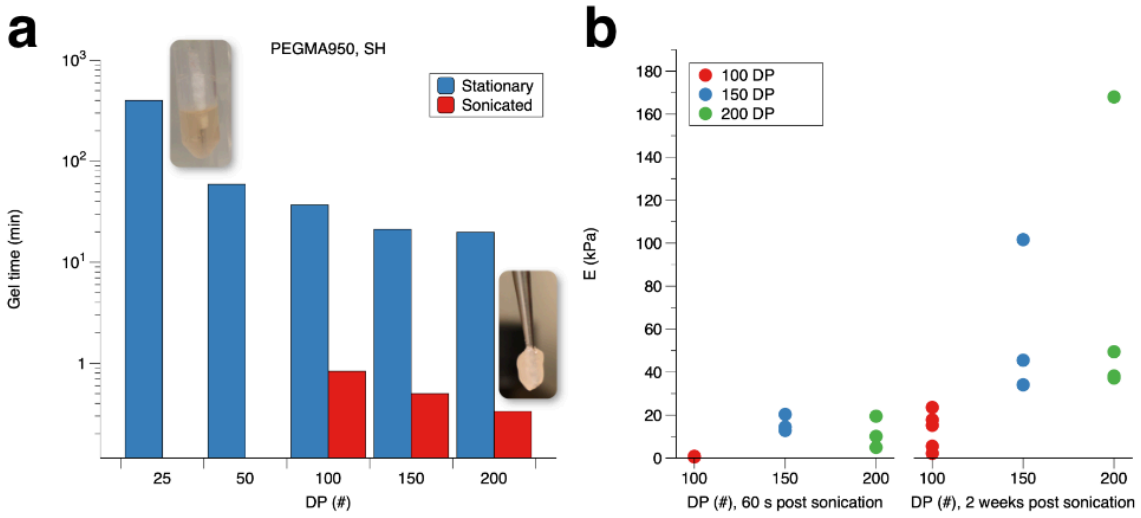

Figure 17: Sonication induces shielded polymer crosslinking. (a) Gel time of poly(GMA-*co*-PEGMA950) under static and sonicated conditions at varying DP with 1:1 molar ratio. Samples at 25 and 50 DP did not form a gel. Insets show a liquid polymer solution during a bubble test and a polymer cured through sonication, still attached to the sonicator probe. (b) Elastic modulus of poly(GMA-*co*-PEGMA950) cured with sonication as measured *via* NIC. Samples were crosslinked with a 1:1 molar ratio of thiol to epoxy and at a DP of 100, 150, or 200 and measured 60 s post sonication and after two weeks.

Crosslinking of shielded polymers induced *via* sonication was assessed at DP of 25 to 200 monomer units per chain (Figure 17 a). Each polymer sample was prepared at 1 M epoxide group concentration and reacted with EDT catalyzed by LiOH. Utilizing an ultrasonic probe immersed in polymer solutions, samples were subjected to ultrasonic waves for 5 s at a time, with 10 s of pause in between to prevent probe overheating. All conditions have delayed gelation at static conditions, allowing for the characterization of faster crosslinking with induced strain. At DP equal or greater to 100, samples gelled within 60 s of sonication time. At 100 DP, I observed a two order of magnitude decrease in gelation time when comparing unperturbed samples with sonicated samples. Samples of DP 150 and 200 gelled more rapidly, within 30 and 20 seconds of sonication time, respectively. Poly(GMA-*co*-PEGMA950) of lower DP (25 and 50) did not show any strain responsiveness, and the solution boiled before any gelation or viscosity change was observed due to the heat generated by the ultrasonic probe, reaching a temperature of 56 °C measured through an IR thermometer, at which point the solution began to boil while sonication was being applied. Counterintuitively, the heat generated by sonication is counterproductive to gelation of this system, possibly due to changes in the conformation of PEGMA shielding groups at higher temperatures (Figure 18). It is well understood that PEGMA copolymers have a lower critical solution temperature in water that is dependent on the polyether length and the ionic strength of the environment,[194] but it is not clear that this behavior extends into aprotic organic solvents. Gelation time under static conditions decreased as a function of DP like sonicated samples but showed a

leveling off after 150 DP unlike the sonicated samples. This decrease in gel time is likely due to the longer backbone lengths of the polymers beginning closer to the percolation threshold for gelation, resulting in fewer epoxide-thiol reactions needing to take place to form a volume spanning elastic path and a shorter time to the critical gel.[195,196]

It has been shown that polymers of sufficient molecular weight are sensitive to shear forces. The large size of polymers results in restriction of bond angle conformers

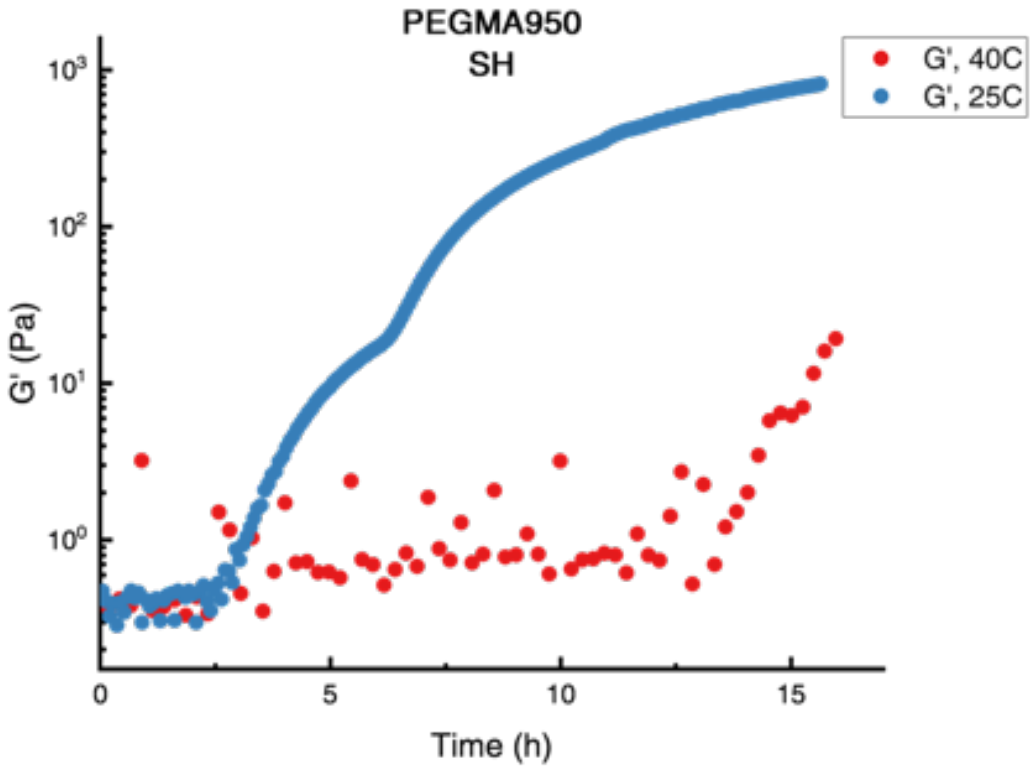

Figure 18: Evolution of G' for poly(GMA-*co*-PEGMA950) at a 1:1 molar ratio of comonomers and 25 DP during parallel plate rheology. Frequency sweeps were run from 1 to 100 rad/s over 17.5 hrs using a 20 mm top plate. Data plotted at 1 Hz and 1% strain. At 25 °C the sample increases in modulus rapidly after a 2.5 hr latency period. At 40 °C the same shows a small uptick in modulus after 12.5 hrs and never fully gels during the measurement period.

available due to chain and bond torsional strain, meaning polymers can accumulate force along their backbone as entropic potential energy.[197–200] High molecular weight polymers undergo chain scission in response to strong shear forces generating two distinct carbon-centered radicals.[201,202] These sufficiently strong shear forces result in overstreched segments of polymer adjacent to the chain center, generating a tensile force that drives mechanochemical reactions.[58] The chain scission rate increases with molecular weight.[203] This molecular weight dependence is more accurately described as a polymer length dependence.[204] It follows that shielded poly(GMA-*co*-PEGMA950) of sufficient DP is more easily influenced by shear forces in solution if the chain length is long enough, surpassing at least 100 units in length. The increased DP of the polymer also increases the viscosity of the sample. Prior literature has shown that highly viscous media decreases the effectiveness of ultrasonic micromixing,[205] making it less likely that the dependence of gel time on DP is a result of mixing phenomena. This study does not elucidate the mechanism for this system's strain sensitivity. It is not clear what aspect of crosslinking is sped up by the application of ultrasound, the addition of EDT to polymer or the addition of polymer+EDT to another polymer. Future studies using mono-thiols functionalized with UV tags would shed light on the precise molecular mechanism of strain-sensitive crosslinking.

Cavitation rheology was used to assess post-gelation elastic moduli of gels formed *via* sonication (Figure 17 b). NIC has previously been shown to be effective at extracting elastic modulus information from soft materials.[186] Sonicated samples were measured to

have an elastic modulus near 1 kPa for samples starting at 100 DP, and 20 kPa for samples between 150 and 200 DP as measured by NIC. After a week of resting in a sealed tube to allow for residual epoxides to be consumed by thiols, the modulus of each sample increased to an average of 20 kPa for samples starting at 100 DP and 60 kPa for samples starting at 150 to 200 DP. The final modulus for 150 and 200 DP polymers had a wide range, varying from 30 to 170 kPa. This variance is likely error from cavitation rheology, which tends to have higher variance for samples with higher elastic moduli.[206,207] The modulus derived from NIC shows polymers shielded with PEGMA950 cure into relatively weak materials.

2.4.4 Ultrahard materials from shielded copolymers

Conventional epoxy resins and composites can attain G' values approaching and surpassing 10^9 Pa.[208,209] Choosing this value as a benchmark for comparison, I formulated poly(GMA-*co*-PEGMA2000) copolymers at a 1:1 monomer ratio and 670 DP. The extremely long shielding group and long DP were chosen to provide a material that had both maximum latency and sensitivity to ultrasound. After sonicating these samples and leaving them to cure for 48 hr, the polymer crosslinked into an opaque white solid. Samples were prepared as 5x4 mm cylinders, and their moduli were assessed on a rheometer via compression with a 4 mm diameter plate. An elastic modulus value of 62 MPa was extracted from the resultant stress-strain curve (Figure 19 a), approaching that of conventional epoxy materials. Immersing gels of this copolymer into acetone and ethanol showed no visible change in the material, but in MeCN, DCM, and water the gels crumbled into insoluble

chunks (Figure 19 b), leading me to conclude that the material's strength comes from a combination of epoxide-thiol covalent crosslinks and PEG side chain crystallization. It is well known that graft copolymers with crystallizable side chains will form crystal domains.[210,211] Using DSC I was able to measure a melting temperature for a cured GMA:PEGMA2000 sample. confirming the material is partially crystallized (Figure 20). Using a steric shielding approach, I created an ultrahard material through an unexpected combination of crystallinity and covalent bonding.

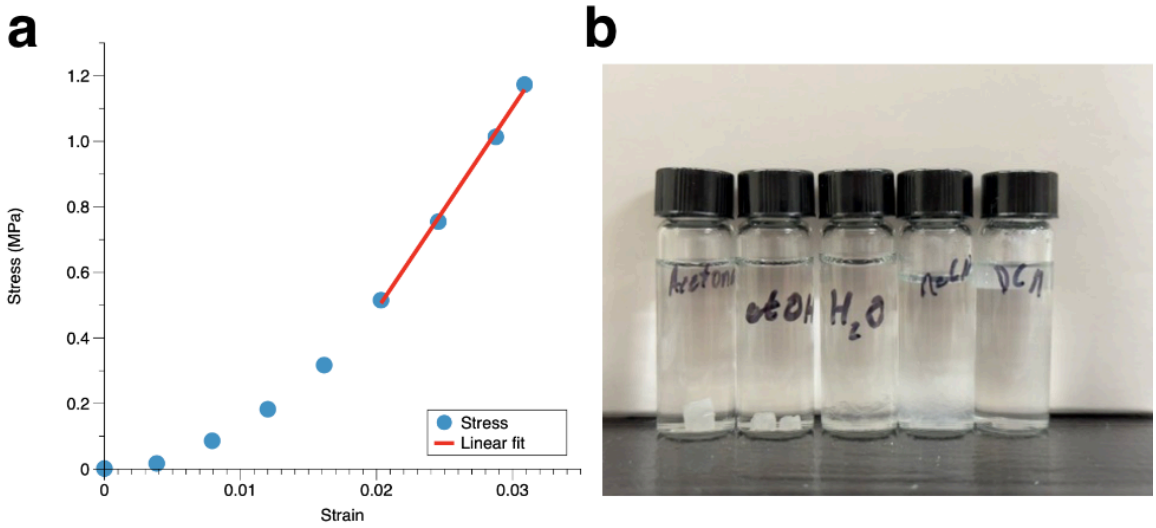

Figure 19: Shielded copolymers create ultrahard and durable materials. (a) Compression modulus of a fully cured poly(GMA-*co*-PEGMA2000) with 1:1 molar ratio of monomers. Elastic modulus is calculated by taking the slope during the linear portion of the stress-strain curve. Red line shows the linear best fit through four points. (b) Fully cured poly(GMA-*co*-PEGMA2000) gels immersed into acetone, ethanol, water, acetonitrile, and dichloromethane.

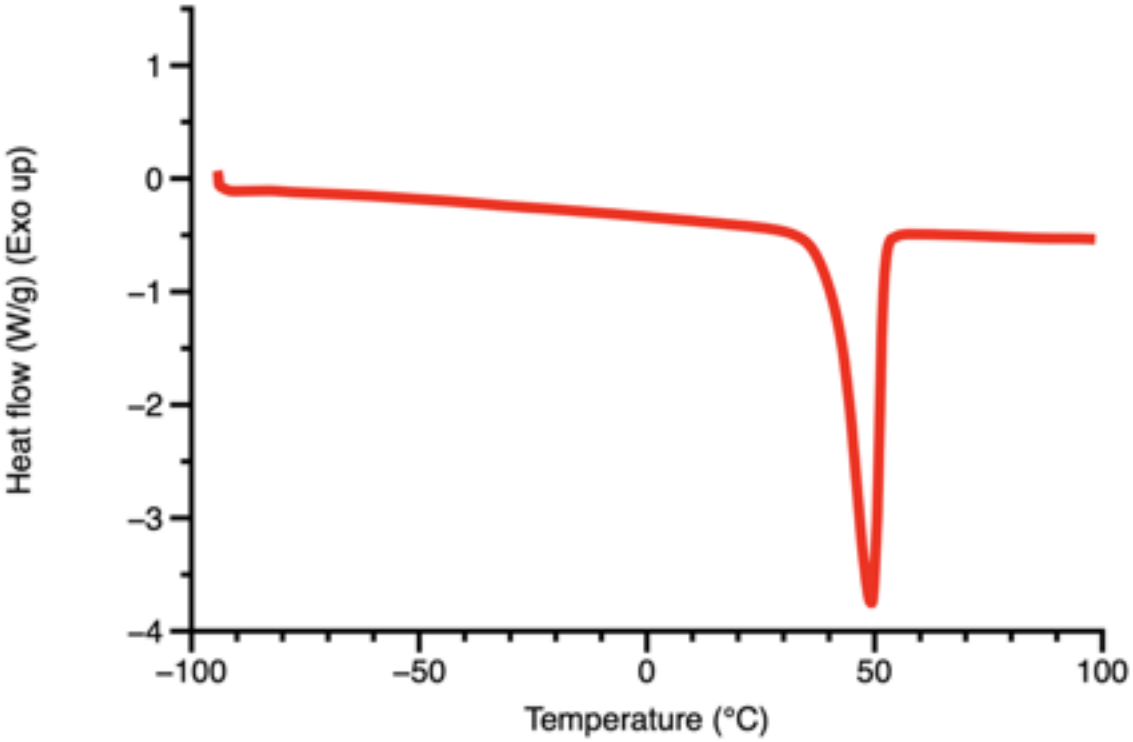

Figure 20: Differential scanning calorimetry thermogram of 1:1 GMA:PEGMA2000 crosslinked with EDT with all acetonitrile solvent evaporated off. ΔH_m of the sample was calculated to be 97.9 J/g with T_m at 49.29 °C.

2.5 Conclusion

We synthesized novel strain-sensitive shielded polymers containing both reactive epoxides and molecular shields. These shielding PEG chains provide a steric barrier to an otherwise powerful and efficient crosslinking reaction between amines or thiols and epoxides. This approach to creating strain sensitive materials provides a facile route to creating strain responsive coatings and adhesives, using well-known and commercially available monomers. Through this I demonstrated, for the first time, a liquid-to-solid transition accelerated under force using shielded reactive polymers. I showed that force stimulated gelation could be achieved with ultrasound. I further showed that steric shielding can

create ultrahard materials. Suppressed gelation without force, combined with ultrasound sensitivity, make this polymer an ideal candidate for an adhesive in a heat or light sensitive application.

The work in this chapter represents a collaboration with Jichao Song and Professor Jessica Schiffman from the Chemical Engineering Department at University of Massachusetts Amherst. DSC measurements in Figure 20 were conducted and data analyzed by Jichao Song. NIC data was collected and analyzed by Hsu Shwe Yee Naing.

Chapter 3

Highly crosslinked, ultra-hard networks from polymer combs

Publication in preparation

3.1 Abstract

Comb polymers are branched macromolecules used as compatibilizers, surface modifiers, and, when polymerized, as strong networks. Comb polymers are typically synthesized to contain different backbone and sidechain chemistries, which can result in multifunctional reactivity and strong phase separation from different polymer domains. Here, we explored designing comb polymers that could result in high modulus, tough networks by synthesizing polymers with glycidyl methacrylate sidechains capable of participating in dense crosslinking reactions. We synthesized several comb polymers containing homopolymer, block, or random copolymer sidechains, and compared their mechanical properties and network structures to their linear counterparts. Comb polymers with random copolymer side chains had superior toughness, even compared to their linear counterparts. I hypothesize that statistical distribution of monomers along the grafts break up crosslinking sites, disfavoring intramolecular crosslinks and favor intermolecular crosslinks. I expect these polymers to be useful for multi-functional coatings and as adhesives with high modulus and toughness.

3.2 Introduction

Comb polymers are macromolecules with polymers grafted onto a main polymer backbone. They are increasingly popular for their low viscosity,[212] ease of side-chain functionalization,

quick gelation times,[29] complex phase behavior,[213] and large parameter design space.[214] Comb polymers have applications ranging from next-generation compatibilizers between immiscible polymer phases,[104] tough networks and adhesives,[105,106] anionic exchange resins,[215] viscosity modifiers,[103] tough resins with crystalline domains.[100,101] The low viscosity of these polymers and polymer solutions offers the additional benefit of requiring less energy to process.[102]

Previously, our group has created mechanosensitive networks from comb copolymers with reactive monomers along the main backbone.[101] Using poly(ethylene glycol) (PEG) grafts as molecular shields blocking the reactive sites on the main backbone, I produced crosslinked materials upon application of ultrasound. In that system, the material mass was dominated by inert PEG side chains. This resulted in low overall density of crosslinks, limiting the maximum modulus of the polymers. To address this limitation, here I have developed a suite of reactive comb polymers, where each sidechain is itself reactive and crosslinkable, significantly increasing the potential for new crosslinks and high modulus networks. I hypothesized that GMA containing grafts would allow for an increase in crosslinking density while still providing ultrasound activated crosslinking. This work was focused on the mechanical properties of these graft polymers.

Most comb polymers used to create networks have crosslinking sites along the main polymer backbone, while the grafts do not contribute to the modulus. In contrast, I synthesized a well-defined methacrylic polyinitiator (pBIEM), where each monomer on the chain contains a pendent alkyl bromine capable of initiating atom transfer radical

polymerization (ATRP). Homo- and co-polymers of GMA and BMA were then grown off the backbone using a "grafting from" approach to prepare densely grafted comb polymers. I then crosslinked the polymer combs to form networks with elastic moduli of 1 GPa and with toughnesses of 500kPa. I anticipate that this work will provide strategies for preparing high modulus, tough comb polymer coatings and adhesives.

3.3 Materials and methods

3.3.1 Chemical sourcing

Materials were purchased from Sigma-Aldrich unless otherwise mentioned. 2-Hydroxyethyl methacrylate (HEMA, 98%), α-bromoisobutyryl bromide (99%), pyridine (anhydrous, 99%), dichloromethane (DCM, anhydrous, 99%), dioxane (99%), $CuBr_2$ (99%), 1,5,7-triazabicyclo[4.4.0]dec-5-ene (TBD, 98%), ethyl α-bromophenylacetate (EBPA, 97%), N,N,N',N",N"-pentamethyldiethylenetriamine (PMDETA, 99%), 1,1,3,3-tetramethylguanidine (TMG, 99%), and azobisisobutyronitrile (AIBN, 99%), were used as received. Glycidyl methacrylate (GMA, 99%), butyl methacrylate (BMA, 99%) were passed through a column of basic alumina to remove inhibitors. CuBr (99.9%) was purified by stirring in glacial acetic acid. Tris(2-pyridylmethyl)amine (TPMA, 98%), tris 2-(dimethylamino)ethyl amine (Me6TREN, 98%), cyclopentylmethyl ether (CPME, 99%), and 2-cyano-2-propyl dodecyl trithiocarbonate (CPDT, 97%) was purchased from TCI (Tokyo, Japan) and used as received. Methanol (99%), toluene (99%), dimethylformamide (DMF, 99%), isopropanol (99%), calcium chloride (99%) diethyl ether (anhydrous, 99%), tetrahydrofuran (THF, 99%),

HCl (concentrated), reduced iron powder, copper turnings, basic alumina, and neutral alumina were purchased from Thermo Fisher (Waltham, MA) and used as received.

3.3.2 2-(2-Bromoisobutyryloxy)ethyl methacrylate (BIEM) synthesis

BIEM was synthesized according to a previously published protocol.[216] Briefly, to a 250 mL three-necked round bottom flask (RBF), 50 mL of anhydrous DCM, 10 mL of HEMA (0.1 mol), and 10 mL of anhydrous pyridine (0.12 mol), and a magnetic stir bar are added. The RBF is then lowered into an ice bath and stirred for ten minutes. Meanwhile, a drying tube filled with calcium chloride, an addition funnel attached to a bubbler filled with silicone oil, and a glass adaptor attached to a nitrogen line are attached to each neck of the flask. 7 mL of α-bromoisobutyryl bromide (0.1 mol) is dissolved into 20 mL of anhydrous DCM and added to the addition funnel. The α-bromoisobutyryl bromide solution is added dropwise to the RBF over 15 minutes, after which the reaction is allowed to stir in the ice bath for a further 45 minutes, followed by removal from the ice bath. After stirring at room temperature for two hours, the crude product is filtered through cotton to remove pyridine salts and then concentrated under vacuum. The product is purified by flash chromatography over silica gel with chloroform, yielding a clear colorless oil after evaporation of the chloroform.

3.3.3 Copper activation and stirbar cleaning

Copper turnings were activated by tying around a magnetic stir bar followed by immersion in conc. HCl for 15 minutes to remove copper oxides followed by rinsing with methanol.

Stir bars were cleaned of residual metals by submerging in concentrated HCl overnight, followed by washing with DI water and ethanol.

3.3.4 CuBr purification

To a 500 mL beaker was added 250 mL of glacial acetic acid followed by 25 g of CuBr and a magnetic stirbar. The beaker was covered with parafilm and allowed to stir vigorously for two days. After two days, the glacial acetic acid had turned blue as $CuBr_2$ is dissolved by the acetic acid. The insoluble CuBr was collected by vacuum filtration, and the cake washed three times with −20 °C methanol, then three times with −20 °C diethyl ether. The now damp white powder was collected into a 50 mL RBF and dried under vacuum overnight.

3.3.5 PolyGMA synthesis

We synthesized polyGMA according to a previously published protocol.[217] Briefly, to a 20 mL scintillation vial with a magnetic stirbar, 2.84 g GMA (0.02 mol), 10 µL PMDETA ($4.8e^{-5}$ mol), 0.001 g CuBr ($8e^{-6}$ mol), 2.84 mL of DMSO and 70 µL of EBPA ($4e^{-4}$ mol) is added. The reaction was sealed with a rubber septum stirred at 60 °C overnight, after which it was diluted with THF, passed through a short plug of alumina, and precipitated into cold methanol.

3.3.6 pGMA-*b*-BMA and pGMA-*co*-BMA synthesis

We synthesized linear copolymers by adapting a previously published protocol.[218] Briefly, to a 20 mL scintillation vial 29 µL TMG ($2.3e^{-4}$ mol), 0.005 g $CuBr_2$ ($2.3e^{-5}$ mol), and 1.65 g of BMA (0.011 mol) is added. For the block polymer, 1.65 g of pGMA (0.011 mol) and 0.625 mL of DMSO is added. For the random copolymer, 1.65 g of GMA (0.011 mol), and 1.25

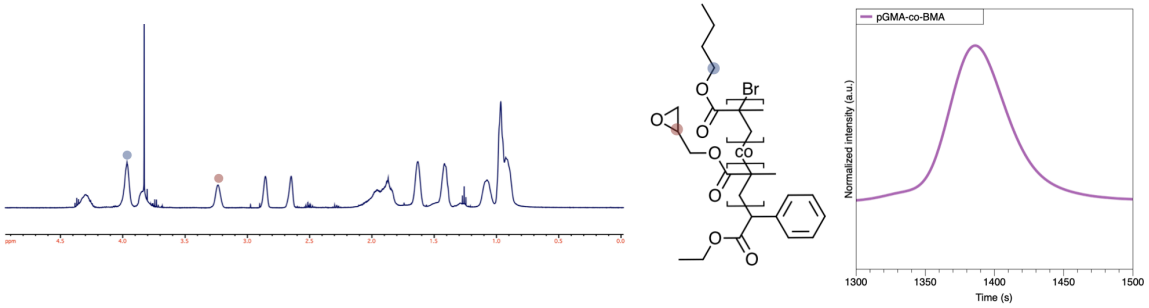

Figure 21: ^{1}H NMR and GPC of pGMA-*co*-BMA. Spectra recorded at 500 MHz in $CDCl_3$. THF used as eluent.

mL of DMSO is added. The vial is capped with a rubber septum and nitrogen is bubbled through the solution for 15 minutes, after which a magnetic stirbar with an activated copper turning tied around it is added. The reaction is stirred overnight at 30 °C, after which it was diluted in THF, passed through a short plug of alumina, and precipitated into cold methanol. Spectra for all linear polymers are shown in Figure 21 and Figure 22.

3.3.7 PolyBIEM (pBIEM) synthesis

We synthesized polyBIEM by RAFT polymerization. To a 20 mL scintillation vial 5.56 g of BIEM (0.02 mol), 0.014 g CPDT (0.04 mmol), 0.0013 g AIBN (0.008 mmol), 5.56 mL dioxane, and a new magnetic stir bar is added. The vial is capped with a new rubber septum and degassed for 15 minutes by sparging with nitrogen using new needles. After degassing,

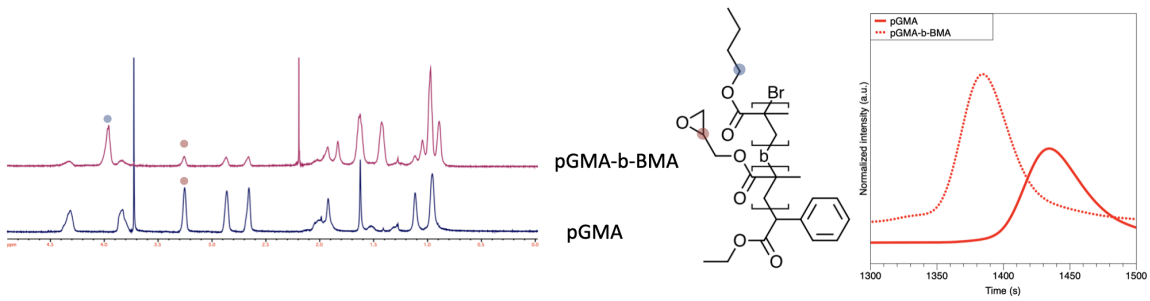

Figure 22: ^{1}H NMR and GPC of pGMA and pGMA-*b*-BMA. Spectra recorded at 500 MHz in $CDCl_3$. THF used as eluent.

the vial is added to an aluminum reaction block thermostatted at 60 °C to react overnight. The next day, the reaction was diluted with dioxane, precipitated into cold diethyl ether, and dried under vacuum at 0.001 mbar overnight.

3.3.8 Comb polymer synthesis

The synthesis procedure for comb polymers follow similar reaction setup. Reagents and detailed conditions are described after the general procedure is outlined and in Table 2. Synthesis was undertaken according to an adapted protocol for synthesizing polyGMA[219] *via* SARA ATRP. For each reaction, reagents were prepared in a 20 mL scintillation vial. The vial was sealed with a rubber septum and after reagent dissolution, the vial was degassed by sparging with nitrogen for 15 min, after which either a stir bar with activated copper turnings wrapped around it or 0.011 g iron powder was added to the vial (Table 2). The vial was added to an aluminum reaction block at varying temperatures for one hour, until the reaction had increased in viscosity. The crude polymer was diluted in THF and passed through a short plug of neutral alumina to remove dissolved copper salts, precipitated in −20 °C methanol, and dried under vacuum at 0.001 mbar for one hour. The polymer was used immediately after drying.

PolyBIEM-*g*-(GMA-*co*-BMA): 2.8 g GMA (0.02 mol), 0.064 g pBIEM ($4e^{-4}$ mol), 0.061 g TPMA ($2e^{-4}$ mol), 0.0045 g $CuBr_2$ ($2e^{-5}$ mol), and 2.8 mL of 70/30 v/v toluene/DMF.

polyBIEM-*g*-(GMA-*co*-BMA): 2.8 g BMA (0.02 mol), 2.8 g GMA (0.02 mol), 0.064 g pBIEM ($4e^{-4}$ mol), 0.061 g TPMA ($2e^{-4}$ mol), 0.0045 g $CuBr_2$ ($2e^{-5}$ mol), and 5.6 mL of 70/30 v/v toluene/DMF.

Comb Polymer	Reducing agent	Temperature (°C)	Methanol acidified?
PolyBIEM-*g*-GMA	Iron	30	No
polyBIEM-*g*-(GMA-*b*-BMA)	Copper	30	Yes
PolyBIEM-*g*-(BMA-*b*-GMA)	Copper	50	Yes
PolyBIEM-*g*-BMA	Copper	50	Yes
PolyBIEM-*g*-(GMA-*co*-BMA)	Iron	30	Yes

Table 2: Synthetic setup for comb polymerizations.

Name	GMA (%)	Mn (g/mol)	Đ
pGMA	100	5,907	1.12
pGMA-*b*-BMA	45	11,436	1.12
pGMA-*co*-BMA	50	11,942	1.09
pBIEM	—	57,641	1.3
pBIEM-*g*-GMA	100	275,294	1.17
pBIEM-*g*-BMA	—	415,543	1.36
pBIEM-*g*-(GMA-*b*-BMA)	55	491,777	1.24
pBIEM-*g*-(BMA-*b*-GMA)	45	551,826	1.31
pBIEM-*g*-(GMA-*co*-BMA)	51	423,522	1.3

Table 3: Tabulated properties of polymers used in this study.

PolyBIEM-*g*-(GMA-*b*-BMA): 2 mL of BMA (0.014 mol), 1 g of polyBIEM-*g*-GMA (0.007 mol), 0.0045 g CuBr2 ($2e^{-5}$ mol), 64 µL Me6TREN ($2e^{-4}$ mol), and 4 mL of 70/30 v/v toluene/DMF.

PolyBIEM-*g*-BMA: 2.8 mL of BMA (0.02 mol), 0.064 g of polyBIEM (0.007 mol), 0.0045 g $CuBr_2$ ($2e^{-5}$ mol), 64 µL Me6TREN ($2e^{-4}$ mol), and 2.8 mL of 70/30 v/v toluene/DMF.

PolyBIEM-*g*-(BMA-*b*-GMA): 2 g BMA (0.014 mol), 1 g pBIEM-*g*-BMA (0.007 mol), 0.061 g TPMA ($2e^{-4}$ mol), 0.0045 g CuBr ($2e^{-5}$ mol), and 2.8 mL of 70/30 v/v toluene/DMF.

3.3.9 Polymer characterization

Polymer molecular weight was determined by GPC. GPC was conducted on an Agilent 1260 with a PL gel 5 μm guard column and three 5 μm analytical mixed C columns (Agilent). THF was used as the eluent at a flow rate of 1 mL/min. The column was standardized with pMMA calibration standards and toluene was used as a flow marker. ^{1}H NMR spectra were measured on a Bruker Avance 500 spectrometer with deuterated chloroform as the solvent. Properties are compiled in Table 3.

3.3.10 Sample preparation

In general, to prepare a crosslinked thermoset, polymer was dissolved in acetone, and succinic acid was added to create a solution with a 1:1 molar ratio of oxirane:COOH. 0.05 eq of TBD was added as a catalyst and the solution was stirred at 100 °C until most acetone had evaporated and a partially crosslinked solid remained. The polymer was then pressed in a mold at 150 °C for 10 minutes, and the flexible solid was cut to shape and left in an oven at 120 °C overnight to complete the curing process.

3.3.11 DMA

To determine the modulus of the crosslinked samples, I performed DMA measurements with a DMA 850 (TA Instruments) equipped with a tension clamp. Frequency sweeps were performed at 0.01 % strain with a preload of 0.01 N at room temperature.

3.3.12 Swelling ratio

To determine their equilibrium swelling ratio, fragments of each polymer were weighed and added into excess xylenes, chosen to be a good solvent for these polymers.[220] The

samples were then placed in an aluminum reaction block thermostatted to 100 °C for 48 hours to reach their equilibrium swelling ratio. After the 48 hours, the samples were carefully removed or filtered from the xylene and weighed, with the difference being used to calculate the swelling ratio.

3.3.13 Toughness measurements

To determine the toughness of the crosslinked samples, I conducted uniaxial extension measurements with a Texture Analyzer (Stable Microsystems) equipped with a 50 N load cell. The crosshead displacement rate was controlled at a speed of 0.1 mm/s. The samples were stretched until the samples broke at the center of the sample in between the grips.

3.4 Results and discussion

3.4.1 Controlled synthesis of reactive combs

We synthesized a suite of different comb polymer architectures with the goal of determining how graft density and structure affected eventual network modulus and toughness, as well as a set of analogous linear polymers. I kept monomer ratio and degree of polymerization consistent between linear and comb grafts to best compare resultant material properties. I synthesized four comb polymers: pBIEM-*g*-GMA (homopolymer GMA side chains), pBIEM-*g*-(GMA-*co*-BMA) (random GMA copolymer sidechains, inset of Figure 23 b), pBIEM-*g*-(GMA-*b*-BMA) ("hidden" GMA block copolymer sidechains, inset of Figure 23 c), and pBIEM-*g*-(BMA-*b*-GMA) ("exposed" GMA block copolymer sidechains, inset of Figure 23 d). I then synthesized three linear polymers analogous to the sidechains of the comb polymers: pGMA (compared to comb polymers with homopolymer side chains),

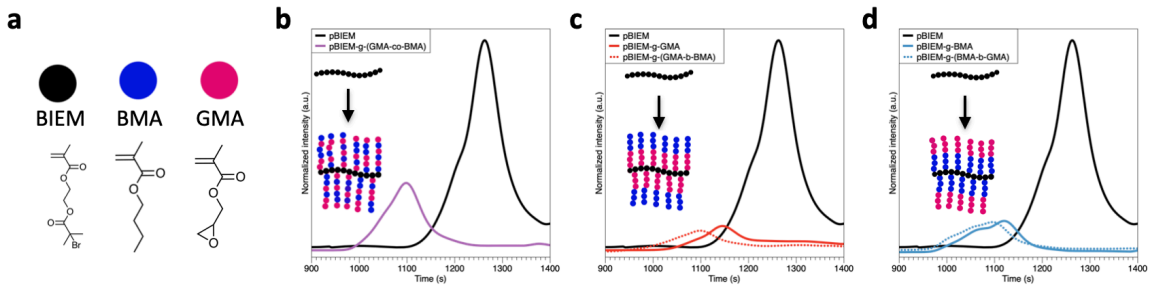

Figure 23: SARA-ATRP produces narrowly dispersed, well defined comb polymers. (a) Illustrations of the monomers used in this paper. (b) GPC chromatogram showing the shifting of precursor polymer to earlier elution times, demonstrating the successful chain extension with GMA-*co*-BMA. (c) GPC chromatogram showing successful chain extensions of pBIEM with first GMA and then BMA to create block copolymer side chains. (d) GPC chromatogram showing successful chain extensions of pBIEM with first BMA and then GMA to create block copolymer side chains. For (b-d), insets depict the idealized structure of the initial and final polymer.

pGMA-*co*-BMA (compared to comb polymer with random side chains), and pGMA-*b*-BMA (compared to comb polymers with both "hidden" and "exposed" sidechains).

First, I synthesized linear polymers *via* ATRP, and determined they had well-defined molecular weights and narrow dispersities *via* GPC (pGMA: Mn = 5,907 g/mol, Đ = 1.12; pGMA-*co*-BMA: M_n = 11,942 g/mol, Đ = 1.09; pGMA-*b*-BMA: M_n = 11,436 g/mol, Đ = 1.12). I then created copolymers of GMA and BMA with matched lengths, and measured that all polymers had comparable amounts of GMA.

In order to produce graft polymers, I used a "grafting from" approach to grow GMA and BMA from a pBIEM backbone (Figure 23 a). To accomplish this, I polymerized an inimer (a dual functional small molecule acting as initiator and monomer) of BIEM *via* RAFT to create a linear polyinitiator ~500 monomers long. I chose CPDT as the chain transfer agent as trithiocarbonates have been shown to not participate in the necessary

ATRP to create the ensuing linear-block-comb architectures.[221] Successful synthesis of pBIEM showed a modest final Đ = 1.3, higher than would be expected for a RAFT polymerization (Figure 23 b). This was likely due to small amounts of contaminating crosslinking, as indicated by a small shoulder in the GPC chromatograms at lower elution times. The Đ was similar to other reported polymerizations of BIEM.[222]

Using two distinct reversible deactivation radical polymerizations, well-defined and narrowly disperse comb polymers were synthesized. First, I created a comb architecture with random side chains (Figure 23 b). pBIEM-*g*-(GMA-*co*-BMA) was synthesized by initiating polymerization from pBIEM using GMA and BMA as comonomers in a 1:1 molar feeding ratio (pBIEM-*g*-(GMA-*co*-BMA, M_n = 423,522 g/mol, Đ = 1.3). The final monomer ratio was confirmed *via* ^{1}H NMR at 51 mol% GMA (Figure 24). I then created a second comb architecture with a "hidden" block architecture. In this structure, the reactive GMA monomers are closest to the backbone (Figure 23 c). pBIEM-*g*-(GMA-*b*-BMA) was synthesized in a sequential polymerization process. First, polymerization of GMA from pBIEM yielded pBIEM-*g*-GMA (Mn = 275,294 g/mol, Đ = 1.17). Next, BMA was polymerized from the ends of the grafted GMA of pBIEM-*g*-GMA to create pBIEM-*g*-(GMA-*b*-BMA) (Mn = 491,777 g/mol, Đ = 1.24). Final monomer ratio was confirmed *via* ^{1}H NMR at 51 mol% GMA (Figure 25).Finally, I synthesized a comb with an "exposed" block architecture, where the reactive GMA monomers were furthest away from the comb backbone *via* sequential polymerizations of BMA to create pBIEM-*g*-BMA (Mn 415,543 g/mol, Đ 1.36), and then GMA to create pBIEM-*g*-(BMA-*b*-GMA) (Mn 551,826 g/mol, Đ

1.31) (Figure 23 d). Feed ratio was confirmed *via* ^{1}H NMR at 51 mol% GMA (Figure 26). All these "grafting from" reactions showed no measurable increase in the dispersity of the polymers relative to the pBIEM backbone.

3.4.2 Crosslinking and storage modulus of reactive comb polymers

After successfully preparing the reactive comb polymers, determined the effect of polymer architecture on the bulk properties of their crosslinked resins. I began by crosslinking the

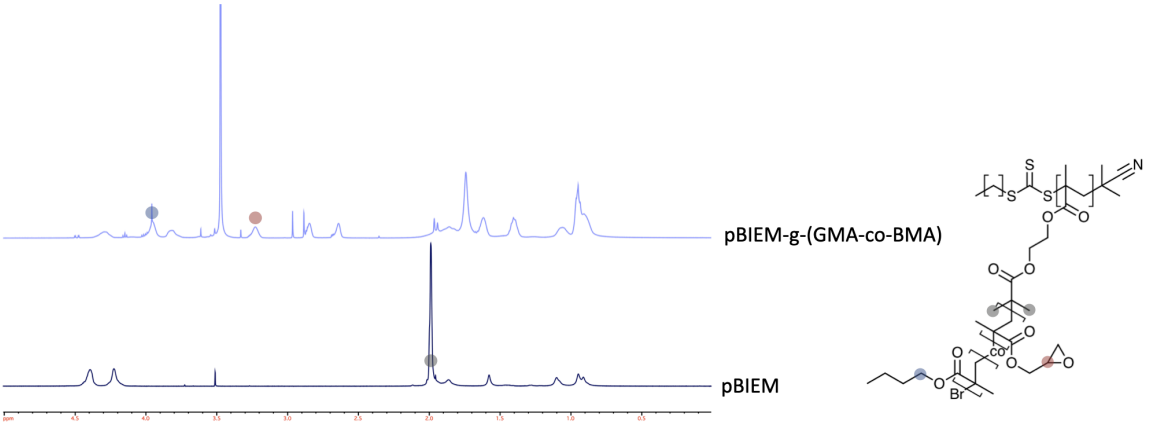

Figure 24: ^{1}H NMR of pBIEM-*g*-(GMA-*co*-BMA) after successive polymerizations. Spectra recorded at 500 MHz in $CDCl_3$.

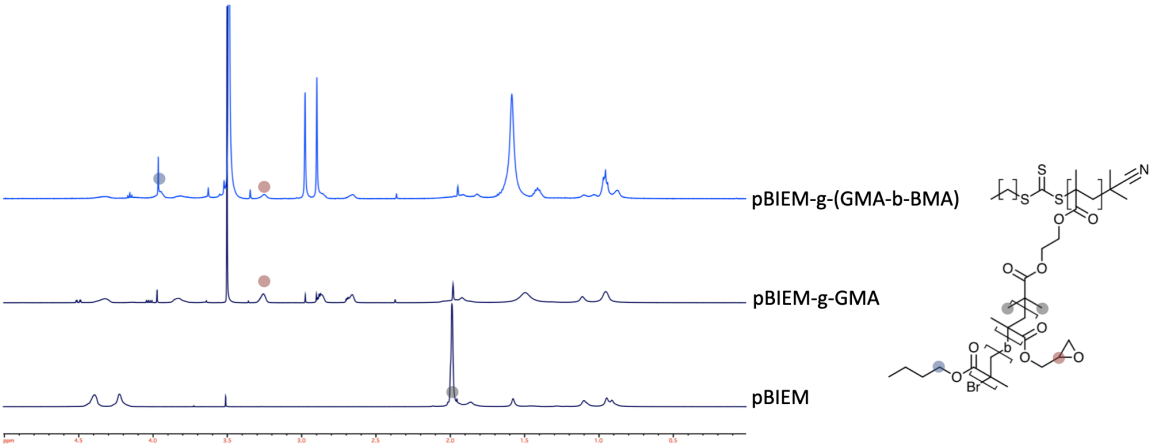

Figure 25: ^{1}H NMR of pBIEM-*g*-(GMA-*b*-BMA) after successive polymerizations. Spectra recorded at 500 MHz in $CDCl_3$.

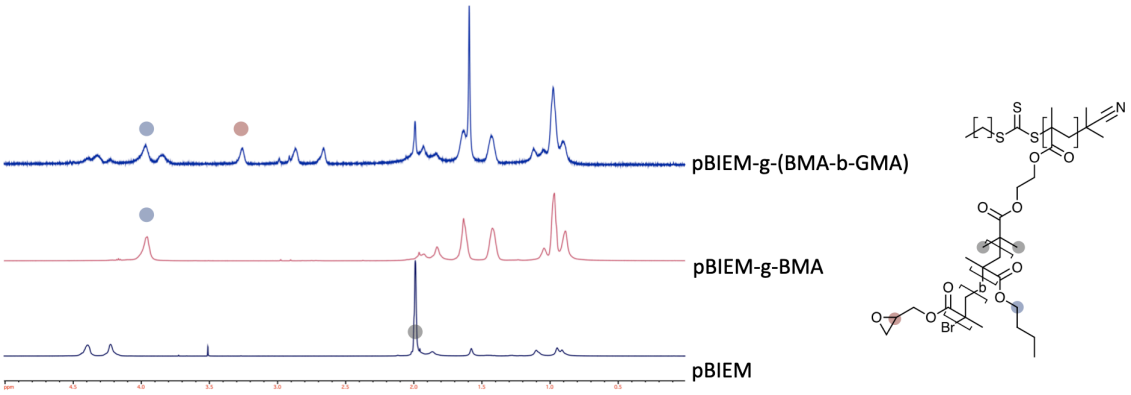

Figure 26: ^{1}H NMR of pBIEM-*g*-(BMA-*b*-GMA) after successive polymerizations. Spectra recorded at 500 MHz in $CDCl_3$.

thermosets with succinic acid, chosen due to its small molecular weight and functionality (Figure 27 a). Small molecular weight crosslinkers enable high crosslink density, somewhat offsetting the diluting effect of BMA comonomer, and the carboxylic acid functionality facilitates step-growth polymerization with the epoxy groups of GMA. A 1:1 ratio of acid:epoxy (succinic acid:GMA) was utilized, again to achieve a high crosslink density. Additionally, a catalyst was used increase the rate of crosslinking (TBD at 5 mol% relative to epoxy). All linear and comb polymers were crosslinked identically.

We first crosslinked and characterized the modulus of the block polymers (Figure 27 b). Successful crosslinking was identified by visual inspection. Polymers were measured under tensile conditions at 1 Hz (6.28 rad/s) frequency, resulting in storage moduli of pGMA-*b*-BMA = 584.0 MPa, pBIEM-*g*-(BMA-*b*-GMA) = 410.0 MPa, and = 410.0 MPa. The linear copolymer had the highest modulus of the three, and shows some frequency dependency, overlapping with the comb block polymers at lower frequencies. Strong phase separation of the BMA blocks resulting in a dynamic glass transition is likely the

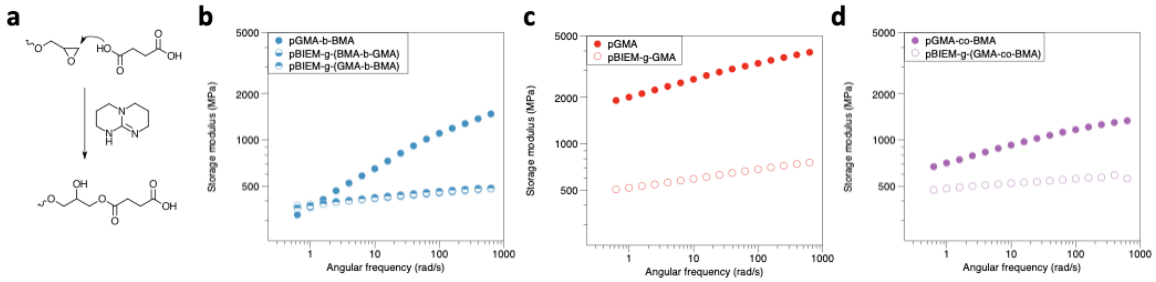

Figure 27: Comb polymers crosslink to form high modulus materials. (a) Schematic of the crosslinking reaction between glycidyl esters and succinic acid, catalyzed by TBD. (b) Storage modulus of block polymers crosslinked with succinic acid, as measured by DMA. (c) Storage modulus of homopolymers crosslinked with succinic acid, as measured by DMA. (d) Storage modulus of random copolymers crosslinked with succinic acid, as measured by DMA.

cause of the frequency dependent behavior of pGMA-*b*-BMA. Both comb block polymers had nearly identical moduli.

We then prepared crosslinked homopolymer and homopolymer graft thermosets in an identical manner to the block polymers. At 1 Hz, the measured storage moduli of pGMA = 2,484 MPa and pBIEM-*g*-GMA = 577.1 MPa (Figure 27 c). In this case, the linear homopolymer had a far higher modulus than the comb homopolymer, showing a roughly five-fold increase.

Finally, I prepared crosslinked random copolymer thermosets in the same manner. At 1 Hz, the measured storage moduli of pGMA-*co*-BMA = 881.0 MPa and = 515.0 MPa (Figure 27 d). Here, the linear polymer has a modulus almost twice as high as the comb polymer.

The highest modulus value belonged to pGMA and pBIEM-*g*-GMA for linear and comb polymers, respectively, is expected, as the overall crosslinking density of these

samples should be the highest. As crosslinking was mediated *via* epoxy groups, the GMA homopolymers have the greatest degree of epoxy crosslinks without other comonomers to dilute it. More surprising is that all comb polymers consistently show a lower modulus compared to their linear counterparts. I hypothesized that this was due to increased intramolecular crosslinking occurring between comb hairs of block copolymer and homopolymer samples. In densely grafted comb polymers, GMA monomers would be forced very near to GMA on combs within the same polymer, favoring intramolecular crosslinks. These intramolecular crosslinks would create loop defects that do not contribute to the modulus of the final thermoset.

3.4.3 Network architecture effects on material properties

To interrogate the network structure of each crosslinked polymer, we conducted swelling studies. Fragments of all samples were submersed in mixed xylenes at 100 °C for 48 hours to reach equilibrium swelling, and swelling ratio was determined by the difference in mass before and after swelling. Resultant values for block copolymers were pGMA-*b*-BMA = 1.85, pBIEM-*g*-(BMA-*b*-GMA) = 1.91, and pBIEM-*g*-(GMA-*b*-BMA) 1.2 times. For homopolymers, swelling ratios for pGMA = 1.34 times and pBIEM-*g*-GMA = 0.85. Random copolymers pGMA-*co*-BMA = 1.95 and pBIEM-*g*-(GMA-*co*-BMA) = 1.68 (Figure 28 a). All comb polymers, with the exception of pBIEM-*g*-(GMA-*co*-BMA) crumbled into small insoluble particles, indicating either that the solid was held together primarily by intermolecular interactions, or that the network topology was uneven, resulting in rapid material failure.[223] Linear polymers retained their original shape (Figure 29). Additionally,

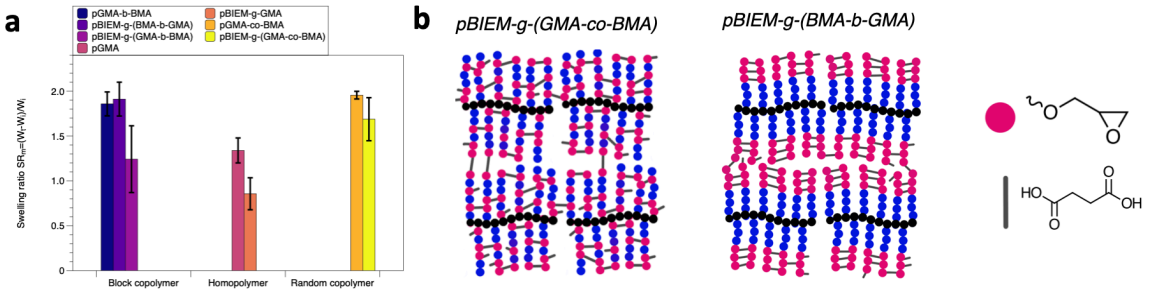

Figure 28: Swelling of thermosetting polymers. (a) Swelling ratios of crosslinked polymers in mixed xylenes. n = 3 (b) Cartoon depiction of comb copolymers with random (left) and block (right) sidechains.

all comb polymers, with the exception of pBIEM-*g*-(BMA-*b*-GMA), showed lower swelling ratios than their linear counterparts.

According to Flory,[19] swelling ratio is directly related to degree of polymerization between crosslinks, which in turn is directly related to modulus. According to the swelling data then, each comb polymer should have a higher modulus. To explain this, after comparing the storage modulus data to the swelling data, I hypothesized that

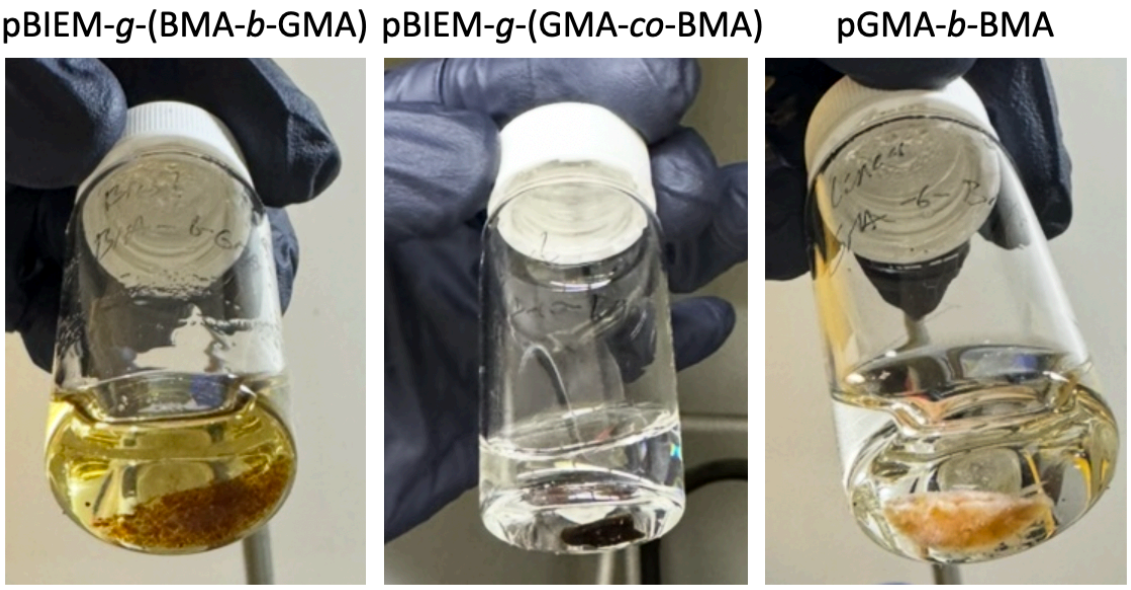

Figure 29: pBIEM-*g*-(BMA-*b*-GMA), pBIEM-*g*-(GMA-*co*-BMA), and pGMA-*b*-BMA swelling in xylenes.

comb polymers contain a high degree of intramolecular crosslinking compared to linear polymers. The intramolecular crosslinks would form microgels and small loop defects, which would not contribute to the formation of elastically active network chains that are able to dissipate stress and increase the storage modulus (Figure 28 b). Additionally, these intramolecular crosslinks contribute to a more inhomogeneous network structure, which reduces the swelling ratio of crosslinked networks, as the network is less easily able to expand to accommodate additional solvent.[224]

If these materials do contain a high degree of intramolecular crosslinks, they may contain fewer intermolecular covalent crosslinks or entanglements, resulting in reduced bulk mechanical properties. Intramolecular crosslinks would form highly crosslinked microgels, but adjacent polymers are loosely connected. Then, in addition to dissociating in solvent, I would expect these materials to have much lower toughness compared to samples that do not contain as many of these defects. To examine this, I conducted tensile tests to determine the toughness of the crosslinked thermosets.

Each sample was cut into rectangles of approximately 6.5 mm in width and 1.5 mm in thickness. The samples were pulled until they broke in half and the toughness calculated from the measured force, elongation at break, and sample cross-sectional area. Block polymers, pGMA-*b*-BMA had a toughness of 180.0 kPa, pBIEM-*g*-(BMA-*b*-GMA) had a toughness of 95.60 kPa, and pBIEM-*g*-(GMA-*b*-BMA) had a toughness of 93.30 kPa. In contrast, random copolymers, pGMA-*co*-BMA had a toughness of 578.0 kPa, and pBIEM-

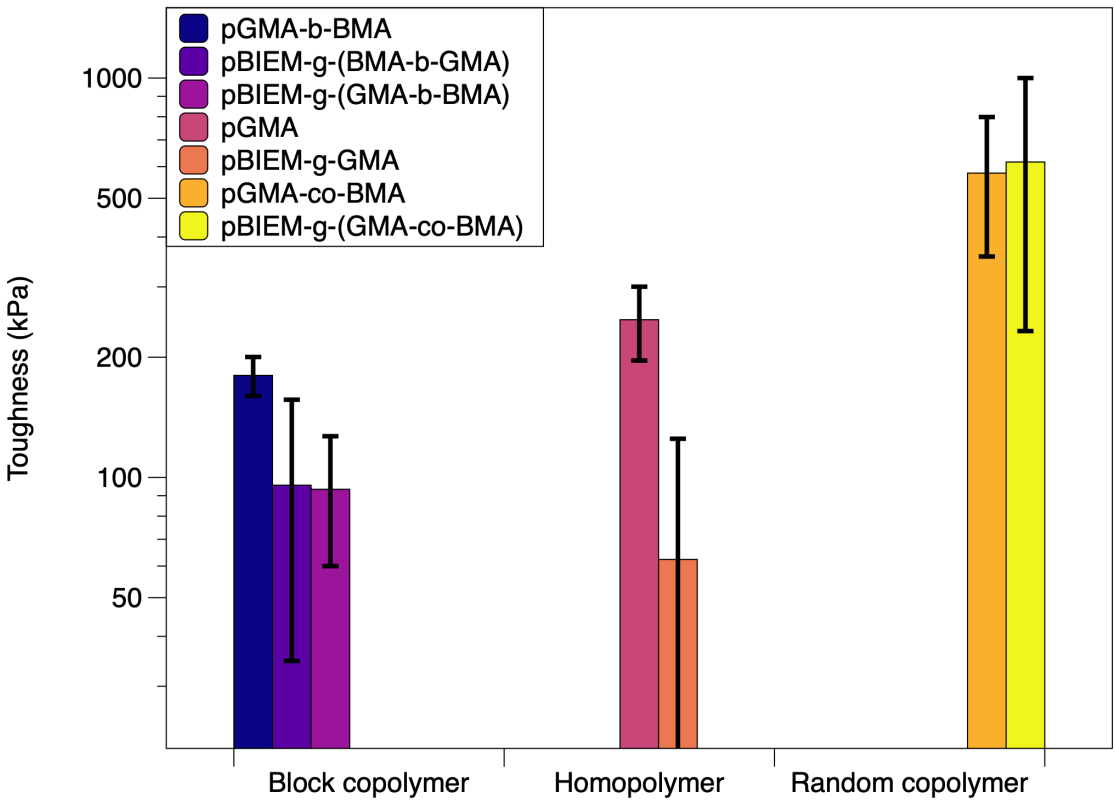

Figure 30: Random comb sidechains suppress intermolecular crosslinking and create tougher materials. Tensile toughness of comb and linear polymers. n = 3

g-(GMA-*co*-BMA) had a toughness of 616.0 kPa (Figure 30). Homopolymers, pGMA had a toughness of 248.0 kPa, and pBIEM-*g*-GMA had a toughness of 62.30 kPa.

In the case of both block polymers and homopolymers, the comb polymers had lower toughness. These results are somewhat contrary to conventional block polymers, as the phase separation between segments of block polymers and resultant self-assembly is routinely exploited to create rubbery microdomains capable of dissipating stress and increasing the toughness of thermosetting resins. Linear block polymers[225] and comb block polymers[121] have been demonstrated to improve the toughness of epoxy resins, and it was expected that comb polymers with a rubbery core would show superior toughness.

I attribute this to intramolecular crosslinking forming loops and microgels that do not create elastically active network chains. Unsurprisingly, the comb homopolymer showed the worst toughness. BMA is known to increase toughness of crosslinked networks,[226,227] and its absence in the homopolymers leads to increased brittleness. Most surprisingly, the random copolymers showed the highest toughness, with the comb polymer even achieving higher toughness compared to the linear polymers. It is worth noting that the highest measured toughness of pBIEM-*g*-(GMA-*co*-BMA) was 1,088 kPa, versus 883.0 kPa for pGMA-*co*-BMA. I hypothesize that the randomly distributed BMA monomers space apart the reactive GMA monomers, making it less probable that they will react to form loops with adjacent sidechains. This tensile data shows that I are ultimately able to create high modulus materials with toughness comparable to their linear analogues using highly crosslinked comb polymers.

3.5 Conclusion

We synthesized novel thermosetting comb polymers containing both reactive glycidyl groups and rubbery butyl methacrylate. Block and homopolymer comb polymers showed low modulus and toughness due to intermolecular crosslinking creating loop defects. Using a random copolymerization of reactive and rubbery monomers, I was able to suppress intermolecular crosslinks and increase the toughness of highly crosslinked comb polymers. Through this, I demonstrated a method for creating very high molecular weight thermosetting polymers with high toughness and modulus. High molecular weight and

a tunable density of epoxy functionality make this material and attractive option for fast setting coatings and adhesives.

Chapter 4

Fast, oxygen-tolerant RAFT polymerization of hydrogels

Publication in preparation

4.1 Abstract

Synthetic hydrogels are an attractive platform for cell culture, as they are water-rich, and they can often be used to encapsulate cells within a three-dimensional matrix under the right chemical conditions. Many hydrogels form *via* free radical polymerization in the presence of initiating species under UV light. The combination of free radicals and UV light during polymerization can lead to decreased viability and cellular stress. Here, I demonstrate a photoiniferter strategy to polymerize hydrogel networks without exogenous initiators and UV light. We demonstrate formation of soft hydrogels with xanthate-functional polymers with visible light. Importantly, polymerization proceeds equally well under nitrogen and in ambient conditions with a range of monomers. I suggest this process as a way to diversify monomer choice for synthetic hydrogel development in the absence of UV-light and free radical initiators.

4.2 Introduction

Hydrogels made from synthetic polymer precursors span a wide range of applications, from injectable redox-based hydrogels,[228] to antifouling coatings,[229] to cell culture environments[30,230] and tissue engineering.[231] Hydrogels are highly useful networks for cell culture applications due to their affinity for water, their stability at physiological conditions, and their 3D matrix structure that surrounds cells.[232,233] Most commonly,

hydrogels are formed by crosslinking polymer chains into a network *via* free radical polymerization of vinyl functional monomers, initiated by redox or UV-sensitive species. Limitations of this standard approach include toxic byproducts[155,223,234] and high energy light,[235] both of which can be damaging to embedded cells. Michael-addition reactions of multifunctional polymers are a popular alternative to free radical-initiated network formation, though tuning the kinetics of Michael-addition reactions can be difficult within the strict confines of physiological conditions.[148] I sought to find an alternative solution to this issue by in situ reversible addition-fragmentation chain transfer (RAFT) polymerization. RAFT polymerizations are traditionally highly oxygen sensitive and polymerize slowly, so they are rarely used for cell applications.[236] The goal of my work was to explore whether specialized RAFT polymerizations could be effectively tuned to create soft hydrogels quickly and in oxygen-tolerant conditions.

RAFT polymerizations offer several advantages to free radical polymerizations. RAFT polymerizations use far lower radical concentrations than typical free radical polymerizations, potentially reducing oxidative stress on cells. Owing to their reversibility, they can be started and stopped at will, enabling the synthesis of complex structures and sequences through careful reaction design. Additionally, polymers with RAFT endgroups are nontoxic to cells.[237] A final benefit of RAFT-crosslinked hydrogels is their ability to produce highly homogeneous[238] crosslinked networks with chain-end functionality, enabling the preparation of living hydrogels that can be modified after fabrication.[239,240]

A key limitation in the use of RAFT for biocompatible hydrogel fabrication is its high sensitivity to oxygen.[241,242] Oxygen is a well-known radical scavenger; but molecular oxygen is required for viable cell culture. Several techniques have been developed to impart oxygen tolerance to RAFT polymerizations such as employing alkyl amine electron donors or photoredox catalysts.[243] Alternatively, the oxygen can be overwhelmed with excess radicals from the initiating species. Here, I have taken inspiration from this last concept by exploiting the high radical flux produced by xanthates in photoiniferter (PI)-RAFT polymerization to rapidly consume environmental oxygen during polymerization, followed by rapid reoxygenation by diffusion to maintain cell viability.[244]

The photoiniferter (PI) concept was recently described by Otsu,[245] and it uses molecules that can simultaneously act as **ini**tiator, trans**fer** agent, and **ter**minator. This means no exogenous initiators are needed, which simplifies reaction set-up and reduces concerns of byproduct cytotoxicity. Given that xanthates enable polymerization and crosslinking in air,[246] and that trithiocarbonate disulfides can mediate PI-RAFT and produce telechelic polymers,[247,248] I hypothesized that xanthate disulfides would provide a facile way to produce telechelic polymers, similar to trithiocarbonate disulfides, and produce gels rapidly in open air, similar to traditional xanthates. To do this, I employed a bisxanthate proposed by Huang *et al.*,[249] and translated it to an aqueous system to support future cell applications.

4.3 Materials and methods

4.3.1 Reagents used

Reagents were purchased from Sigma-Aldrich unless otherwise noted. Methyl acrylate (MA, 99%), ethyl acrylate (EA, 99%), n-butyl acrylate (nBA, ≥ 99%), 2-hydroxyethyl acrylate (HEA, 96%), acrylamide (AAm, 99%), N,N-dimethylacrylamide (DMAa, 99%), acrylic acid (AA, 99%), and isodecyl acrylate (iDA, 99%) were each passed over alumina to remove inhibitors before use. N-isopropylacrylamide (NIPAM, 97%), carbon disulfide (redistilled, ≥99.9%), iodine (≥99.8%), (DCTB, ≥99.0%), 1,4-dioxane (dioxane, ≥99.0%), deuterated DMSO (99.8%), and sodium thiosulfate (99%) were used as received. Potassium hydroxide (KOH, 99.98%), ethanol (anhydrous, 90%), methanol (99.8%), hexanes (99%), and diethyl ether (anhydrous, 99%) were purchased from ThermoFisher and used as received. Sodium trifluoroacetate (NaTFA) was synthesized as described by Prakesh and Matthew.[250]

4.3.2 Instrumentation

Poly(iDA) molecular weight and dispersity were measured by GPC on an Agilent 1260 with a PL gel 5 μm guard column and three, 5 μm analytical mixed C columns (Agilent). THF was used as the eluent at a flow rate of 1 mL/min. The column was standardized with pMMA calibration standards and toluene was used as a flow marker. All other polymer molecular weights and dispersities were determined on an Agilent Tech 1260 Infinity DMF GPC, with a Gel 5 μm guard column, a PL Gel 5 μm mix D 1° column, a PL Gel 5 μm Mix C 1° column, and a refractive index detector using a 20 μL sampling loop. Analyses were run at 50 °C using DMF with 0.01 M LiCl at a flow rate of 1.0 mL/min with toluene

as a flow marker (Figure 31). ^{1}H NMR spectra were recorded using a 400 MHz Avance Bruker spectrometer (Figure 32 - Figure 37).

4.3.3 Polymerization kinetics

A 50 wt% solution of MA monomer solution (1 eq of bis(xan), 50 eq of MA, and deuterated DMSO queued to 50 wt%) was prepared in a 20 mL vial. The solution was added to an NMR tube either sparged with nitrogen or not. A ^{1}H spectra was taken at t = 0 min using a 400 MHz Avance Bruker spectrometer (Bruker Scientific LLC). The tubes were then placed in a photoreactor under a 405 nm lamp at 4.1 mW/cm$^{2.}$ Spectra were collected at 1, 5, and 10 minutes to monitor monomer conversion. Reactions were stopped when 90+ % conversion was reached. Conversion was determined by integrating the vinyl protons and acrylic backbone protons (Figure 38 and Figure 39).

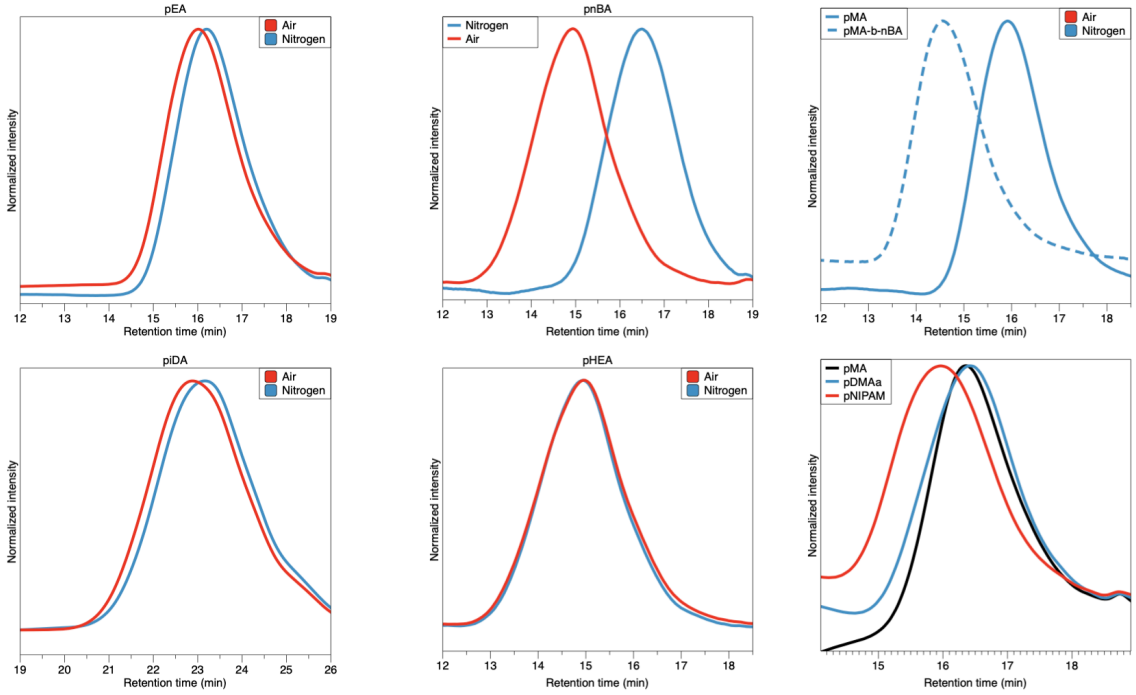

Figure 31: GPC traces of polymers studied, synthesized in air or nitrogen.

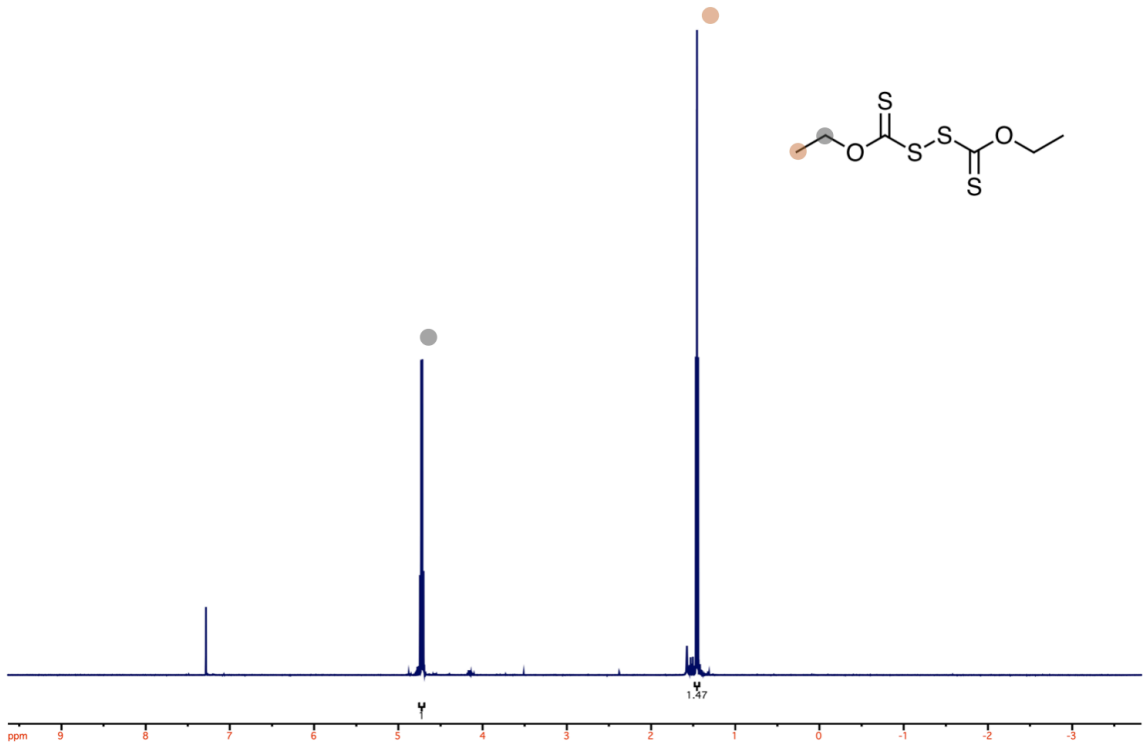

Figure 32: ^{1}H NMR of bis(xan). Spectra recorded at 300 MHz in $CDCl_3$.

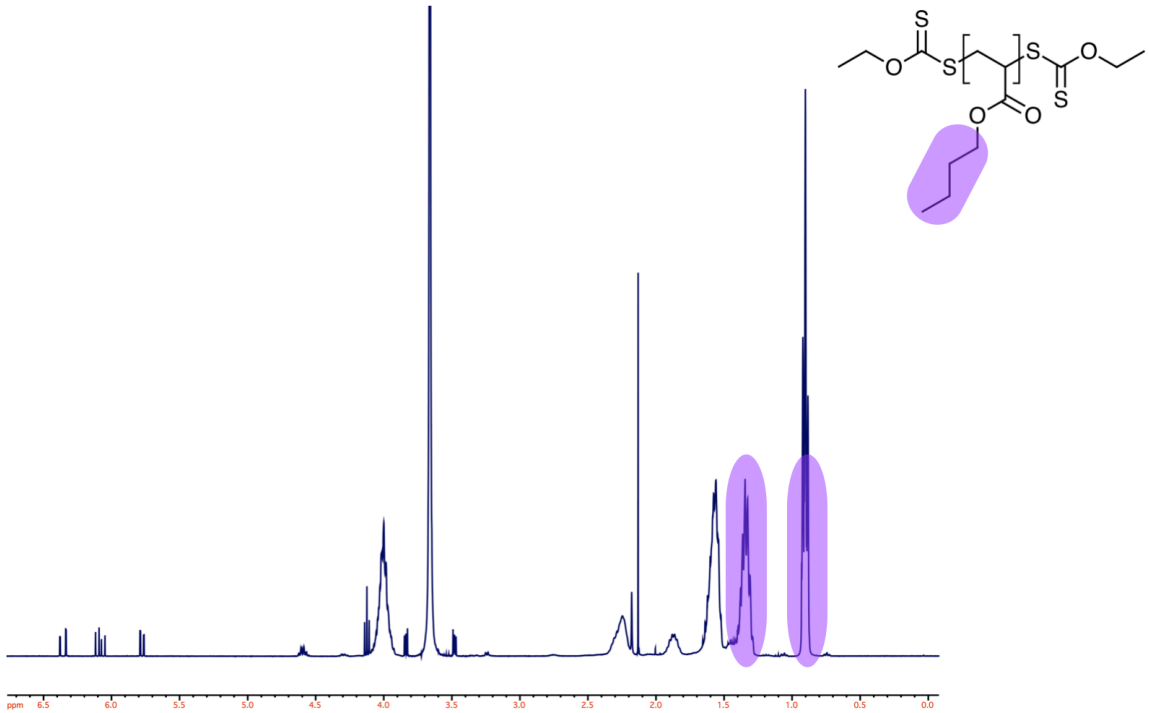

Figure 33: ^{1}H NMR of pnBA. Spectra recorded at 300 MHz in $CDCl_3$.

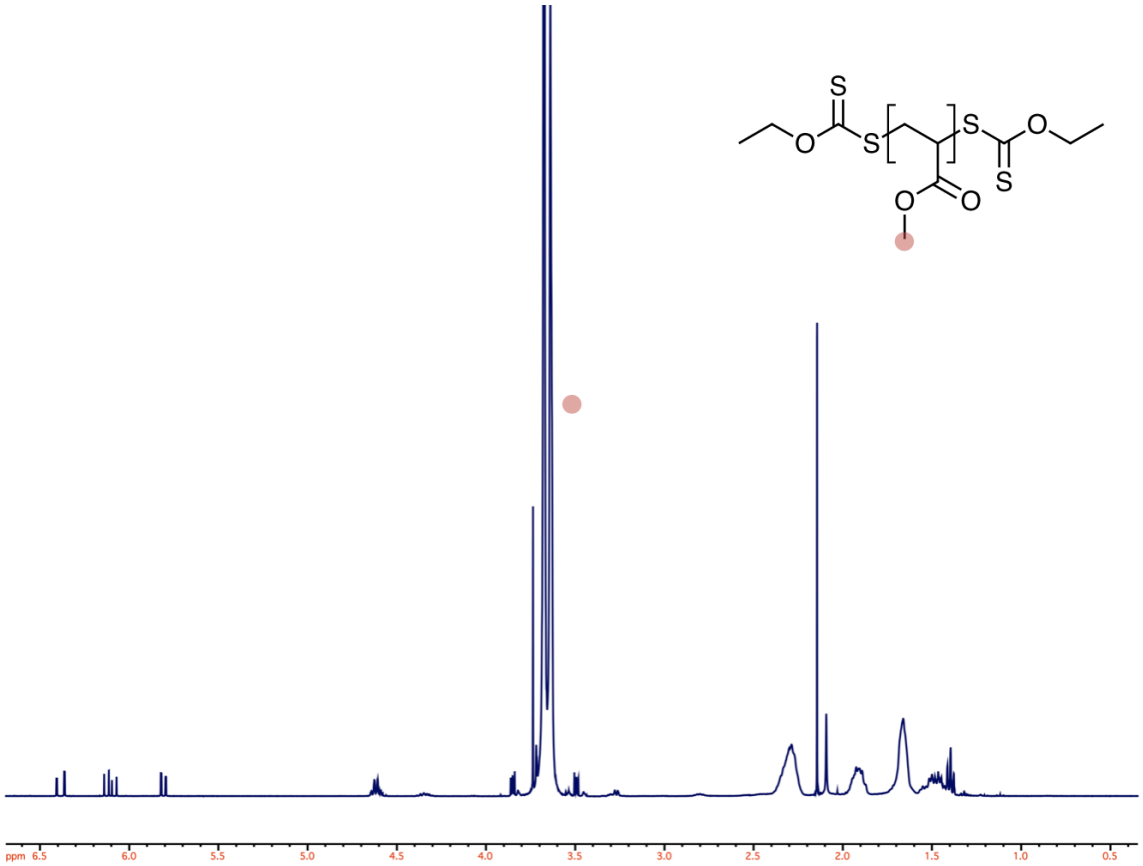

Figure 34: ^{1}H NMR of pMA. Spectra recorded at 300 MHz in $CDCl_3$.

4.3.4 Synthesis of O,O-diethyl 1,2-disulfanedicarbothioate (bis(xan))

KOH (5 g) was added to anhydrous ethanol (200 mL) in a 500 mL round bottom flask and stirred until dissolved. The flask was then cooled to 0 °C on ice. Carbon disulfide (5 mL) was added to the solution dropwise. Immediately, the solution turned bright yellow. Subsequently, the round bottom flask was stirred for three hours at room temperature. The solution was precipitated in diethyl ether (1 L) to yield potassium ethyl xanthogenate as a slightly off white solid. The solid was collected by vacuum filtration and further dried under 0.001 mbar vacuum overnight. Once dry, 10 g of the pure solid was added to a methanol (50 mL) in a 100 mL round bottom flask and dissolved. Iodine (2.5 g) was added

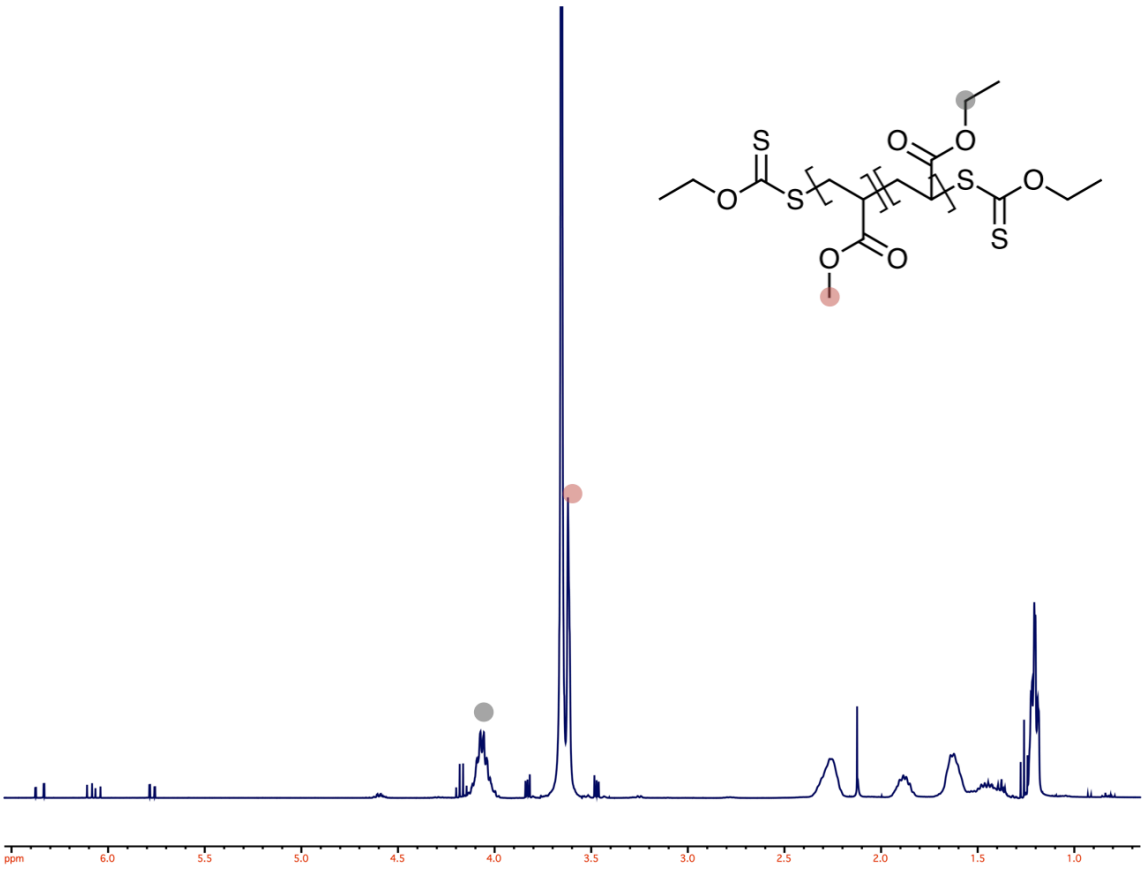

Figure 35: ^{1}H NMR of pMA-*b*-EA. Spectra recorded at 300 MHz in $CDCl_3$.

portionwise, and the solution was stirred for three hours at room temperature. The solution was precipitated in ice cold DI water (2 L), yielding O,O-diethyl 1,2-disulfanedicarbothioate as a bright yellow solid. The solid was washed with saturated sodium thiosulfate solution and DI water, then dried in a vacuum dessicator to yield the final product.

4.3.5 Photopolymerization

Polymerizations from methyl acrylate (MA), ethyl acrylate (EA), n-butyl acrylate (nBA), isodecyl acrylate (iDA), acrylic acid (AA), hydroxyethylacrylate (HEA), acrylamide (AAm), N,N-dimethylacrlamide (DMAa), and N-isopropylacrylamdie (NIPAM) monomers were conducted in similar fashions. Briefly, a 50 wt% solution of monomer was prepared in

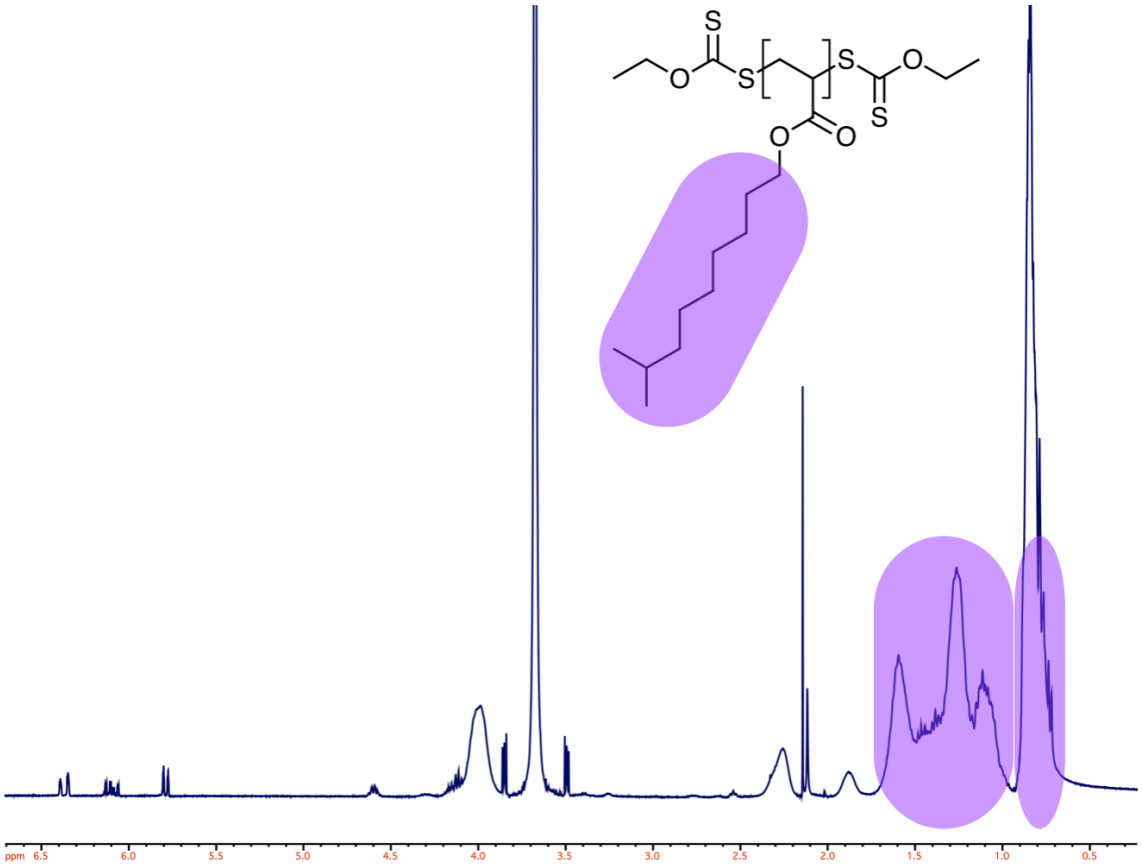

Figure 36: ^{1}H NMR of piDA. Spectra recorded at 300 MHz in $CDCl_3$.

a 20 mL vial (1 eq bis(xanthate), 50 eq of monomer, and 50 wt% dioxane). The vial was then sealed with a rubber septum and either left under air or sparged with nitrogen for 15 minutes. Next, the vial was placed into a photoreactor under a 405 nm lamp either in a ventilated (MA, EA, nBA, iDa, AA, and HEA) or in a saled chamber (AAm, DMAa, and NIPAM) at 4.1 mW/cm^2 for 30 min. A small aliquot of the resultant polymer solution was reserved to measure monomer conversion, and the remainder was diluted with dioxane. Polymers containing nBA or iDA were precipitated in cold methanol, and all other polymers were precipitated in cold hexanes.

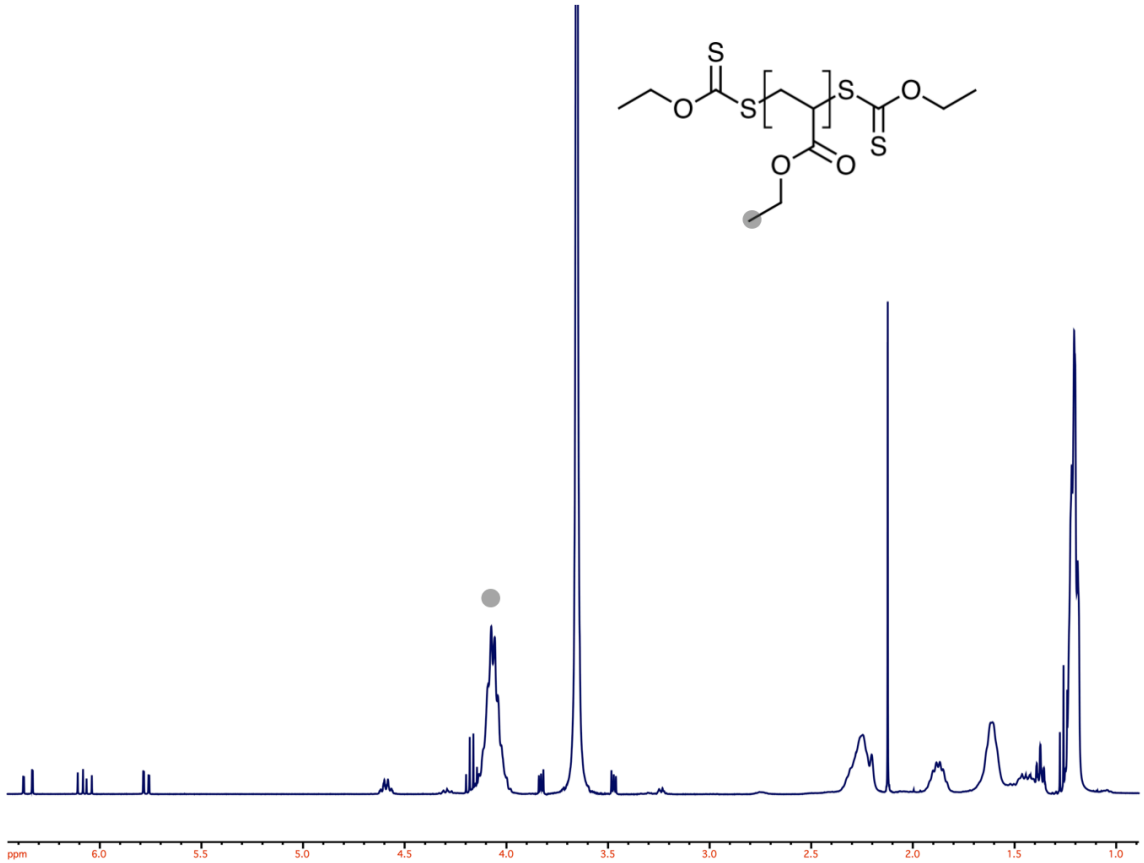

Figure 37: ^{1}H NMR of pEA. Spectra recorded at 300 MHz in $CDCl_3$.

4.3.6 Hydrogel preparation

Bis(xan) (1 eq) and hydroxyethyl acrylate (100 eq) were vortexed in a 20 mL vial until the iniferter dissolved. Then 1 wt% trimethylolpropane triacrylate and 50wt% DI water

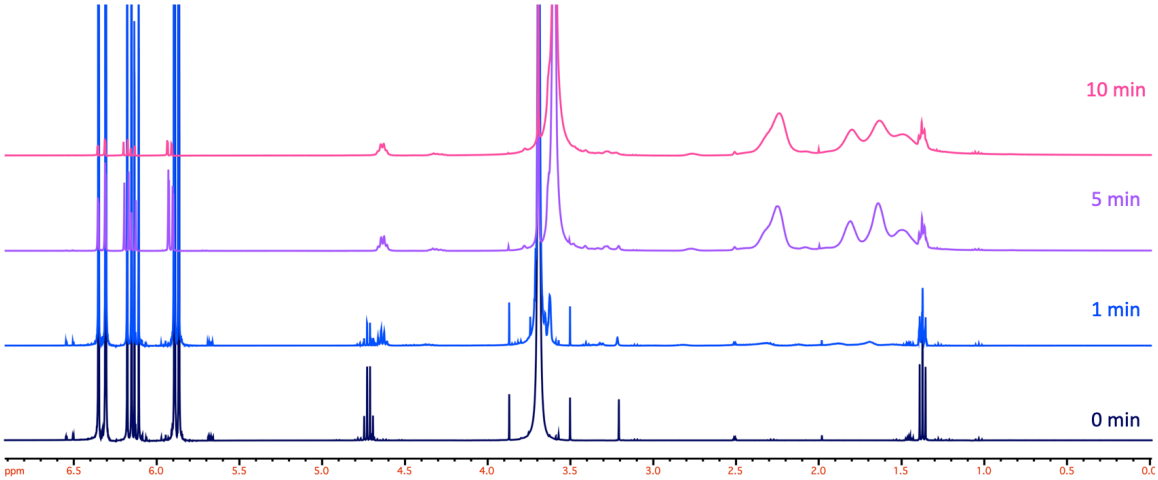

Figure 38: ^{1}H NMR of bis(xan) and MA evolution over time under 405 nm light in nitrogen.

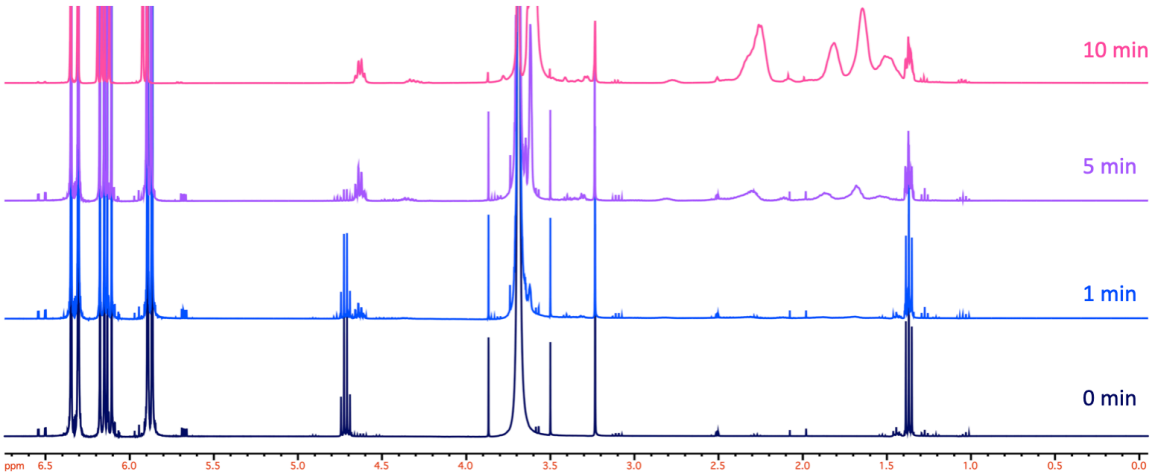

Figure 39: ^{1}H NMR of bis(xan) and MA evolution over time under 405 nm light in air.

were added resulting in precipitation of the bis(xan). Under agitation, 100 µL of the well-mixed, cloudy mixture was quickly pipetted into a 24 well plate. The hydrogel solution was then placed under a 405 nm LED lamp for ten minutes. The circular, clear gels were then removed from the wells and placed into 100 mL 1X PBS pH 7.4 buffer for 48 hours to fully swell, exchanging the PBS buffer after 24 hours.

4.3.7 Rheological characterization of hydrogels

After they reached equilibrium swelling, the storage and loss moduli were measured by oscillatory shear rheology using a Kinexus Pro parallel plate rheometer (Netzsch, Selb, Bayern, Germany) with a 20 mm diameter platens. Each platen was affixed with 60-grit sandpaper to prevent slippage. Measurements were conducted at room temperature at 0.1% strain, 0.1 and 1 Hz, and a constant 0.01 N normal force. A solvent trap filled with DI water was used to maintain gel hydration.

4.3.8 MALDI-ToF

To characterize the mass distribution of polymers, I adapted a MALDI-ToF technique described in Beres *et al.*[247] Briefly, we dissolved (DCTB) as the matrix (40 mg/mL), sodium trifluoroacetate (NaTFA, 1 mg/mL) as a cationizing agent, and the polymer sample (10 mg/mL) in spectroscopy grade acetonitrile. 5 µL each of matrix and sample and 1 µL of salt were mixed, and 1 µL of this mixture was deposited onto a ground steel target. Data was acquired on an Ultraflex III MALDI-TOF/TOF mass spectrometer equipped with a smartbeam laser (Bruker) operating in linear or reflectron positive ion mode. External calibration was performed using mixtures of commercial PEGs to overlap with the m/z range of interest. Spectra were generated by averaging 5,000-10,000 shots from non-overlapping positions. Data was analyzed using FlexAnalysis v3.4 and PolyTools v1.31 (Bruker).

4.4 Results and discussion

4.4.1 Kinetics and livingness

Our goal was to develop a new approach to synthesize polymers and hydrogels rapidly, without toxic radicals and side products, in the presence of oxygen and water. If successful, this would represent a fundamentally new strategy to form polymers and hydrogels in the presence of living cells. To accomplish this, I employed xanthate-mediated PI-RAFT polymerizations because of their fast kinetics.[251–253] Inspired by recent work on bis(trithiocarbonates)[247,248] and xanthates, I selected a xanthogen disulfide (bis(xan)) as the PI.

Polymerization reactions of bis(xan) follow a traditional RAFT mechanism. 405 nm light puts bis(xan) into an excited state where it can fragment through β-scission into two thiyl radicals. These radicals can then react with vinyl monomers through a single unit monomer insertion (SUMI) pathway (Figure 40).[247] The addition of a monomer into bis(xan) changes its chemistry, resulting in better initiating radicals upon excitation and fragmentation relative to thiyl radicals. When the xanthates are again excited by light, a secondary carbon radical is formed that propagates rapidly. From there, the growing polymer enters RAFT equilibrium.

We assessed the compatibility of bis(xan) to create polymers with a suite of acrylic monomers (Table 4) under nitrogen atmosphere in dioxane. Water insoluble monomers tested were alkyl esters, including methyl acrylate (MA), ethyl acrylate (EA), n-butyl acrylate (nBA), and isodecyl acrylate (iDA). Water soluble monomers tested included acrylates (and hydroxyethylacrylate (HEA)) and acrylamides (acrylamide (AAm), (DMAa), and N-isopropylacrylamdie (NIPAM)).

All polymerizations save for AAm yielded a viscous liquid after 30 minutes. For the alkyl esters, smaller pendent alkyl groups corresponded to better controlled polymerizations than their larger counterparts (pEA, pnBA, piDA, Table 4). The largest pendent alkyl group polymer, piDA, had a large dispersity ($Đ > 2$) and several unidentified smaller peaks in the chromatogram (Figure 31). For the acrylamides, only monomers with substituted amides polymerized. AAm did not polymerize, whereas pDMAA and pNIPAAm formed readily with pDMAA showing lower dispersities than pNIPAAm (Figure 31). The amide protons

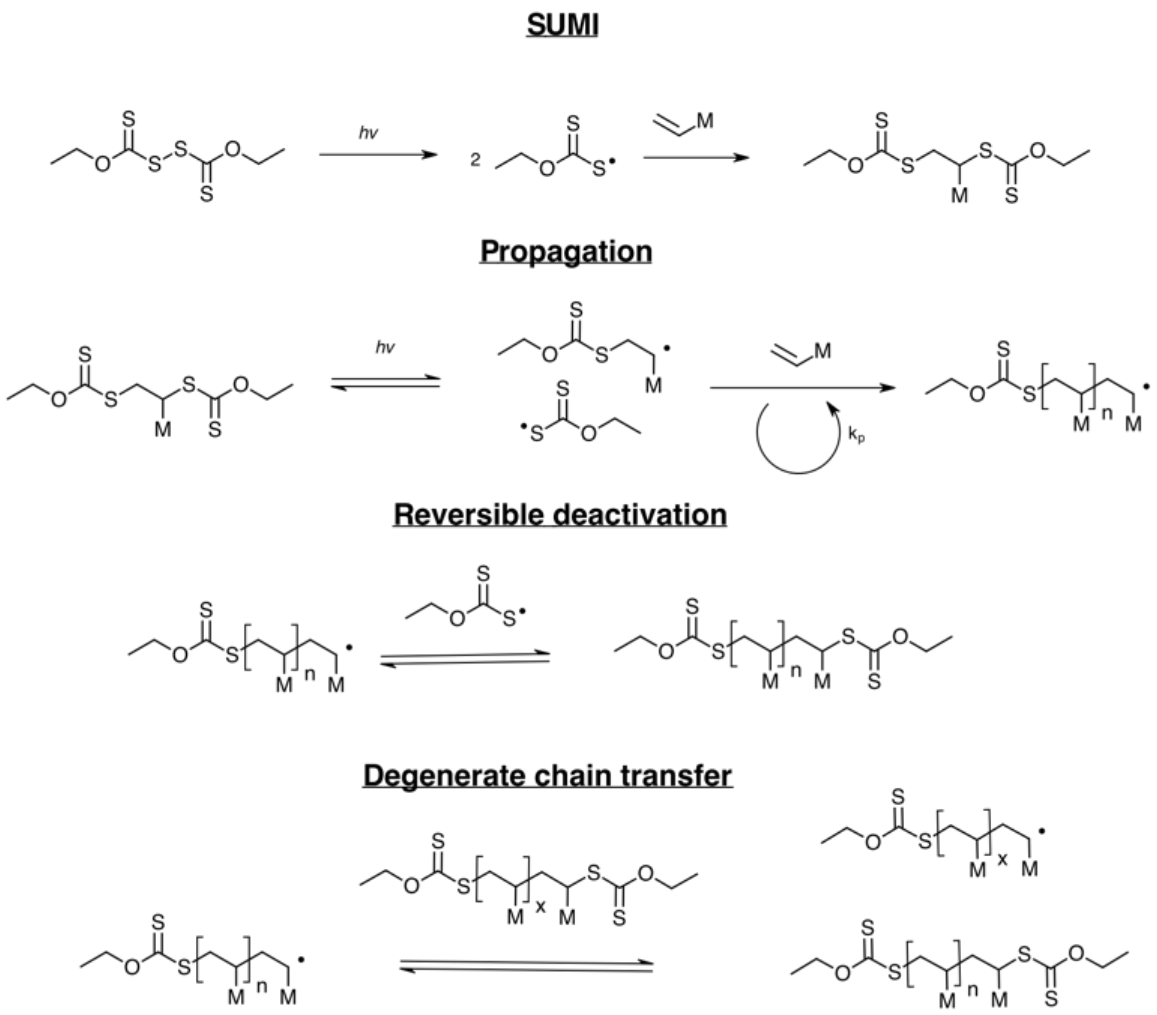

Figure 40: Schematic of photoiniferter polymerization of vinyl monomers. PI polymerization proceeds through a SUMI step to yield a better initiating R group capable of initiating the propagation step, followed by conventional RAFT kinetics.

are likely responsible for the large dispersity and failed polymerizations due to aminolysis reactions of bis(xan).[254] Regardless, the polymers that did form represent a wide range pendent functionality, demonstrating broad utility and applicability of bis(xan).

To determine the air tolerance and suitability towards cell encapsulation of these polymerizations, the same monomers were polymerized with bis(xan), this time without nitrogen purging to remove air. Mirroring the Nitrogen condition, all polymerizations

Polymer	Temp (°C)	Atm	Target DP	Measured DP	Mn (g/mol)	Đ	Conv (%)
PMA	38	Air	50	57	5773	1.46	96
PMA	38	N2	50	45	4562	1.49	97
PEA	38	Air	50	49	4969	1.63	95
PEA	38	N2	50	41	4180	1.59	97
PnBA	38	Air	50	38	3847	1.6	96
PnBA	38	N2	50	41	4106	1.41	98
PHEA	38	Air	50	139	13993	1.81	95
PHEA	38	N2	50	154	15411	1.66	96
PiDA	38	Air	50	73	7361	2.26	90
PiDA	38	N2	50	63	6364	2.25	92
PDMAa	60	Air	50	44	4457	1.32	N/A
PNIPAM	60	Air	50	66	6613	1.4	N/A

Table 4: Characterization of xanthate polymerizations for a range of monomers. Polymerization conditions (temperature, atmosphere, targeted DP) and characterization (measured DP, molecular weight (M_n), dispersity (Đ), and conversion are detailed.

except AAm yielded a viscous liquid after 30 minutes. Further, similar molecular weights and dispersities were observed when polymerizations were conducted in air and nitrogen (Table 4).

To further investigate the influence of air on these reactions, we analyzed polymerization kinetics. Ideally, polymerizations would approach full conversion within ten minutes to be useful for encapsulating cells. To this end, a MA polymerization under air or nitrogen was monitored *via* NMR. Polymerizations were conducted in air or under nitrogen with 405 nm light at 38 °C with spectra collected at 0, 1, 5, and 10 minutes (Figure 41 a). Polymerization under nitrogen or air displayed nearly identical kinetics, each reaching 97% conversion within 10 min. The polymerization is remarkably fast compared to prior publications using 365 nm light.[249]

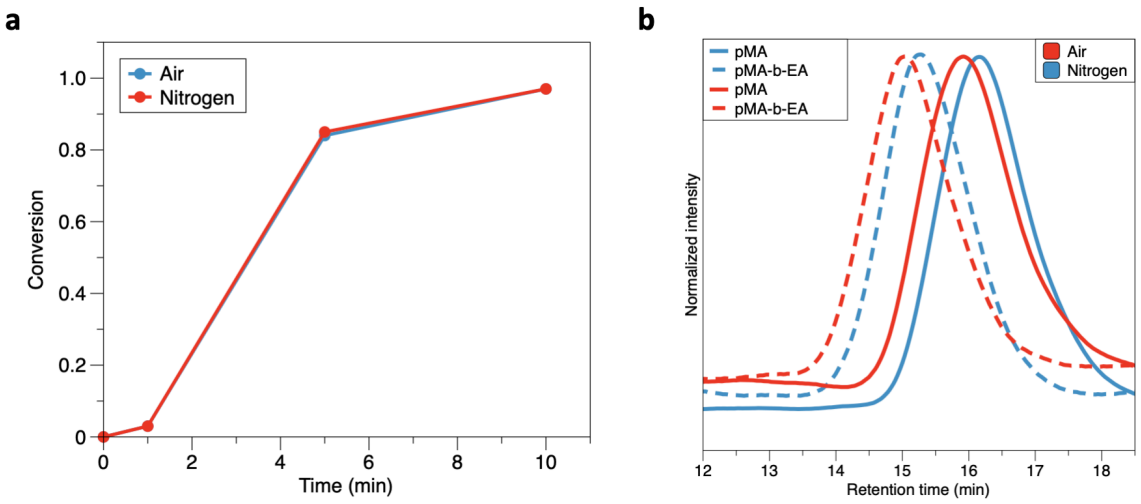

Figure 41: Bis(xanthates) mediate ultra-fast polymerizations of acrylates and produce living polymers. (a) Conversion over time of xanthate-mediated PI polymerization of 50 wt% MA under air and nitrogen atmosphere. (b) GPC chromatogram showing degree of polymerization of pMA and pMA-*b*-EA synthesized in air and under nitrogen.

A brief study was then conducted to determine the impact of heat on the polymerization reactions was conducted with MA monomers. I compared reactions at 38°C and 60°C in air (Table 5). In comparison to pMA synthesized at 38°C, pMA synthesized at 60 °C was more narrowly dispersed. This is most likely due to the change in the RAFT equilibrium at elevated temperatures.[255] Although not useful for cell applications, temperature could be another useful handle for controlling this polymerization.

To further characterize the air tolerance, I conducted further analysis on the degree of polymerization (DP) *via* GPC. Polymerizations of MA in air and nitrogen with a targeted DP of 25 were conducted using a monomer:bis(xan) ratio of 25:1. The resultant polymers

Polymer	Temp (°C)	Atm	Target DP	Measured DP	Mn (g/mol)	Đ	Conv (%)
PMA	38	Air	50	57	5773	1.46	96
PMA	60	Air	50	84	8496	1.25	N/A

Table 5: Impact of temperature on xanthate polymerization of pMA.

yielded DP of 32 and 35 monomers per chain for air and nitrogen respectively (Figure 41 b, Table 6). I then attempted to re-initiate polymerization by redissolving the pMA poymers and adding EA (1 eq. bis(xan): 1 eq. EA). Successful chain extension was demonstrated for both samples *via* the shift to earlier elution times (Figure 41 b). Interestingly, the final DP measured by GPC were nearly twice as high as the targeted DP in both air and under nitrogen. This behavior is consistent with prior reports studying bis(trithiocarbonates),[247] though the reason for this doubling of DP is not clear. Despite the higher than predicted DP, I was able to produce living polymers capable of further reaction in open air and in nitrogen.

4.4.2 End group fidelity of polymers

To confirm the telechelic nature of polymers resulting from synthesis via bis(xan), I analyzed the structure of pMA *via* MALDI-ToF, GPC, and NMR (Figure 42). For these reactions, pMA was synthesized at a target DP of 25 (25:1 MA:bis(xan)), either in air or nitrogen, and characterized by MALDI-ToF (Figure 42 a,b). MALDI-ToF showed that pMA polymerized through a photoiniferter approach with bis(xan) is well controlled, with

Polymer	Temp (°C)	Atm	Target DP	Measured DP	Mn (g/mol)	Đ	Conv (%)
PMA	38	Air	25	32	3278	1.45	94
PMA	38	N2	25	35	3578	1.4	95
PMA-*b*-EA	38	Air	64	115	11559	1.32	94
PMA-*b*-EA	38	N2	70	114	14414	1.32	95

Table 6: GPC characterization of polymerizations of MA and block polymers built from living PMA.

polymerizations done in air and in nitrogen having a dispersity of 1.11 (Figure 43 and Figure 44). The MALDI-ToF spectra also showed air and nitrogen synthesized polymers to have very similar molecular weights (Mn = 4584 g/mol in nitrogen, M_n = 4821 in air). Additionally, MALDI-ToF analysis detected the sodiated forms of both polymers, consistent with pMA bearing the α and ω functionality expected in the telechelic polymer (Figure 40).

GPC confirmed the polymers had nearly identical molecular weights and dispersities (Figure 42 c). ^{1}H NMR results revealed CH_3-$\mathbf{CH_2}$-O peaks characteristic of chain end O-

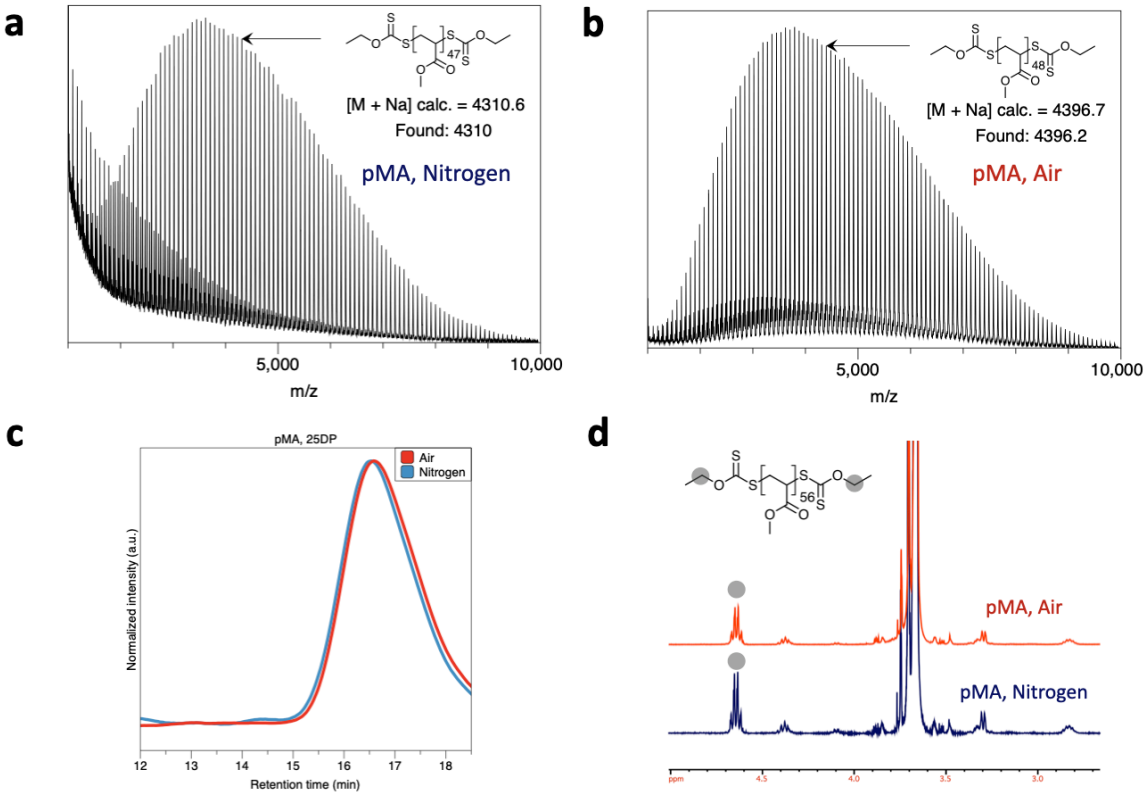

Figure 42: Structural characterization of pMA synthesized with bis(xanthates) in air and nitrogen. (a) MALDI-ToF spectra of pMA synthesized in nitrogen (Mn = 4310 g/mol). (b) MALDI-ToF spectra of pMA synthesized in air (Mn = 4396.2 g/mol). (c) GPC (DMF) chromatogram of pMA polymers with a targeted DP of 25 (d) ^{1}H NMR spectra showing characteristic xanthate peaks.

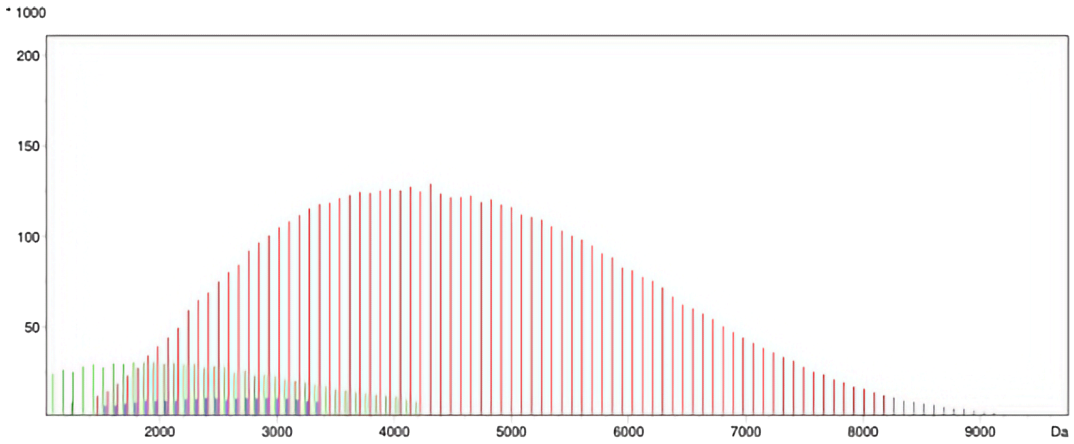

n	ser.	rep.unit	orig. resid.	resid.	end1	end2	cation	Mn	Mw	pd	DP	% I.	cnt	Kendrick
1	1	86.1000	1.24831	1.24831				4584.19	5104.40	1.11348	53.2427	66.8	86	
2	2	86.1000	55.3085	55.3041				2158.06	2563.98	1.18809	25.0646	11.9	38	
3	3	86.1000	71.0313	71.0313				2475.68	2587.36	1.04511	28.7535	2.7	22	

Figure 43: Linear MALDI-ToF of pMA synthesized under nitrogen.

ethyl xanthates, attached to pMA synthesized in air and under nitrogen (Figure 42 d). Further, these results unambiguously showed end group fidelity *via* a downward shift in the xanthate functional groups in pMA relative to their ppm in the bis(xan) precursor (4.6 ppm Figure 42 d, 4.7 ppm Figure 32).

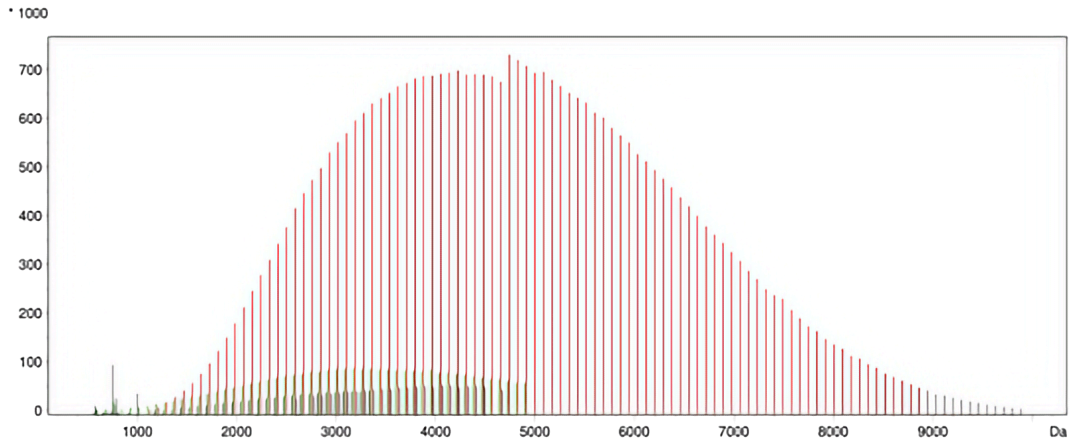

n	ser.	rep.unit	orig. resid.	resid.	end1	end2	cation	Mn	Mw	pd	DP	% I.	cnt	Kendrick
1	1	86.0238	5.51614	5.51614				4821.30	5370.53	1.11392	56.0461	86.8	98	
2	2	86.0238	74.2184	74.2184				3175.53	3510.05	1.10534	36.9145	7.6	51	

Figure 44: Linear MALDI-ToF of pMA synthesized under air.

4.4.3 Rapid hydrogel fabrication

We then set about testing their utility in forming hydrogels. The goal for hydrogel fabrication is to enable a hydrogel system useful for tissue engineering, namely cell culture. Hydrogels for cell culture should reach the critical gel point within ten minutes without agitation so that cells do not settle to the bottom of the solution. Gelation cannot be too fast, as proper mixing must occur to limit heterogeneity.[148] I hypothesized that a fast gelation rate could be attained in water with one of the water soluble polymers synthesized *via* bis(xan).

To test gelation rate, pHEA was selected as a model hydrophilic polymer. First, HEA was polymerized in water *via* bis(xan). After ten minutes of 405 nm light irradiation, a trifunctional vinyl crosslinker trimethylolpropane triacrylate was added to be 1 wt% of the

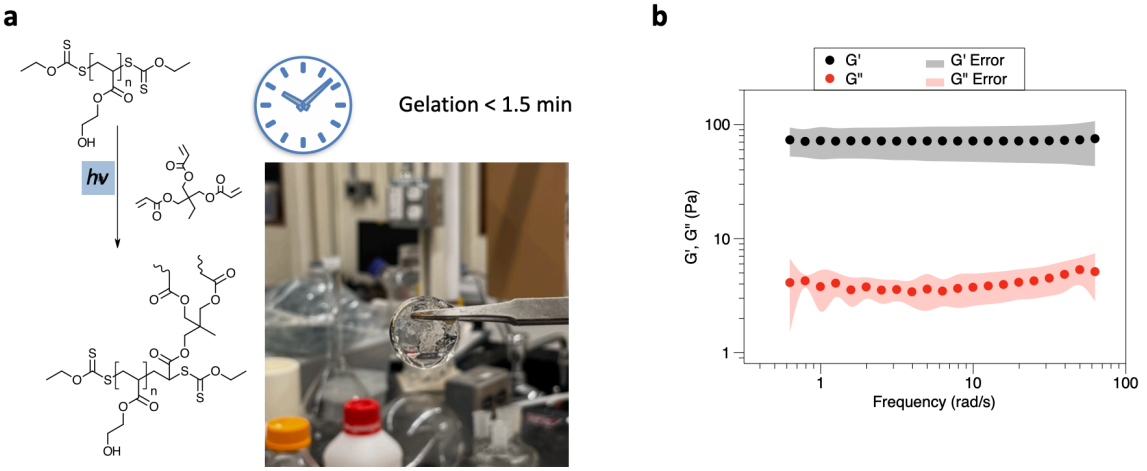

Figure 45: Structural characterization of pMA synthesized with bis(xanthates) in air and nitrogen. (a) MALDI-ToF spectra of pMA synthesized in nitrogen (Mn = 4310 g/mol). (b) MALDI-ToF spectra of pMA synthesized in air (Mn = 4396.2 g/mol). (c) GPC (DMF) chromatogram of pMA polymers with a targeted DP of 25 (d) ^{1}H NMR spectra showing characteristic xanthate peaks.

solution. The sample was again irradiated and within 1.5 min, a crosslinked gel formed. Following the successful fabrication of gels in water, several gels were prepared by the same protocol and left to swell in PBS for 48 hrs. The resultant gels were colorless and optically transparent (Figure 45 a). To determine the properties of the resultant hydrogels, modulus was then characterized using parallel plate rheology. The G' and G'' values of the gels were determined, resulting in a G' of 72 ± 24 Pa and G'' of 4.5 ± 0.9 Pa at 1 Hz (Figure 45 b). G' and G'' were observed to be frequency independent, indicating that the samples had reached the critical gel point defined by the Winter-Chambon criterion.[181] The small standard deviation of these modulus values indicates the hydrogel formed had consistent network properties. Therefore, using bis(xan), I was able to rapidly fabricate soft hydrogels in water with consistent modulus values.

4.5 Conclusion

In this study, I demonstrated bis(xan)-mediated PI polymerizations to be very fast and not impacted by the presence of oxygen. The polymers produced could be chain extended with additional monomers. Finally, hydrogels were fabricated using pre-synthesized polymer and a tri-functional crosslinker in 1.5 min. This approach provides a facile route to quick hydrogel fabrication using light in the visible spectrum at physiological temperature without radical initiators and their decomposition products. Overall, my approach enables an optimal combination of rapid polymerization/gelation kinetics, and water and air tolerance while producing well defined telechelic polymers with minimal components.

These properties make this system suitable for preparing custom water-soluble acrylic and acrylamide polymers used to form hydrogels to culture cells *via* crosslinking.

MALDI-ToF spectra of pMA were collected and analyzed by Dr. Cedric Bobst.

Chapter 5

Conclusions, limitations, and future directions

5.1 Conclusions

This dissertation has presented novel methods to design mechanosensitive graft polymers, highly crosslinked bottlebrush polymers, and living hydrogels. Utilizing shielding PEG chains to provide a steric barrier to an otherwise efficient crosslinking reaction between amines or thiols and epoxides, I was able to produce mechanosensitive polymers that undergo a sol-gel transition in response to ultrasound. This approach to creating strain sensitive materials provides a facile route to creating strain responsive materials using commercially available monomers and simple techniques. I demonstrated, for the first time, a sol-gel transition accelerated under force using shielded reactive polymers. I synthesized novel thermosetting bottlebrush polymers containing both reactive glycidyl groups and rubbery butyl methacrylate. By adjusting polymer architecture I was able to suppress intermolecular crosslinks and increase the toughness of highly crosslinked bottlebrush polymers. In doing so I demonstrated a method for creating very high molecular weight thermosetting polymers with high toughness and modulus. Additionally, I demonstrated bis(xan)-mediated PI polymerizations to be tolerant to oxygen and produce telechelic polymers. Xanthate-capped hydrophilic polymers were shown to crosslink in the presence of a tri-functional crosslinker in $\sim$1.5 min. This approach provides a facile route to quick hydrogel fabrication using light in the visible spectrum, at physiological temperature, in air and water, and without radical initiators and their decomposition products. In all cases,

careful design of initiator structure and polymer architecture enabled the production of novel materials. I foresee that this work will enable the development of new high performance coatings, adhesives, and biocompatible materials.

5.2 Materials and methods

5.2.1 Chemical sourcing

Materials were purchased from Sigma-Aldrich unless otherwise mentioned. (APMA, 98%), Jeffamine ED-600, poly(ethylene glycol) (PEG) methyl ether methacrylate (950 g/mol, PEGMA950), 2-Hydroxyethyl methacrylate (HEMA, 98%), (CPA), (99%), pyridine (anhydrous, 99%), dichloromethane (DCM, anhydrous, 99%), dioxane (99%), $CuBr_2$ (99%), 1,5,7-triazabicyclo[4.4.0]dec-5-ene (TBD, 98%), (EBPA, 97%), (, 99%), 1,1,3,3-tetramethylguanidine (TMG, 99%), and azobisisobutyronitrile (AIBN, 99%), were used as received. Glycidyl methacrylate (GMA, 99%), butyl methacrylate (BMA, 99%), 2-ethyhexyl methacrylate (EHMA, 98%), 2-methoxyethyl methacrylate (MEMA, 99%), and 2-(methacryloyloxy)ethyl methacrylate (AAEM, 95%) were passed through a column of basic alumina to remove inhibitors. CuBr (99.9%) was purified by stirring in glacial acetic acid. Tris(2-pyridylmethyl)amine (TPMA, 98%), tris 2-(dimethylamino)ethyl amine (Me_6TREN, 98%), cyclopentylmethyl ether (CPME, 99%), and 2-cyano-2-propyl dodecyl trithiocarbonate (CPDT, 97%) was purchased from TCI (Tokyo, Japan) and used as received. Methanol (99%), toluene (99%), dimethylformamide (DMF, 99%), isopropanol (99%), calcium chloride (99%) diethyl ether (anhydrous, 99%), tetrahydrofuran (THF, 99%),

HCl (concentrated), reduced iron powder, copper turnings, basic alumina, and neutral alumina were purchased from Thermo Fisher (Waltham, MA) and used as received.

5.2.2 Synthesis of polyinitiator and vitrimers containing GMA

Details of the synthesis of poly(BIEM), linear vitrimers, and bottlebrush vitrimers, and their formulation can be found in Chapter 3.2.

5.2.3 Representative PEG shielded and control polymer synthesis

Poly(GMA-*co*-PEGMA950), poly(AAEM-*co*-PEGMA950), and of all molar ratios and degree of polymerization (DP) were synthesized by reversible addition-fragmentation chain transfer (RAFT) polymerization. Each reaction was fed 0.01 moles of monomer total. For example, 0.71 g (0.005 mol) GMA, 0.72 g (0.005 mol) MEMA, 0.0559 g CPA (0.2 mmol), 6.6 mg AIBN (0.04 mmol) ([50]:[1]:[0.2] [M]:[CTA]:[I], where [M]:[CTA] defines the DP), 4 mL of 1,4-dioxane, and a stir bar were added to a 20 mL scintillation vial. Polymers containing APMA were synthesized in 1:1 dioxane:water. The vial was sealed with a rubber septum and the solution was purged with N_2 (g) for ∼20-30 min in an ice bath to prevent solvent and monomer evaporation (PEGMA solutions were bubbled in cool water to prevent PEG crystallization). Subsequently, the vial was placed in a thermostated aluminum reaction block at 60 °C on top of a magnetic stir/hot plate. The reaction was left to stir overnight, yielding a viscous liquid. The solution was removed from heat and exposed to air to terminate the polymerization. The solution was precipitated into cold (-20 °C) ether, the solid washed twice more with cold ether, and dried at 0.01 mbar

overnight. Polymers containing APMA were poured into a small amount of cold ether, shaken, then isopropanol was added to precipitate the polymer.

5.2.4 Copolymer solution preparation

Polymer solutions were initially prepared to be 50 wt% polymer. For example, 0.3 g of polymer was dissolved in 0.3 g of solvent, and crosslinker was added such that the nucleophilic functional group was equimolar with the total epoxide concentration. To control for the concentration of crosslinking points in solution, polymers were subsequently formulated to be 1 M of epoxide in solution. Each sample was vortexed for 5 sec to ensure complete mixing before proceeding with rheometry or sonication.

For all experiments crosslinked with amines, reactions were conducted in a solvent system of 1:1 BuOH:DMF. Alcohols are known to catalyze the reaction between amines and epoxides through the formation of a trimolecular complex.[179] Thiol-crosslinked reactions were conducted in MeCN with 10 μL of 2 M LiOH as a catalyst, necessary to deprotonate the thiols in order to perform a nucleophilic attack on the epoxide ring.[180] Poly(APMA-*co*-MEMA) was first treated with pyridine to deprotonate the pendent amines.

5.2.5 Parallel plate rheology

Gelation times and storage moduli (G'), and tanδ of polymer solutions/gels were determined on a Kinexus Pro parallel plate rheometer (Netzsch, Selb, Bayern, Germany). Measurements were run on a 20 mm plate with a 1 mm gap at 1 % strain and 1 – 100 rad s^{-1} frequency sweep. Each frequency sweep lasted approximately 5 min, and the entire measurement lasted approximately 15 hr. The gel point was defined using the Winter-Chambon criterion,

for which the time of gelation is defined as the point at which tanδ becomes frequency independent at small frequencies.[181–183] For samples with very high modulus, the elastic modulus was determined using compressive rheology by taking the slope of the stress strain curve of cured gels with a 4 mm diameter. Rheological experiments were analyzed using IRIS Rheo-Hub (IRIS Development, Amherst, MA).[184] For samples treated with 30 % strain, single frequency measurements were conducted at 1 Hz and 30 % strain for 10 minutes in between each frequency sweep.

5.2.6 Time-temperature superposition measurements

Time-temperature superposition was conducted by performing frequency sweeps at 30 °C intervals with a DMA 850 (TA Instruments) equipped with a tension clamp. Frequency sweeps were performed at 0.01 % strain with a preload of 0.01 N .

5.3 Limitations

Thermosetting materials have come far from the crosslinked latex rubbers first developed by ancient Mesoamericans, and have transformed the world along the way. Polymer chemists have and continue to produce ever more sophisticated ways to prepare narrowly disperse polymers with diverse functionality enabling the synthesis of more and more exotic polymer architecture. Taking advantage of multiple methods of controlled/living polymerization enabled the bottom up molecular design of novel mechanosensitive comb polymers, highly crosslinked molecular bottlebrushes, and living hydrogels. While these materials do fill unmet needs for thermosetting resins and soft biocompatible materials,

they still suffer from several drawbacks. Here I will detail the limitations of my approaches and how they might be overcome.

5.3.1 PEG-shielded polymers require high strain and/or strain rates to induce crosslinking

Ultrasound is a convenient method for applying strong shear forces at high shear rates to polymers in solution on a laboratory scale. However, it is not necessarily a scaleable technique or easily accessible outside of laboratory environments. More relevant techniques involve parallel plate shear by forcefully spreading liquid on a solid substrate or extrusion of liquids through a narrow opening. To simulate these methods of straining polymer solutions, solutions pGMA-*co*-PEGMA950 and ethylene diamine were subjected to 30 % shear at 1 Hz on a parallel plate rheometer and extruded through a 27 Ga needled. Neither method showed any increase in the rate of gelation. Shear thinning was observed in the polymer solution, evidenced by a decrease in G' after strain was applied (Figure 46). At a minimum, 20 kHz ultrasound at 10 % amplitude (50 W) was required to induce gelation of PEG shielded polymers. To enable more diverse applications, thermosetting polymers that are more sensitive to mechanical force should be developed.

5.3.2 Steric shielding by PEG is not generalizable to all crosslinking chemistries

Although the PEG shielding groups are easily accessible and installed alongside reactive monomers on polymer backbones, they are not suitable for shielding all kinds of reactive monomers. Different applications demand different crosslinking chemistry. For example, ethylene diamine can be replaced with Jeffamines for decorative applications that require

high clarity and transparency. Jeffamines are a class of amine terminated poloxamers developed specifically for preparing crosslinked epoxies, and their structure can be tuned to modulate the properties of the final crosslinked material. However, their large polymeric structure prevents them from diffusing to reactive sites flanked by large PEG shielding groups and forming crosslinks (Figure 47).

Other applications require quicker crosslinking kinetics[256] or reversible crosslinks.[257] For such applications, acetoacetoxy functional polymers offer an attractive option, forming vinylogous urethane bonds in the presence of primary amines. However, the (acetoacetoxy)ethyl ester is quite large, and most likely significantly alters chain conformations, lessening the steric effects of pendent PEG. Additionally, the tendency of the acetoacetoxy pendent groups to self assemble through hydrogen-bonding[258] likely preemptively brings reactive monomers into contact, increasing the apparent rate of

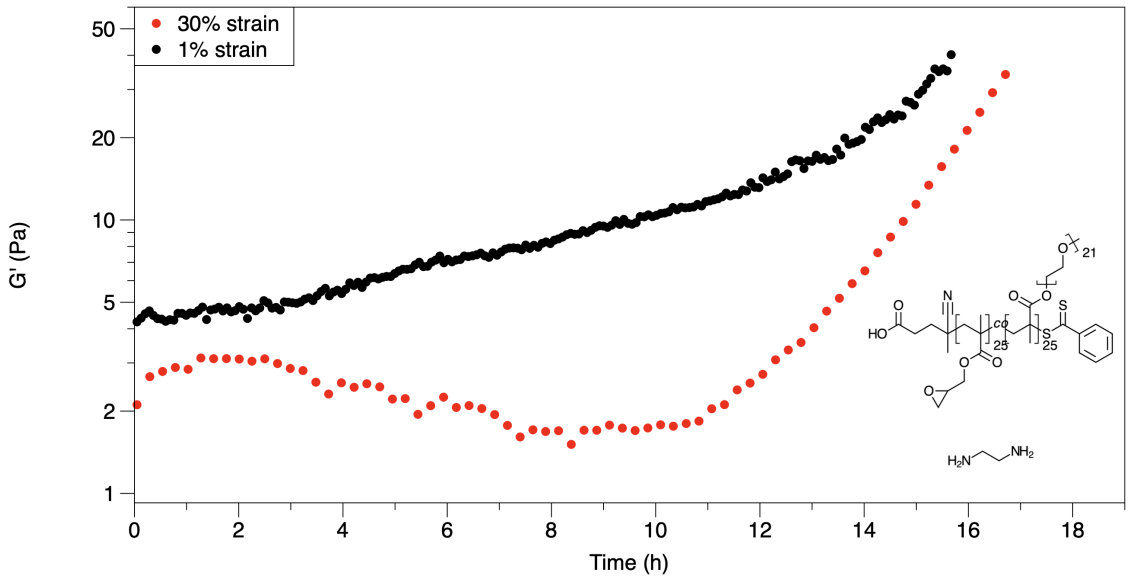

Figure 46: PEG shielded polymers are not activated by parallel plate shear. G' evolution over time of pGMA-*co*-PEGMA950 at 1 % and 30 % strain.

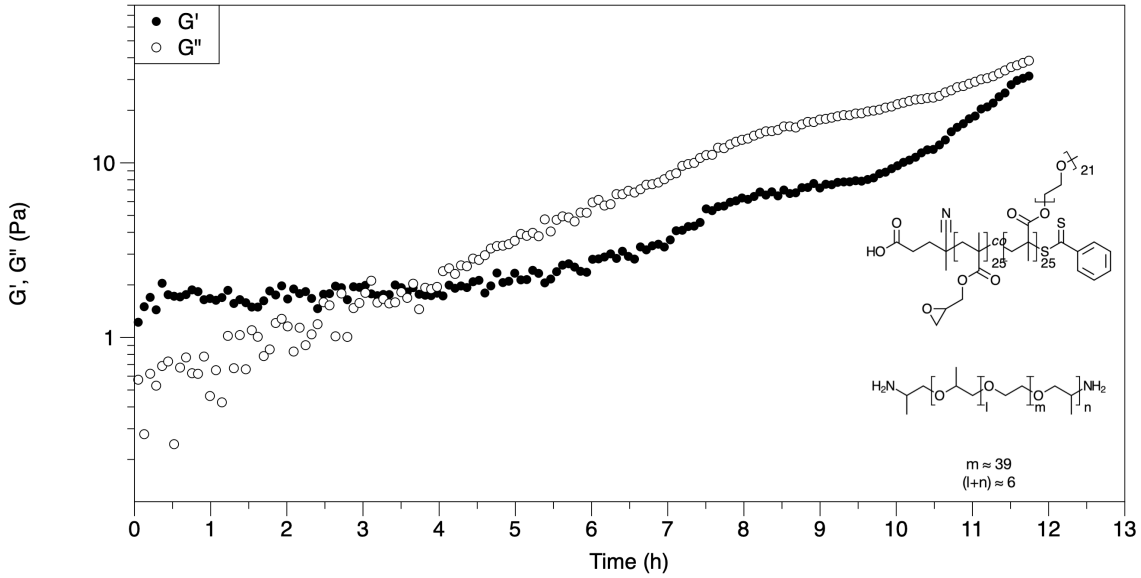

Figure 47: PEG shielding completely prevents gelation with Jeffamine. G' evolution over time of pGMA-*co*-PEGMA950 in the presence of Jeffamine ED-900.

crosslinking. As such, PEG shielding groups are insufficient to protect acetoacetoxy reactive groups (Figure 48). To overcome this, more aggressive shielding methods are required.

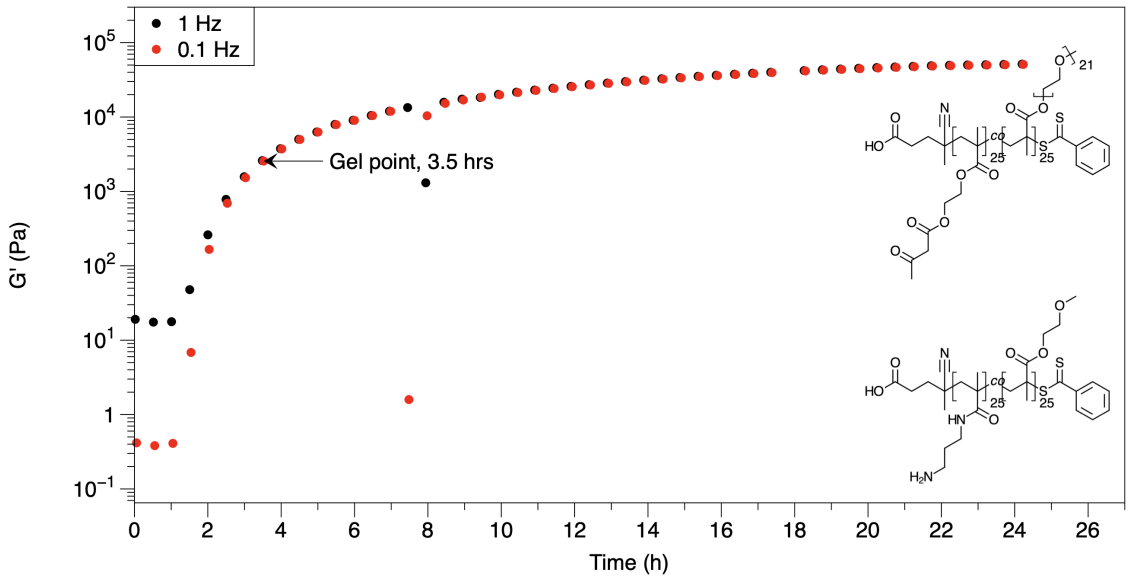

Figure 48: pAAEM-*co*-PEGMA950 rapidly gels in the presence of primary amines. G' evolution over time of pAAEM-*co*-PEGMA950 in in the presence of pAPMA-*co*-MEMA.

5.3.3 Grafting-from produces unstable brushes

One of the most important properties of thermosetting coatings and adhesives is shelf stability. The formulated resin should remain inert until the user desires the material to crosslink. To simplify application, one pot formulations are ideal. To produce highly shielded acetoacetoxy polymers, I turned to core-shell bottlebrush polymers composed of an inner core of crosslinkable AAEM and an outer shell of rubbery EHMA. These polymers were prepared by the "grafting from" method as it enables longer side chain lengths. Initially it was believed that ATRP of AAEM would be impossible due to the 1,3-dicarbonyl interfering with the copper complex. However, some reports have shown the controlled polymerization of AAEM through traditional ATRP mediated by CuBr.[259]

To minimize the amount of copper halide required, poly(AAEM) was synthesized by SARA ATRP with Cu(0) as the reducing agent. This produced a polymer with a bimodal molecular weight distribution with the peak at shorter retention time being roughly double the molecular weight of the peak at longer retention time (Figure 49 a). It is assumed that this is due to radical-radical coupling facilitated by chelation of coper bringing growing chains into close proximity. ^{1}H NMR clearly showed the presence of the acetoacetoxy group as well as the methacrylate backbone (Figure 49 b). Replacing Cu(0) with Fe(0) as the reducing agent produced no polymer. This is to my knowledge the first SARA ATRP reported of AAEM.

Still, bottlebrush polymers with AAEM and ethylhexyl methacrylate copolymer sidechains were prepared by the same technique. However, all copolymers prepared were

extremely unstable, often forming insoluble gels instantaneously upon precipitation. Only a single sample, pBIEM-*g*-(AAEM-*b*-EHMA), could be analyzed by NMR and GPC. GPC of showed a small shoulder at shorter retention times, indicating some amount of radical-radical coupling Figure 50 a). ^{1}H NMR clearly showed the successful sequential polymerization of AAEM and EHMA from the BIEM backbone (Figure 50 b).

Bottlebrush polymers prepared by ATRP "grafting from" are known to form C–C crosslinks at sidechain ends in the solid phase, even in the presence of ppm amounts of copper.[260] Removal of copper from AAEM bottlebrushes was very difficult, presumably as a result of chelation between brush hairs, with copper being clearly visible even after

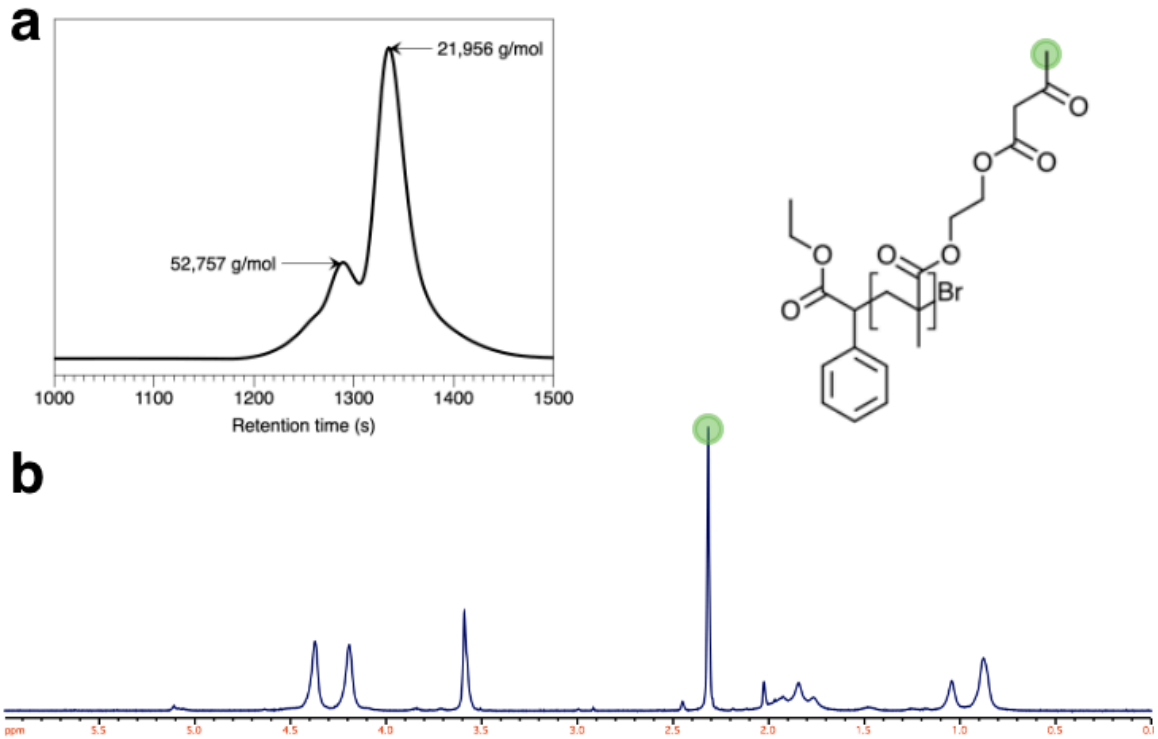

Figure 49: Characterization of pAAEM produced by SARA ATRP. (a) GPC chromatogram of pAAEM. (b) ^{1}H NMR of pAAEM. Spectra recorded at 500 MHz in $CDCl_3$. THF used as eluent.

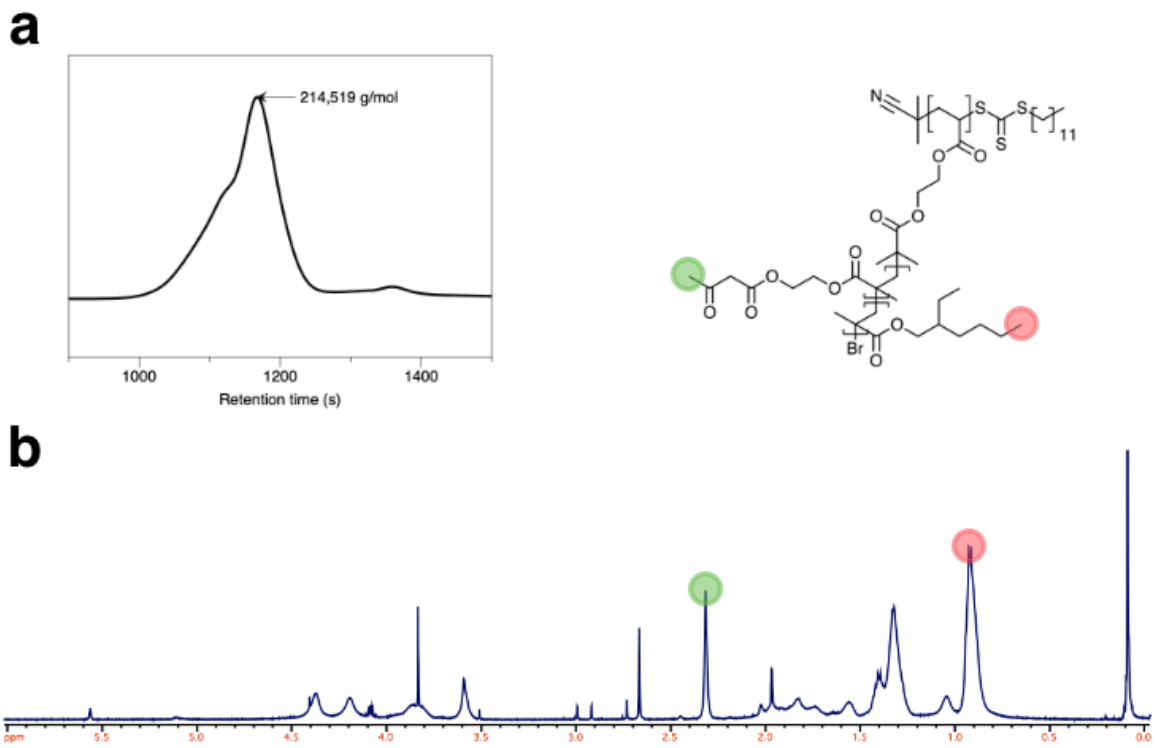

Figure 50: Characterization of pBIEM-*g*-(AAEM-*b*-EHMA) prepared by SARA ATRP. (a) GPC chromatogram of pBIEM-*g*-(AAEM-*b*-EHMA). (b) ^{1}H NMR of pBIEM-*g*-(AAEM-*b*-EHMA). Spectra recorded at 500 MHz in $CDCl_3$. THF used as eluent.

passing through alumina. To make it easier to produce shelf stable bottlebrushes, AAEM was replaced with GMA, and EHMA was replaced with BMA. These bottlebrush polymers were able to be isolated as white solids after passing over alumina to remove the copper salts, but still were only stable for a few days at −20 °C. A different approach to synthesis would be required to produce highly shielded, reactive bottlebrush polymers with a long shelf life.

5.3.4 GMA is not suitable for transesterification based vitrimers

Crosslinked bottlebrushes with GMA (co)polymer sidechains tend to have substantially lower elastic moduli compared to their linear counterparts. Controlling for total number

of crosslinks possible, this suggests that not all crosslinking sites are being utilized. I hypothesized that the onset of vitrification during the cure process prevented the full conversion of epoxides by restricting chain mobility. In an attempt to overcome this and improve the elastic modulus of the bottlebrush polymers, I formulated vitrimers by incorporating a transesterification catalyst, TBD. Described in 2011 by Montarnal et al., vitrimers (sometimes referred to as covalent adaptable networks) are crosslinked thermosets with dynamic bonds that flow like glasses above a certain temperature.[261]

TBD is well understood to enable network topology rearrangement above its characteristic topology freezing temperature through bond exchange reactions at β-

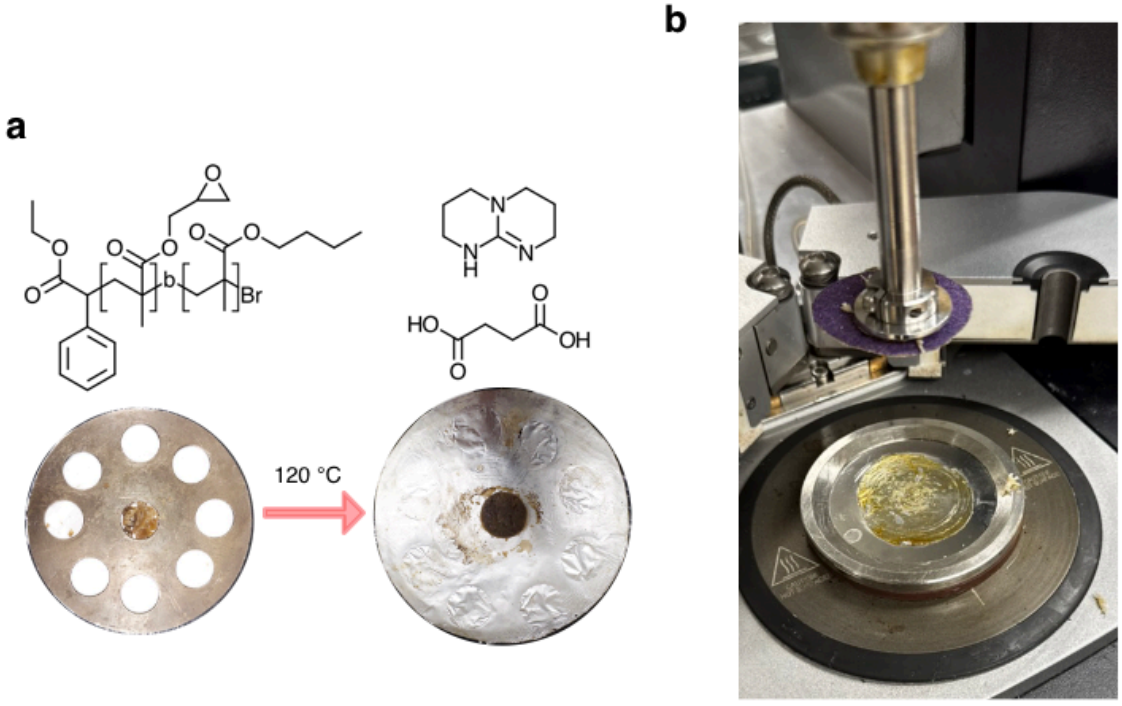

Figure 51: pGMA-*b*-BMA performs well as a reprocessible adhesive. (a) Fragments of crosslinked pGMA-*b*-BMA are melt pressed into a homogeneous solid. (b) An image of a rheometer stage showing that the epoxy adhesive securing sandpaper to the bottom plate has failed, while pGMA-*b*-BMA is still adhering the bottom sandpaper and top plate.

hydroxyl-esters. As a practical test, crosslinked pGMA-*b*-BMA was broken into pieces and pressed in a mold at 120 °C, reforming into a disk within minutes (Figure 51 a). Remarkably, it even outperformed a commercial epoxy glue during parallel plate rheology at 155 °C (Figure 51 b). To attempt to measure the activation energy of vitrimer flow, I employed time-temperature superposition measurements using DMA.[262] However, we were unable to cleanly superimpose the elastic modulus data (Figure 52 a) and no such vitrimer flow was recorded by DMA, even at temperatures exceeding 180 °C (Figure 52 b). It remains unclear what exactly caused this behavior. Additionally, pGMA, pGMA-*co*-BMA, pBIEM-*g*-GMA, pBIEM-*g*-(GMA-*b*-BMA), pBIEM-*g*-(BMA-*b*-GMA), and pBIEM-*g*-(GMA-*co*-BMA) all failed to superimpose cleanly and showed no ability to be reformed by melt pressing. Different dynamic crosslinking chemistry is required to drive polymeric vitrimers to full conversion.

5.4 Future directions

5.4.1 Improving elastic modulus of thermoset bottlebrushes

High-performance thermosetting resins are prized for their resistance to creep, temperature, and solvent, as well as their light weight. These same properties however make reprocessing and recycling impossible. Covalently crosslinked thermosets traditionally do not dissolve in solvent or melt at high temperature, unlike thermoplastics, meaning their shape is set at the onset of gelation. Additionally, the onset of gelation imposes vitrification on thermosetting resins whose $T_{cure} < T_g$, hampering further conversion of reactive sites. This is particularly problematic for bottlebrush polymers, whose large size produces

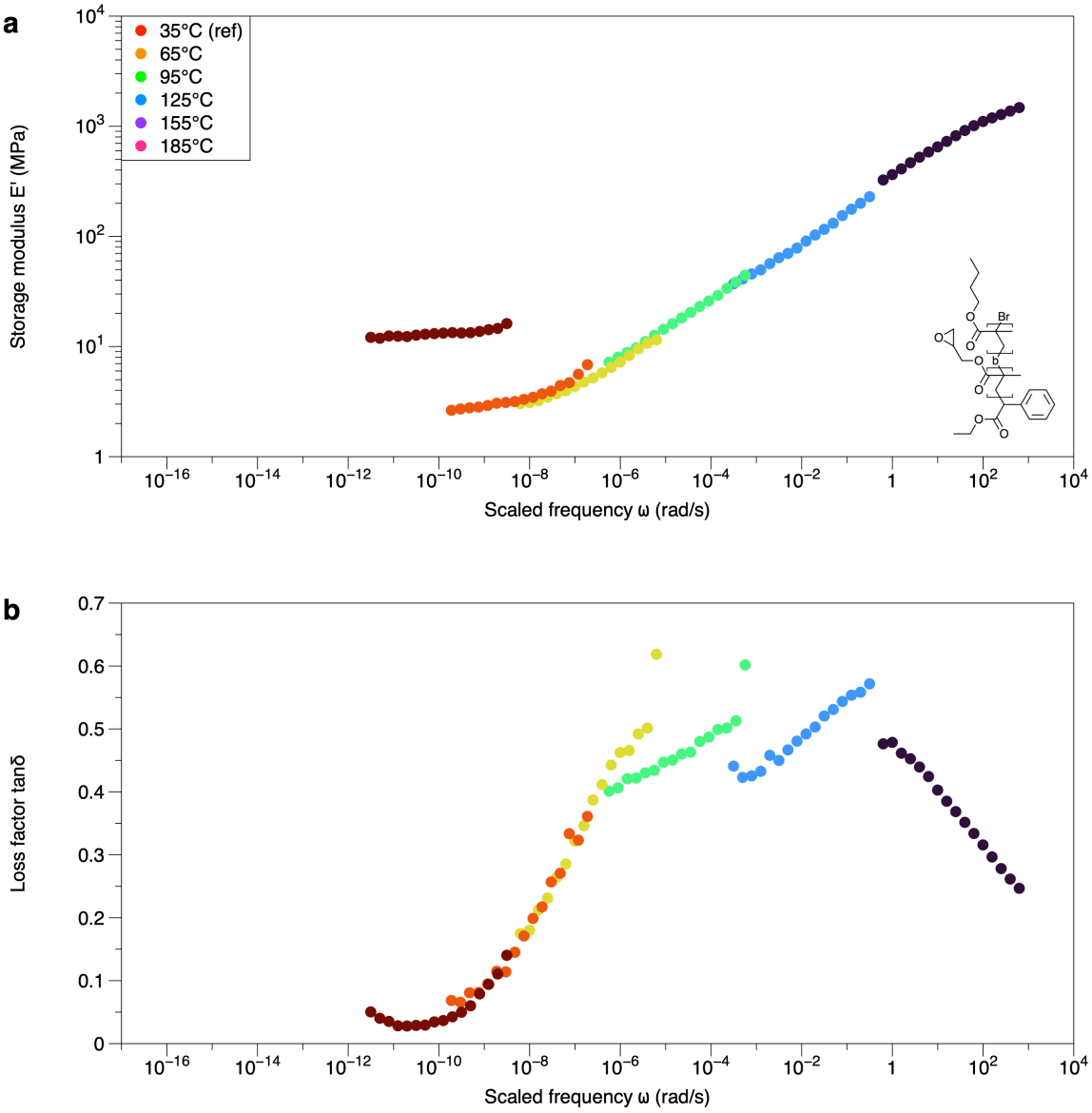

Figure 52: Time-temperature superposition of pGMA-*b*-BMA. (a) Time-temperature superposition of the elastic modulus of pGMA-*b*-BMA. (b) Time-temperature superposition of the loss factor of pGMA-*b*-BMA.

already sluggish motion, making it very difficult to achieve full conversion and maximum modulus. I propose to introduce dynamic crosslinks to bottlebrush polymers in order to maximize the elastic modulus of bottlebrush thermosets by facilitating bond exchange through melt processing.

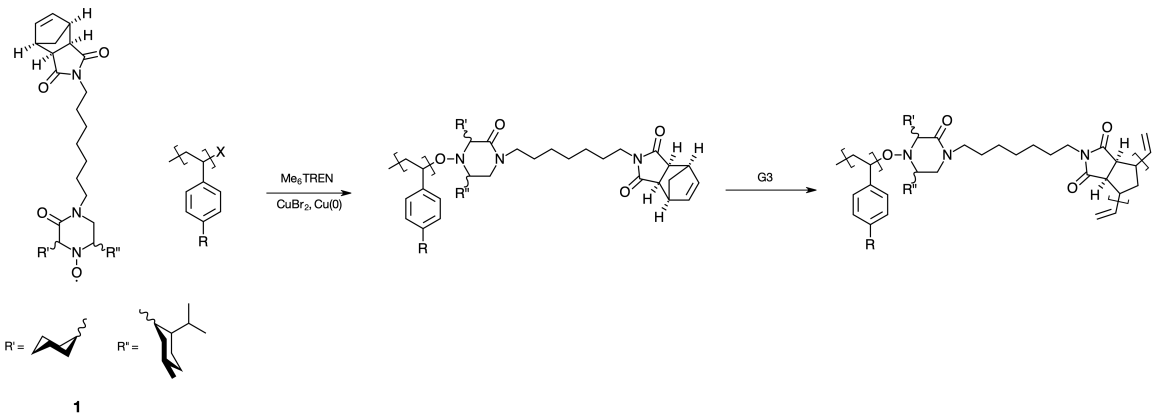

Figure 53: Proposed route to reactive bottlebrush polymers with labile side chains.

Though there are many available chemistries used to prepare vitrimers, imine exchange is most commonly used for polymeric vitrimers. Imine crosslinked polymers can be prepared by reacting aldehyde functional polymers in the presence of primary amines. Copolymer vitrimers based on 2-(methacryloyloxy)ethyl vanillin, and aldehyde functional monomer, and plasticizing monomers have been demonstrated to undergo dynamic bond exchange.[263] Additionally, imine exchange requires no additional catalyst and occurs at lower temperatures. To prepare bottlebrush vitrimers in particular the use of styrenic monomers is preferred, both for their superior hydrolytic stability compared to (meth)acrylic monomers as well as for access to atom transfer nitroxide radical coupling reactions (ATNRC) for facile transformations of chain end halogens (Figure 53).[264] 4-vinylbenzaldehyde (VBA) is an easily accessible monomer, though not commercially available. There are many reported routes to VBA, but I will relay two that give VBA in high yield, one by hydrolysis of p-(chloromethyl)styrene followed by oxidation to VBA (Figure 54 a),[265] another by Wittig olefination of 4-(diethoxymethyl)benzaldehyde followed

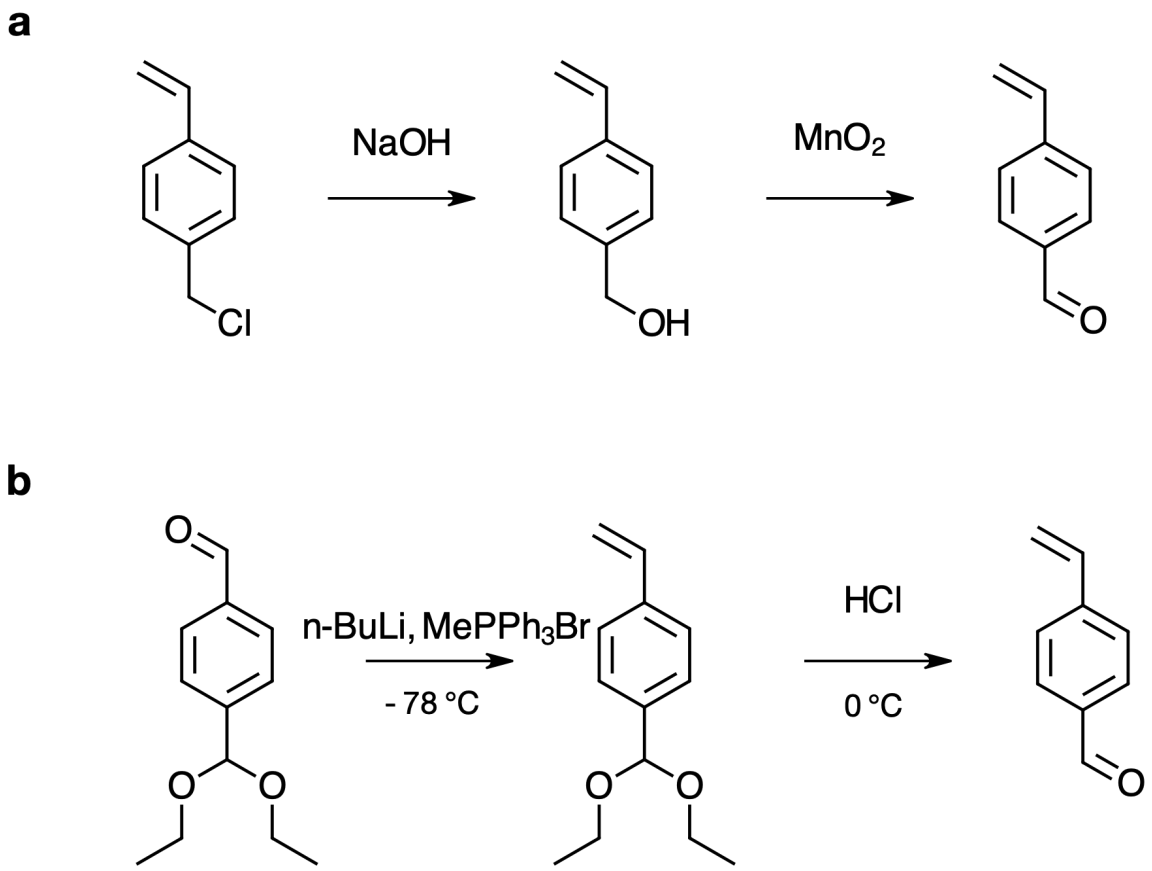

Figure 54: Proposed routes to aldehyde functionalized styrenic monomer for improved reactive bottlebrush polymers.

by deprotection (Figure 54 b).[266] RAFT polymerization of VBA has been reported,[266] but not ATRP.

5.4.2 Mechanosensitive nanocapsule thermosets

While the "grafting from" method excels at producing bottlebrush polymers with long side chains, it also produces ill-defined polymers. Residual initiating sites on side chain ends can also cause irreversible crosslinking in the solid phase, limiting their shelf life. Additionally, control over the final brush architecture is limited to only being able to adjust the sequence of the side chains, meaning the ends of the brush always presented exposed reactive groups to the environment, resulting in rapid crosslinking. Though it was not quantified,

the initiation efficiency and monomer conversion for the bottlebrush side chains was likely quite low.[267] It's possible this could be avoided by an ATRP approach favoring deactivation of the propagating radicals.[268] I propose to use the "grafting through" technique, by which olefin terminated macromonomers are polymerized into bottlebrushes, to create a new class of mechanosensitive "nanocapsule" bottlebrush thermosets that are able to crosslink in response to weak shear forces.

While the "grafting through" technique is not able to prepare bottlebrushes with side chain lengths matching that of "grafting from," it possesses several advantages of its own. Linear macromonomers are able to be easily characterized prior to polymerization into bottlebrush polymers, meaning the length of bottlebrush hairs can be precisely tuned. Different bottlebrush morphologies (comb, rodlike side chain, stretched backbone, stretched sidechain) can be precisely prepared. Bottlebrush block copolymers can be easily prepared by sequential addition of macromonomers. Additionally, bottlebrush polymers prepared this way possess a side chain on every monomer (if only macromonomers are polymerized).

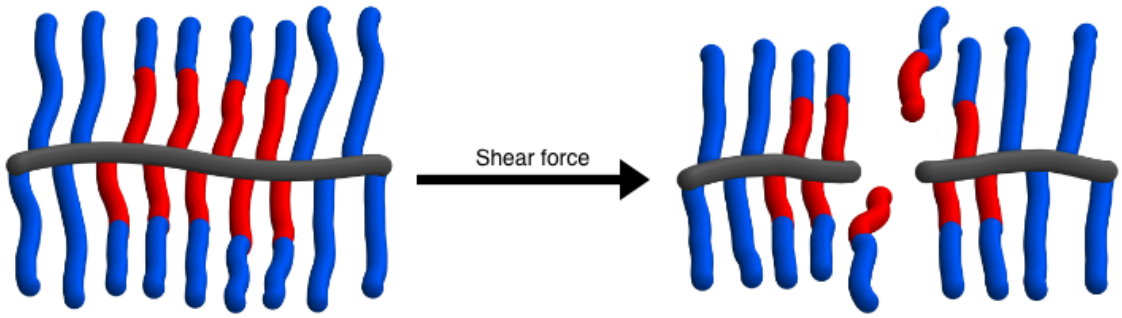

Figure 55: Mechanosensitive nanocapsule thermosets expose a reactive core in response to shear forces.

Steric repulsion between side chains of densely grafted bottlebrush polymers is known to induce significant tension along the polymer backbone, on the order of nanonewtons,[107] the same or higher than the force required to break C–C bonds.[77,84] These prestrained brushes may be easier to mechanochemically cleave, exposing the reactive core (Figure 55). Indeed, it has been shown that the limiting contour length for bottlebrush polymers is dramatically shorter than linear polymers, and bottlebrush polymers approach this limit under sonication much more quickly.[269] Other methods of inducing strain, such as parallel plate shear or extrusion, may be able to "activate" molecular brushes with a reactive core more easily, particularly those in the stretched backbone regime or those adsorbed to surfaces, which can experience up to 100 nN of tension along the backbone. Scission at the hair-backbone junction will also generate unshielded reactive linear polymers.[122,123,270] Further, the propensity for hairs to be released into solution can be tuned by weakening the alkoxyamine C–O bond with highly sterically hindered nitroxides (proposed structure **1**),[271,272] or by preparing bottlebrush polymers in the stretched side chain regime.

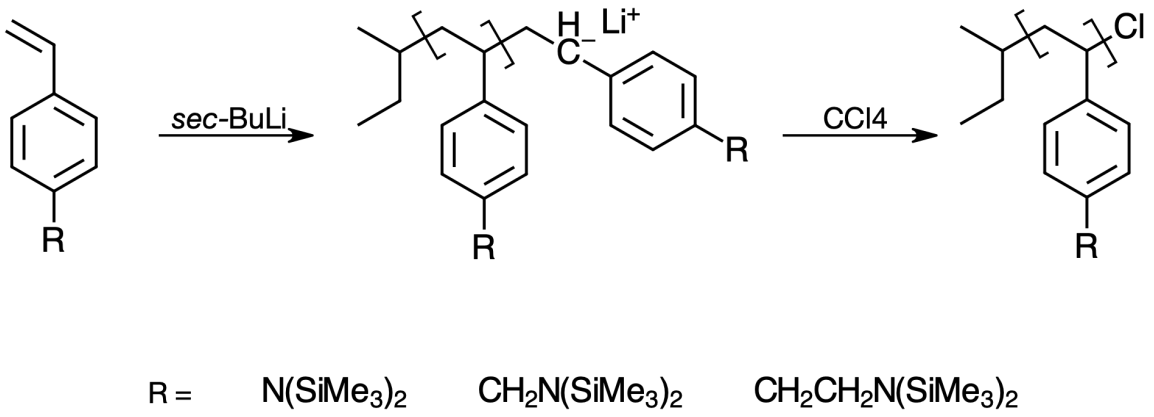

Figure 56: Proposed polymerization and chain-end chlorination of amine functional styrenes.

Complementary amine functionalized bottlebrush crosslinkers should be prepared as well. Amine functional styrenes protected with trimethylsilane groups have been prepared by living anionic polymerization.[273] Carbanion chain ends of polymers prepared by living anionic polymerization can be easily converted to terminal chlorines for use in ATNRC (Figure 56).[274] It's possible that protected amine functional styrenes could be directly polymerized by ATRP, though aryl amines (R = NH_2) will likely polymerize slowly if at all by increasing the dissociation energy of the chain end carbon-halogen bond and slowing propagation.[275] Choosing a strongly hydrogen bonding solvent may be able to overcome this by reducing the electron donating ability of the amine through intermolecular interactions. There are some reports of polymerization of unprotected 4-(vinylaniline) by ATRP.[276] In any case, the amines should remain protected until use as they will both deactivate the ROMP catalyst preventing bottlebrush synthesis[277] and the unprotected amines are unstable in air.[278]

Alternative reactive monomers include 4-vinylphenyloxirane, 4-vinylphenyl glycidyl ether, 4-vinylphenol, 4-vinylthiophenol, 4-(2-mercaptoethyl)styrene, and 4-vinylbenzoic acid.

5.4.3 Xanthogen disulfide optimization and hydrogel stereolithography

The design and synthesis of chain transfer agents for the RAFT process has been much studied since the process was first introduced.[161] RAFT agents typically take the form of **2** (Figure 57). The Z group (in this case O-ethyl) is generally responsible for modifying the rate of addition of propagating radicals and the rate of fragmentation of intermediate

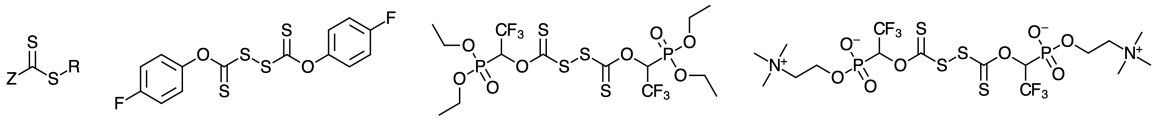

2 **3** **4** **5**

Figure 57: Proposed xanthate structures.

radicals in the main RAFT equilibrium. R is generally meant to act as an excellent homolytic leaving group capable of initiating polymerization. I use a symmetrical xanthogen disulfide, meaning modifications to the R group can be ignored.

Xanthogens (Z = OR′) are chiefly used for the polymerization of less activated monomers. Xanthates have dramatically lower reactivity towards radical addition, qualitatively understood by the resonance contribution of the oxygen lone pair to the C=S double bond, meaning more activated monomers ((meth)acryloyl monomers) which produce less reactive radical species do contributing to lower transfer constants of the xanthate and poorer control. However, the C=S double bond can be made more reactive by lessening the contribution of the oxygen lone pair by installing electron withdrawing groups attached to the oxygen, lessening the contribution of the oxygen lone pair on the C=S double bond. Xanthates possessing the Z groups of **3**[253] and **4**[279] have shown superior control over polymerization of acrylic monomers, importantly with no change in polymerization kinetics, and should be explored as xanthogen disulfide photoiniferters.

More pressingly for biomedical applications is the solubility of the chain transfer agent. My chosen xanthate is easy to synthesize, but is not water soluble, nor are **3** or **4**. Thus, I propose to develop zwitterionic xanthogen disulfides as photoiniferters. **5** will likely provide excellent control of acryloyl functional monomers and excellent solubility.

It should be cautioned however that while adding electron withdrawing Z (where Z is O–R' and R' is alkyl or aryl) groups to the RAFT agent will improve the control of certain monomers, it will also increase the susceptibility of it to aminolysis and hydrolysis, which will complicate cytocompatible polymerizations in water.[254,280] Tertiary alcohols should be avoided such that Z does not become a good homolytic leaving group.[281,282]

Additionally, I propose to utilize the dormant xanthogen chain ends to introduce and pattern hydrogels post polymerization. The 3D network structure of synthetic hydrogels nicely mimics the mechanical properties of the native cellular environment, but not the chemical properties. Synthetic materials, like PEG, tend to be both chemically inert and difficult to for cells to adhere to, long noted for their antifouling properties.[144] Hydrogels should be selectively functionalized by stereolithography with RGD adhesion points, as well as selectively increasing or decreasing the modulus of hydrogels. The necessary N-acryloyl functional oligopeptides are conveniently accessible by protease catalyzed peptide synthesis,[283] and some work has been done polymerizing N-acryloyl amino acids.[284,285]

Bibliography

(1) Krueger, J. I. Gonzalo Guerrero and the Psychology of Identity. *Current Research Journal of Social Sciences and Humanities* **2021**, *4* (2), 122–132.

(2) Pérez, N. A.; Guzmán, V. H.; Ruvalcaba, J. L.; Lucio, O. G. de; Pérez, M.; Nagaya, A.; Cano, N.; Mitrani, A.; Esquivel, B.; Tapia, E.; León, M.; Pilar Ponce, M. del; Carmen Rodríguez, M. del; Ortiz, P. Unraveling the Olmec Rubber Balls from El Manatí, Mexico: A Technological and Compositional Analysis. *Archaeological and Anthropological Sciences* **2024**, *16* (2), 0.

(3) Hickenboth, C. R.; Moore, J. S.; White, S. R.; Sottos, N. R.; Baudry, J.; Wilson, S. R. Biasing Reaction Pathways with Mechanical Force. *Nature* **2007**, *446* (7134), 423–427.

(4) Coe, M. *America's First Civilization*; New Word City, 2017.

(5) Diehl, R. *The Olmecs: America's First Civilization*; Thames \& Hudson, 2004.

(6) Tarkanian, M. J.; Hosler, D. America's First Polymer Scientists: Rubber Processing, Use and Transport in Mesoamerica. *Latin American Antiquity* **2011**, *22* (4), 469–486.

(7) Hosler, D.; Burkett, S. L.; Tarkanian, M. J. Prehistoric Polymers: Rubber Processing in Ancient Mesoamerica. *Science* **1999**, *284* (5422), 1988–1991.

(8) Tarkanian, M. Prehistoric Polymer Engineering: A Study of Rubber Technology in the Americas. *dspace.mit.edu* **2003**.

(9) Ricarte, R. G.; Shanbhag, S. A Tutorial Review of Linear Rheology for Polymer Chemists: Basics and Best Practices for Covalent Adaptable Networks. *Polymer Chemistry* **2024**, *15* (9), 815–846.

(10) Wake, W. C.; Tidd, B. K.; Loadman, M. J. R. *Analysis of Rubber and Rubber-Like Polymers*; Elsevier Science & Technology, 1983; p 358.

(11) Fisher, H. L. VULCANIZATION OF RUBBER Vulcanization of Rubber. *Industrial & Engineering Chemistry* **1939**, *31* (11), 1381–1389.

(12) Guise-Richardson, C. Redefining Vulcanization: Charles Goodyear, Patents, And Industrial Control, 1834-1865. *Technology and Culture* **2010**, *51* (2), 357–387.

(13) Baekeland, L. H. The Synthesis, Constitution, And Uses of Bakelite. *Journal of Industrial & Engineering Chemistry* **1909**, *1* (3), 149–161.

(14) Frey, H.; Johann, T. Celebrating 100 Years of ``polymer Science'': Hermann Staudinger's 1920 Manifesto. *Polymer Chemistry* **2020**, *11* (1), 8–14.

(15) Bruson, H. A.; Staudinger, H. ``cyclopentadiene Rubber'' A. New Cyclic Synthetic Polymerization Product. *Industrial & Engineering Chemistry* **1926**, *18* (4), 381–383.

(16) Veldman, B.; Kaully, T.; Feller, R. K.; Falcao, E.; Wudl, F. Staudinger's Poly(Cyclopentadiene): Sintering Processing of Poly(Diels–alder Cyclopentadiene). *Macromolecules* **2009**, *42* (18), 6848–6850.

(17) Diels, O.; Alder, K. Synthesen in Der Hydroaromatischen Reihe. *Justus Liebigs Annalen der Chemie* **1928**, *460* (1), 98–122.

(18) Flory, P. J. Molecular Size Distribution in Three Dimensional Polymers. I. Gelation1. *Journal of the American Chemical Society* **1941**, *63* (11), 3083–3090.

(19) Flory, P. J.; Rehner, J. Statistical Mechanics of Cross-Linked Polymer Networks II. Swelling. *The Journal of Chemical Physics* **1943**, *11* (11), 521–526.

(20) Flory, P. J.; Rehner, J. Statistical Mechanics of Cross-Linked Polymer Networks I. Rubberlike Elasticity. *The Journal of Chemical Physics* **1943**, *11* (11), 512–520.

(21) SZWARC, M. `living' Polymers. *Nature* **1956**, *178* (4543), 1168–1169.

(22) Georges, M. K.; Veregin, R. P. N.; Kazmaier, P. M.; Hamer, G. K. Narrow Molecular Weight Resins by a Free-Radical Polymerization Process. *Macromolecules* **1993**, *26* (11), 2987–2988.

(23) Kato, M.; Kamigaito, M.; Sawamoto, M.; Higashimura, T. Polymerization of Methyl Methacrylate with the Carbon Tetrachloride/dichlorotris- (Triphenylphosphine)ruthenium(Ii)/methylaluminum Bis(2,6-Di-Tert-Butylphenoxide) Initiating

System: Possibility of Living Radical Polymerization. *Macromolecules* **1995**, *28* (5), 1721–1723.

(24) Wang, J.-S.; Matyjaszewski, K. Controlled/"living" Radical Polymerization. Atom Transfer Radical Polymerization in the Presence of Transition-Metal Complexes. *Journal of the American Chemical Society* **1995**, *117* (20), 5614–5615.

(25) Chiefari, J.; Chong, Y. K. (.; Ercole, F.; Krstina, J.; Jeffery, J.; Le, T. P. T.; Mayadunne, R. T. A.; Meijs, G. F.; Moad, C. L.; Moad, G.; Rizzardo, E.; Thang, S. H. Living Free-Radical Polymerization by Reversible Addition–fragmentation Chain Transfer: The RAFT Process. *Macromolecules* **1998**, *31* (16), 5559–5562.

(26) Alabiso, W.; Schlögl, S. The Impact of Vitrimers on the Industry of the Future: Chemistry, Properties and Sustainable Forward-Looking Applications. *Polymers (Basel)* **2020**, *12* (8), 1660.

(27) Ma, X.; Wu, Y.; Liang, N.; Xu, H.; Xu, Z.; Chen, S.; Zhang, D. High-Efficiently Renewable Hyperbranched Epoxy Resin/carbon Fiber Composites with Both Long Service Life and High Performance. *Composites Communications* **2023**, *40*, 101630.

(28) Wang, C.; Singh, A.; Rognerud, E. G.; Murray, R.; Musgrave, G. M.; Skala, M.; Murdy, P.; DesVeaux, J. S.; Nicholson, S. R.; Harris, K.; Canty, R.; Mohr, F.; Shapiro, A. J.; Barnes, D.; Beach, R.; Allen, R. D.; Beckham, G. T.; Rorrer, N. A. Synthesis, Characterization, And Recycling of Bio-Derivable Polyester Covalently Adaptable Networks for Industrial Composite Applications. *Matter* **2024**, *7* (2), 550–568.

(29) Reynolds, V. G.; Mukherjee, S.; Xie, R.; Levi, A. E.; Atassi, A.; Uchiyama, T.; Wang, H.; Chabinyc, M. L.; Bates, C. M. Super-Soft Solvent-Free Bottlebrush Elastomers for Touch Sensing. *Materials Horizons* **2020**, *7* (1), 181–187.

(30) Jansen, L. E.; Kim, H.; Hall, C. L.; McCarthy, T. P.; Lee, M. J.; Peyton, S. R. A Poly(Ethylene Glycol) Three-Dimensional Bone Marrow Hydrogel. *Biomaterials* **2022**, *280*, 121270.

(31) Arrington, K. J.; Radzinski, S. C.; Drummey, K. J.; Long, T. E.; Matson, J. B. Reversibly Cross-Linkable Bottlebrush Polymers as Pressure-Sensitive Adhesives. *ACS Applied Materials & Interfaces* **2018**, *10* (31), 26662–26668.

(32) Lee, T.-I.; Kim, C.; Kim, M. S.; Kim, T.-S. Flexural and Tensile Moduli of Flexible Fr4 Substrates. *Polymer Testing* **2016**, *53*, 70–76.

(33) Kathalewar, M.; Sabnis, A. Epoxy Resin from Cardanol as Partial Replacement of Bisphenol-a-Based Epoxy for Coating Application. *Journal of Coatings Technology and Research* **2014**, *11* (4), 601–618.

(34) Li, W.; Xiao, L.; Huang, J.; Wang, Y.; Nie, X.; Chen, J. Bio-Based Epoxy Vitrimer for Recyclable and Carbon Fiber Reinforced Materials: Synthesis and Structure-Property Relationship. *Composites Science and Technology* **2022**, *227*, 109575.

(35) Engels, H.-W.; Weidenhaupt, H.-J.; Pieroth, M.; Hofmann, W.; Menting, K.-H.; Mergenhagen, T.; Schmoll, R.; Uhrlandt, S. Rubber, 4. Chemicals and Additives. **2004**, 6.

(36) Abliz, D.; Duan, Y.; Steuernagel, L.; Xie, L.; Li, D.; Ziegmann, G. Curing Methods for Advanced Polymer Composites - a Review. *Polymers and Polymer Composites* **2013**, *21* (6), 341–348.

(37) Raghavan, J.; Baillie, M. R. Electron Beam Curing of Polymer Composites. *Polymer Composites* **2000**, *21* (4), 619–629.

(38) Ernst, O. P.; Lodowski, D. T.; Elstner, M.; Hegemann, P.; Brown, L. S.; Kandori, H. Microbial and Animal Rhodopsins: Structures, Functions, And Molecular Mechanisms. *Chem Rev* **2014**, *114* (1), 126–163.

(39) VISHNIAC, W.; ROSE, I. A. Mechanism of Chlorophyll Action in Photosynthesis. *Nature* **1958**, *182* (4642), 1089–1090.

(40) Shanmugam, S.; Xu, J.; Boyer, C. Utilizing the Electron Transfer Mechanism of Chlorophyll a under Light for Controlled Radical Polymerization. *Chemical Science* **2015**, *6* (2), 1341–1349.

(41) Kumar, P. Sensing Hypoxia in the Carotid Body: From Stimulus to Response. *Essays Biochem* **2007**, *43*, 43–60.

(42) Damaghi, M.; Wojtkowiak, J. W.; Gillies, R. J. Ph Sensing and Regulation in Cancer. *Front Physiol* **2013**, *4*, 370.

(43) Tan, C. L.; Cooke, E. K.; Leib, D. E.; Lin, Y.-C.; Daly, G. E.; Zimmerman, C. A.; Knight, Z. A. Warm-Sensitive Neurons That Control Body Temperature. *Cell* **2016**, *167* (1), 47–59.e15.

(44) Eyckmans, J.; Boudou, T.; Yu, X.; Chen, C. S. A Hitchhiker's Guide to Mechanobiology. *Dev Cell* **2011**, *21* (1), 35–47.

(45) Gee, E. P. S.; Ingber, D. E.; Stultz, C. M. Fibronectin Unfolding Revisited: Modeling Cell Traction-Mediated Unfolding of the Tenth Type-III Repeat. *PLOS ONE* **2008**, *3* (6), e2373.

(46) Gee, E. P. S.; Yüksel, D.; Stultz, C. M.; Ingber, D. E. SLLISWD Sequence in the 10fniii Domain Initiates Fibronectin Fibrillogenesis. *Journal of Biological Chemistry* **2013**, *288* (29), 21329–21340.

(47) Klotzsch, E.; Smith, M. L.; Kubow, K. E.; Muntwyler, S.; Little, W. C.; Beyeler, F.; Gourdon, D.; Nelson, B. J.; Vogel, V. Fibronectin Forms the Most Extensible Biological Fibers Displaying Switchable Force-Exposed Cryptic Binding Sites. *Proceedings of the National Academy of Sciences* **2009**, *106* (43), 18267–18272.

(48) Mao, Y.; Schwarzbauer, J. E. Fibronectin Fibrillogenesis, A Cell-Mediated Matrix Assembly Process. *Matrix Biology* **2005**, *24* (6), 389–399.

(49) Dupont, S.; Wickström, S. A. Mechanical Regulation of Chromatin and Transcription. *Nature Reviews Genetics* **2022**.

(50) Lee, J.; Silberstein, M. N.; Abdeen, A. A.; Kim, S. Y.; Kilian, K. A. Mechanochemical Functionalization of Disulfide Linked Hydrogels. *Materials Horizons* **2016**, *3* (5), 447–451.

(51) Tran, Y. H.; Rasmuson, M. J.; Emrick, T.; Klier, J.; Peyton, S. R. Strain-Stiffening Gels Based on Latent Crosslinking. *Soft Matter* **2017**, *13* (47), 9007–9014.

(52) Sonu, K. P.; Zhou, L.; Biswas, S.; Klier, J.; Balazs, A. C.; Emrick, T.; Peyton, S. R. Strain-Stiffening Hydrogels with Dynamic, Secondary Cross-Linking. *Langmuir* **2023**, *39* (7), 2659–2666.

(53) Rubinstein, M.; Colby, R. H. Polymer Physics. **2003**, 4653.

(54) Graham, M. D. Fluid Dynamics of Dissolved Polymer Molecules in Confined Geometries. *Annual Review of Fluid Mechanics* **2011**, *43* (1), 273–298.

(55) Boger, D. V. Viscoelastic Flows Through Contractions. *Annual Review of Fluid Mechanics* **1987**, *19* (1), 157–182.

(56) Akbulatov, S.; Boulatov, R. Experimental Polymer Mechanochemistry and Its Interpretational Frameworks. *Chemphyschem* **2017**, *18* (11), 1422–1450.

(57) Diesendruck, C. E. How Polymers Dance to the Pulses of Ultrasound. *Nature Chemistry* **2023**, *15* (9), 1199–1201.

(58) O'Neill, R. T.; Boulatov, R. Experimental Quantitation of Molecular Conditions Responsible for Flow-Induced Polymer Mechanochemistry. *Nature Chemistry* **2023**, *15* (9), 1214–1223.

(59) Schmid, G.; Rommel, O. Zerreißen Von Makromolekülen Mit Ultraschall. *Zeitschrift für Physikalische Chemie* **1939**, No. 1, 97–139.

(60) Paulusse, J. M. J.; Sijbesma, R. P. Ultrasound in Polymer Chemistry: Revival of an Established Technique. *Journal of Polymer Science Part A: Polymer Chemistry* **2006**, *44* (19), 5445–5453.

(61) Kuang, X.; Rong, Q.; Belal, S.; Vu, T.; López López, A. M.; Wang, N.; Arıcan, M. O.; Garciamendez-Mijares, C. E.; Chen, M.; Yao, J.; Zhang, Y. S. Self-Enhancing Sono-Inks Enable Deep-Penetration Acoustic Volumetric Printing. *Science* **2023**, *382* (6675), 1148–1155.

(62) Biswal, A. K.; Nandi, A.; Wang, H.; Vashisth, A. Ultrasonic Welding of Fiber Reinforced Vitrimer Composites. *Composites Science and Technology* **2023**, *242*, 110202.

(63) Staudinger, H.; Bondy, H. F. Über Isopren Und Kautschuk, 19. Mitteil.: Über Die Molekülgröße Des Kautschuks Und Der Balata. *Berichte der deutschen chemischen Gesellschaft (A and B Series)* **1930**, *63* (3), 734–736.

(64) Staudinger, H.; Leupold, E. O. Über Isopren Und Kautschuk, 18. Mitteil.: Viscositäts-untersuchungen an Balata. *Berichte der deutschen chemischen Gesellschaft (A and B Series)* **1930**, *63* (3), 730–733.

(65) Staudinger, H.; Heuer, W. Über Hochpolymere Verbindungen, 93. Mitteil.: Über Das Zerreißen Der Faden-moleküle Des Poly-styrols. *Berichte der deutschen chemischen Gesellschaft (A and B Series)* **1934**, *67* (7), 1159–1164.

(66) Kauzmann, W.; Eyring, H. The Viscous Flow of Large Molecules. *Journal of the American Chemical Society* **1940**, *62* (11), 3113–3125.

(67) Tabata, M.; Miyazawa, T.; Kobayashi, O.; Sohma, J. Direct Evidence of Main-Chain Scissions Induced by Ultrasonic Irradiation of Benzene Solutions of Polymers. *Chemical Physics Letters* **1980**, *73* (1), 178–180.

(68) Encina, M. V.; Lissi, E.; Sarasúa, M.; Gargallo, L.; Radic, D. Ultrasonic Degradation of Polyvinylpyrrolidone: Effect of Peroxide Linkages. *Journal of Polymer Science: Polymer Letters Edition* **1980**, *18* (12), 757–760.

(69) Berkowski, K. L.; Potisek, S. L.; Hickenboth, C. R.; Moore, J. S. Ultrasound-Induced Site-Specific Cleavage of Azo-Functionalized Poly(Ethylene Glycol). *Macromolecules* **2005**, *38* (22), 8975–8978.

(70) Li, J.; Nagamani, C.; Moore, J. S. Polymer Mechanochemistry: From Destructive to Productive. *Acc Chem Res* **2015**, *48* (8), 2181–2190.

(71) Woodward, R. B.; Hoffmann, R. The Conservation of Orbital Symmetry. *Angewandte Chemie International Edition in English* **1969**, *8* (11), 781–853.

(72) Raisch, M.; Genovese, D.; Zaccheroni, N.; Schmidt, S. B.; Focarete, M. L.; Sommer, M.; Gualandi, C. Highly Sensitive, Anisotropic, And Reversible Stress/strain-Sensors from Mechanochromic Nanofiber Composites. *Adv Mater* **2018**, *30* (39), e1802813.

(73) Groote, R.; Jakobs, R. T. M.; Sijbesma, R. P. Mechanocatalysis: Forcing Latent Catalysts into Action. *Polymer Chemistry* **2013**, *4* (18), 4846.

(74) Wang, J.; Piskun, I.; Craig, S. L. Mechanochemical Strengthening of a Multi-Mechanophore Benzocyclobutene Polymer. *ACS Macro Letters* **2015**, *4* (8), 834–837.

(75) Groote, R.; Szyja, B. M.; Leibfarth, F. A.; Hawker, C. J.; Doltsinis, N. L.; Sijbesma, R. P. Strain-Induced Strengthening of the Weakest Link: The Importance of Intermediate Geometry for the Outcome of Mechanochemical Reactions. *Macromolecules* **2014**, *47* (3), 1187–1192.

(76) Ramirez, A. L. B.; Kean, Z. S.; Orlicki, J. A.; Champhekar, M.; Elsakr, S. M.; Krause, W. E.; Craig, S. L. Mechanochemical Strengthening of a Synthetic Polymer in Response to Typically Destructive Shear Forces. *Nature Chemistry* **2013**, *5* (9), 757–761.

(77) Willis-Fox, N.; Rognin, E.; Aljohani, T. A.; Daly, R. Polymer Mechanochemistry: Manufacturing Is Now a Force to Be Reckoned with. *Chem* **2018**, *4* (11), 2499–2537.

(78) Ghanem, M. A.; Basu, A.; Behrou, R.; Boechler, N.; Boydston, A. J.; Craig, S. L.; Lin, Y.; Lynde, B. E.; Nelson, A.; Shen, H. The Role of Polymer Mechanochemistry in Responsive Materials and Additive Manufacturing. *Nature Reviews Materials* **2021**, *6* (1), 84–98.

(79) Brantley, J. N.; Wiggins, K. M.; Bielawski, C. W. Polymer Mechanochemistry: The Design and Study of Mechanophores. *Polymer International* **2013**, *62* (1), 2–12.

(80) Kean, Z. S.; Niu, Z.; Hewage, G. B.; Rheingold, A. L.; Craig, S. L. Stress-Responsive Polymers Containing Cyclobutane Core Mechanophores: Reactivity and Mechanistic Insights. *Journal of the American Chemical Society* **2013**, *135* (36), 13598–13604.

(81) Kean, Z. S.; Gossweiler, G. R.; Kouznetsova, T. B.; Hewage, G. B.; Craig, S. L. A Coumarin Dimer Probe of Mechanochemical Scission Efficiency in the Sonochemical

Activation of Chain-Centered Mechanophore Polymers. *Chemical Communications* **2015**, *51* (44), 9157–9160.

(82) Jung, S.; Yoon, H. J. Heterocyclic Mechanophores in Polymer Mechanochemistry. *Synlett* **2021**, a–1703.

(83) Lloyd, E. M.; Vakil, J. R.; Yao, Y.; Sottos, N. R.; Craig, S. L. Covalent Mechanochemistry and Contemporary Polymer Network Chemistry: A Marriage in the Making. *J Am Chem Soc* **2023**, *145* (2), 751–768.

(84) Grandbois, M.; Beyer, M.; Rief, M.; Clausen-Schaumann, H.; Gaub, H. E. How Strong Is a Covalent Bond?. *Science* **1999**, *283* (5408), 1727–1730.

(85) Garnier, L.; Gauthier-Manuel, B.; Vegte, E. W. van der; Snijders, J.; Hadziioannou, G. Covalent Bond Force Profile and Cleavage in a Single Polymer Chain. *The Journal of Chemical Physics* **2000**, *113* (6), 2497–2503.

(86) Rehberg, C. E.; Fisher, C. H. Preparation and Properties of the n-Alkyl Acrylates. *Journal of the American Chemical Society* **1944**, *66* (7), 1203–1207.

(87) Kaufman, H. S.; Sacher, A.; Alfrey, T.; Fankuchen, I. SIDE-CHAIN CRYSTALLIZATION IN ALKYL POLYACRYLATES. *Journal of the American Chemical Society* **1948**, *70* (9), 3147.

(88) Platé, N. A.; Shibaev, V. P. Comb-like Polymers. Structure and Properties. *Journal of Polymer Science: Macromolecular Reviews* **1974**, *8* (1), 117–253.

(89) Vaughn, T. H.; Suter, H. R.; Lundsted, L. G.; Kramer, M. G. Properties of Some Newly Developed Nonionic Detergents. *Journal of the American Oil Chemists' Society* **1951**, *28* (7), 294–299.

(90) Mankowich, A. Micellar Molecular Weights of Selected Surface Active Agents. *The Journal of Physical Chemistry* **1954**, *58* (11), 1027–1030.

(91) Surve, D.; Fish, A.; Debnath, M.; Pinjari, A.; Lorenzana, A.; Piya, S.; Peyton, S.; Kulkarni, A. Sprayable Inflammasome-Inhibiting Lipid Nanorods in a Polymeric Scaffold for Psoriasis Therapy. *Nature Communications* **2024**, *15* (1), 0.

(92) Hadjichristidis, N.; Iatrou, H.; Pitsikalis, M.; Mays, J. Macromolecular Architectures by Living and Controlled/living Polymerizations. *Progress in Polymer Science* **2006**, *31* (12), 1068–1132.

(93) Rempp, P.; Lutz, P.; Masson, P.; Franta, E. Macromonomers - a New Class of Polymeric Intermediates in Macromolecular Synthesis. I - Synthesis and Characterization. *Die Makromolekulare Chemie* **1984**, *8* (S19841), 3–15.

(94) Rempp, P.; Lutz, P.; Masson, P.; Chaumont, P. Macromonomers: A New Class of Polymeric Intermediates in Macromolecular Synthesis - II - Homo- and Copolymerization. *Die Makromolekulare Chemie* **1985**, *13* (S19851), 47–66.

(95) Tsukahara, Y.; Mizuno, K.; Segawa, A.; Yamashita, Y. Study on the Radical Polymerization Behavior of Macromonomers. *Macromolecules* **1989**, *22* (4), 1546–1552.

(96) Tsukahara, Y.; Kohjiya, S.; Tsutsumi, K.; Okamoto, Y. On the Intrinsic Viscosity of Poly(Macromonomer)s. *Macromolecules* **1994**, *27* (6), 1662–1664.

(97) Muehlebach, A.; Rime, F. Synthesis of Well-defined Macromonomers and Comb Copolymers from Polymers Made by Atom Transfer Radical Polymerization. *Journal of Polymer Science Part A: Polymer Chemistry* **2003**, *41* (21), 3425–3439.

(98) Motte, S.; Kaufman, L. J. Strain Stiffening in Collagen I Networks. *Biopolymers* **2013**, *99* (1), 35–46.

(99) Lessard, J. J.; Scheutz, G. M.; Sung, S. H.; Lantz, K. A.; Epps, T. H.; Sumerlin, B. S. Block Copolymer Vitrimers. *Journal of the American Chemical Society* **2020**, *142* (1), 283–289.

(100) Claesson, H.; Scheurer, C.; Malmström, E.; Johansson, M.; Hult, A.; Paulus, W.; Schwalm, R. Semi-Crystalline Thermoset Resins: Tailoring Rheological Properties in Melt Using Comb Structures with Crystalline Grafts. *Progress in Organic Coatings* **2004**, *49* (1), 13–22.

(101) Lorenzana, A. A.; Naing, H. S. Y.; Song, J.; Schiffman, J. D.; Klier, J.; Peyton, S. R. Molecularly Shielded, On-Demand, Ultrasound-Cured Polymer Networks. *Macromolecules* **2024**, *57* (14), 6465–6473.

(102) Kong, D.; Yang, M.; Zhang, X.; Du, Z.; Fu, Q.; Gao, X.; Gong, J. Control of Polymer Properties by Entanglement: A Review. *Macromolecular Materials and Engineering* **2021**, *306* (12), 95.

(103) A New Generation of High Performance Viscosity Modifiers Based on Comb Polymers. *SAE International Journal of Fuels and Lubricants* **2009**, 1511–1516.

(104) Dong, W.; Wang, H.; He, M.; Ren, F.; Wu, T.; Zheng, Q.; Li, Y. Synthesis of Reactive Comb Polymers and Their Applications as a Highly Efficient Compatibilizer in Immiscible Polymer Blends. *Industrial & Engineering Chemistry Research* **2015**, *54* (7), 2081–2089.

(105) Zhang, J.; Schneiderman, D. K.; Li, T.; Hillmyer, M. A.; Bates, F. S. Design of Graft Block Polymer Thermoplastics. *Macromolecules* **2016**, *49* (23), 9108–9118.

(106) Ohnsorg, M. L.; Mash, K. M.; Khang, A.; Rao, V. V.; Kirkpatrick, B. E.; Bera, K.; Anseth, K. S. Nonlinear Elastic Bottlebrush Polymer Hydrogels Modulate Actomyosin Mediated Protrusion Formation in Mesenchymal Stromal Cells. *Adv Mater* **2024**, *36* (28), e2403198.

(107) Panyukov, S.; Zhulina, E. B.; Sheiko, S. S.; Randall, G. C.; Brock, J.; Rubinstein, M. Tension Amplification in Molecular Brushes in Solutions and on Substrates. *J Phys Chem B* **2009**, *113* (12), 3750–3768.

(108) Sheiko, S. S.; Dobrynin, A. V. Architectural Code for Rubber Elasticity: From Supersoft to Superfirm Materials. *Macromolecules* **2019**, *52* (20), 7531–7546.

(109) Xie, G.; Martinez, M. R.; Olszewski, M.; Sheiko, S. S.; Matyjaszewski, K. Molecular Bottlebrushes as Novel Materials. *Biomacromolecules* **2019**, *20* (1), 27–54.

(110) Dalsin, S. J.; Hillmyer, M. A.; Bates, F. S. Molecular Weight Dependence of Zero-Shear Viscosity in Atactic Polypropylene Bottlebrush Polymers. *ACS Macro Lett* **2014**, *3* (5), 423–427.

(111) Liang, H.; Morgan, B. J.; Xie, G.; Martinez, M. R.; Zhulina, E. B.; Matyjaszewski, K.; Sheiko, S. S.; Dobrynin, A. V. Universality of the Entanglement Plateau Modulus of Comb and Bottlebrush Polymer Melts. *Macromolecules* **2018**, *51* (23), 10028–10039.

(112) Liang, H.; Cao, Z.; Wang, Z.; Sheiko, S. S.; Dobrynin, A. V. Combs and Bottlebrushes in a Melt. *Macromolecules* **2017**, *50* (8), 3430–3437.

(113) Dalsin, S. J.; Rions-Maehren, T. G.; Beam, M. D.; Bates, F. S.; Hillmyer, M. A.; Matsen, M. W. Bottlebrush Block Polymers: Quantitative Theory and Experiments. *ACS Nano* **2015**, *9* (12), 12233–12245.

(114) Pan, T.; Patel, B. B.; Walsh, D. J.; Dutta, S.; Guironnet, D.; Diao, Y.; Sing, C. E. Implicit Side-Chain Model and Experimental Characterization of Bottlebrush Block Copolymer Solution Assembly. *Macromolecules* **2021**, *54* (8), 3620–3633.

(115) Bates, C. M.; Bates, F. S. 50th Anniversary Perspective: Block Polymers—Pure Potential. *Macromolecules* **2017**, *50* (1), 3–22.

(116) Dutta, S.; A. Wade, M.; J. Walsh, D.; Guironnet, D.; A. Rogers, S.; E. Sing, C. Dilute Solution Structure of Bottlebrush Polymers. *Soft Matter* **2019**, *15* (14), 2928–2941.

(117) Lecommandoux, S.; Chécot, F.; Borsali, R.; Schappacher, M.; Deffieux, A.; Brûlet, A.; Cotton, J. P. Effect of Dense Grafting on the Backbone Conformation of Bottlebrush Polymers: Determination of the Persistence Length in Solution. *Macromolecules* **2002**, *35* (23), 8878–8881.

(118) Feuz, L.; Leermakers, F. A. M.; Textor, M.; Borisov, O. Bending Rigidity and Induced Persistence Length of Molecular Bottle Brushes:‚äâ a Self-Consistent-Field Theory. *Macromolecules* **2005**, *38* (21), 8891–8901.

(119) Yethiraj, A. A Monte Carlo Simulation Study of Branched Polymers. *J Chem Phys* **2006**, *125* (20), 204901.

(120) Clarke, B.; Witt, C.; Ilton, M.; Crosby, A.; Watkins, J.; Tew, G. Bottlebrush Networks: A Primer for Advanced Architectures. *Angew Chem Int Ed Engl* **2024**, *63* (22), e202318220.

(121) Moon, J.; Huh, Y.; Kim, S.; Choe, Y.; Bang, J. Reactive Core-Shell Bottlebrush Copolymer as Highly Effective Additive for Epoxy Toughening. *Chinese Journal of Polymer Science* **2021**, *39* (12), 1626–1633.

(122) Noh, J.; Peterson, G.; Choi, T. Mechanochemical Reactivity of Bottlebrush and Dendronized Polymers: Solid Vs. Solution States. *Angew Chem Int Ed Engl* **2021**, *60* (34), 18651–18659.

(123) Peterson, G. I.; Choi, T.-L. The Influence of Polymer Architecture in Polymer Mechanochemistry. *Chemical Communications* **2021**, *57* (53), 6465–6474.

(124) Maw, M. R.; Tanas, A. K.; Dashtimoghadam, E.; Nikitina, E. A.; Ivanov, D. A.; Dobrynin, A. V.; Vatankhah-Varnosfaderani, M.; Sheiko, S. S. Bottlebrush Thermoplastic Elastomers as Hot-Melt Pressure-Sensitive Adhesives. *ACS Appl Mater Interfaces* **2023**, *15* (35), 41870–41879.

(125) Daniel, W. F. M.; Burdy≈Ñska, J.; Vatankhah-Varnoosfaderani, M.; Matyjaszewski, K.; Paturej, J.; Rubinstein, M.; Dobrynin, A. V.; Sheiko, S. S. Solvent-Free, Supersoft and Superelastic Bottlebrush Melts and Networks. *Nature Materials* **2016**, *15* (2), 183–189.

(126) Huang, K.; Jacobs, A.; Rzayev, J. De Novo Synthesis and Cellular Uptake of Organic Nanocapsules with Tunable Surface Chemistry. *Biomacromolecules* **2011**, *12* (6), 2327–2334.

(127) Yoshikawa, C.; Takagi, R.; Nakaji-Hirabayashi, T.; Ochi, T.; Kawamura, Y.; Thissen, H. Marine Antifouling Coatings Based on Durable Bottlebrush Polymers. *ACS Applied Materials & Interfaces* **2022**, *14* (28), 32497–32509.

(128) Flemming, H.-C.; Wingender, J. The Biofilm Matrix. *Nat Rev Microbiol* **2010**, *8* (9), 623–633.

(129) Mouw, J. K.; Ou, G.; Weaver, V. M. Extracellular Matrix Assembly: A Multiscale Deconstruction. *Nature Reviews Molecular Cell Biology* **2014**, *15* (12), 771–785.

(130) Seifert, G. J.; Blaukopf, C. Irritable Walls: The Plant Extracellular Matrix and Signaling. *Plant Physiol* **2010**, *153* (2), 467–478.

(131) Ringer, P.; Colo, G.; Fässler, R.; Grashoff, C. Sensing the Mechano-Chemical Properties of the Extracellular Matrix. *Matrix Biol* **2017**, *64*, 6–16.

(132) Lantoine, J.; Grevesse, T.; Villers, A.; Delhaye, G.; Mestdagh, C.; Versaevel, M.; Mohammed, D.; Bruyère, C.; Alaimo, L.; Lacour, S. P.; Ris, L.; Gabriele, S. Matrix Stiffness Modulates Formation and Activity of Neuronal Networks of Controlled Architectures. *Biomaterials* **2016**, *89*, 14–24.

(133) Wei, J.; Yao, J.; Yan, M.; Xie, Y.; Liu, P.; Mao, Y.; Li, X. The Role of Matrix Stiffness in Cancer Stromal Cell Fate and Targeting Therapeutic Strategies. *Acta Biomater* **2022**, *150*, 34–47.

(134) Peyton, S. R.; Kim, P. D.; Ghajar, C. M.; Seliktar, D.; Putnam, A. J. The Effects of Matrix Stiffness and Rhoa on the Phenotypic Plasticity of Smooth Muscle Cells in a 3-D Biosynthetic Hydrogel System. *Biomaterials* **2008**, *29* (17), 2597–2607.

(135) Yeung, T.; Georges, P. C.; Flanagan, L. A.; Marg, B.; Ortiz, M.; Funaki, M.; Zahir, N.; Ming, W.; Weaver, V.; Janmey, P. A. Effects of Substrate Stiffness on Cell Morphology, Cytoskeletal Structure, And Adhesion. *Cell Motil Cytoskeleton* **2005**, *60* (1), 24–34.

(136) Lim, F.; Sun, A. M. Microencapsulated Islets as Bioartificial Endocrine Pancreas. *Science* **1980**, *210* (4472), 908–910.

(137) Kozlowski, M. T.; Crook, C. J.; Ku, H. T. Towards Organoid Culture Without Matrigel. *Commun Biol* **2021**, *4* (1), 1387.

(138) Danno, A. Gel Formation of Aqueous Solution of Polyvinyl Alcohol Irradiated by Gamma Rays from Cobalt-60. *Journal of the Physical Society of Japan* **1958**, *13* (7), 722–727.

(139) WICHTERLE, O.; LÍM, D. Hydrophilic Gels for Biological Use. *Nature* **1960**, *185* (4706), 117–118.

(140) Teichroeb, J. H.; Forrest, J. A.; Jones, L. W.; Chan, J.; Dalton, K. Quartz Crystal Microbalance Study of Protein Adsorption Kinetics on Poly(2-Hydroxyethyl Methacrylate). *J Colloid Interface Sci* **2008**, *325* (1), 157–164.

(141) Nicolson, P. C.; Vogt, J. Soft Contact Lens Polymers: An Evolution. *Biomaterials* **2001**, *22* (24), 3273–3283.

(142) Stafford, J. W. The Radiation Induced Reactions of Aqueous Polyethylene Oxide Solutions. I. Theory of Gelation. *Die Makromolekulare Chemie* **1970**, *134* (1), 57–69.

(143) King, P. A.; Ward, J. A. Radiation Chemistry of Aqueous Poly(Ethylene Oxide) Solutions. I. *Journal of Polymer Science Part A-1: Polymer Chemistry* **1970**, *8* (1), 253–262.

(144) Zhu, J. Bioactive Modification of Poly(Ethylene Glycol) Hydrogels for Tissue Engineering. *Biomaterials* **2010**, *31* (17), 4639–4656.

(145) Tanaka, A.; Yasuhara, S.; Osumi, M.; Fukui, S. Immobilization of Yeast Microbodies by Inclusion with Photo-Crosslinkable Resins. *Eur J Biochem* **1977**, *80* (1), 193–197.

(146) Graham, N. B.; McNeill, M. E. Hydrogels for Controlled Drug Delivery. *Biomaterials* **1984**, *5* (1), 27–36.

(147) Sakai, T.; Matsunaga, T.; Yamamoto, Y.; Ito, C.; Yoshida, R.; Suzuki, S.; Sasaki, N.; Shibayama, M.; Chung, U.-i. Design and Fabrication of a High-Strength Hydrogel with Ideally Homogeneous Network Structure from Tetrahedron-Like Macromonomers. *Macromolecules* **2008**, *41* (14), 5379–5384.

(148) Jansen, L. E.; Negrón-Piñeiro, L. J.; Galarza, S.; Peyton, S. R. Control of Thiol-Maleimide Reaction Kinetics in PEG Hydrogel Networks. *Acta Biomater* **2018**, *70*, 120–128.

(149) Buwalda, S. J.; Boere, K. W. M.; Dijkstra, P. J.; Feijen, J.; Vermonden, T.; Hennink, W. E. Hydrogels in a Historical Perspective: From Simple Networks to Smart Materials. *J Control Release* **2014**, *190*, 254–273.

(150) Metters, A.; Hubbell, J. Network Formation and Degradation Behavior of Hydrogels Formed by Michael-Type Addition Reactions. *Biomacromolecules* **2005**, *6* (1), 290–301.

(151) Caliari, S. R.; Burdick, J. A. A Practical Guide to Hydrogels for Cell Culture. *Nature Methods* **2016**, *13* (5), 405–414.

(152) Chen, A.; Davis, B. H. UV Irradiation Activates JNK and Increases Ai(I) Collagen Gene Expression in Rat Hepatic Stellate Cells. *Journal of Biological Chemistry* **1999**, *274* (1), 158–164.

(153) Peyton, S. R.; Raub, C. B.; Keschrumrus, V. P.; Putnam, A. J. The Use of Poly(Ethylene Glycol) Hydrogels to Investigate the Impact of ECM Chemistry and Mechanics on Smooth Muscle Cells. *Biomaterials* **2006**, *27* (28), 4881–4893.

(154) Galarza, S.; Crosby, A. J.; Pak, C.; Peyton, S. R. Control of Astrocyte Quiescence and Activation in a Synthetic Brain Hydrogel. *Adv Healthc Mater* **2020**, *9* (4), e1901419.

(155) Rizzo, R.; Petelinšek, N.; Bonato, A.; Zenobi-Wong, M. From Free-Radical to Radical-Free: A Paradigm Shift in Light-Mediated Biofabrication. *Adv Sci (Weinh)* **2023**, *10* (8), e2205302.

(156) Paez, J. I.; Farrukh, A.; Valbuena-Mendoza, R.; Włodarczyk-Biegun, M. K.; Del Campo, A. Thiol-Methylsulfone-Based Hydrogels for 3d Cell Encapsulation. *ACS Appl Mater Interfaces* **2020**, *12* (7), 8062–8072.

(157) Darling, N. J.; Hung, Y.-S.; Sharma, S.; Segura, T. Controlling the Kinetics of Thiol-Maleimide Michael-Type Addition Gelation Kinetics for the Generation of Homogenous Poly(Ethylene Glycol) Hydrogels. *Biomaterials* **2016**, *101*, 199–206.

(158) Corbin, D.; Miyake, G. Photoinduced Organocatalyzed Atom Transfer Radical Polymerization (O-ATRP): Precision Polymer Synthesis Using Organic Photoredox Catalysis. *Chem Rev* **2022**, *122* (2), 1830–1874.

(159) Grubbs, R. B. Nitroxide-Mediated Radical Polymerization: Limitations and Versatility. *Polymer Reviews* **2011**, *51* (2), 104–137.

(160) Guégain, E.; Guillaneuf, Y.; Nicolas, J. Nitroxide-Mediated Polymerization of Methacrylic Esters: Insights and Solutions to a Long-Standing Problem. *Macromol Rapid Commun* **2015**, *36* (13), 1227–1247.

(161) Keddie, D. J.; Moad, G.; Rizzardo, E.; Thang, S. H. RAFT Agent Design and Synthesis. *Macromolecules* **2012**, *45* (13), 5321–5342.

(162) Lovestead, T. M.; O'Brien, A. K.; Bowman, C. N. Models of Multivinyl Free Radical Photopolymerization Kinetics. *Journal of Photochemistry and Photobiology A: Chemistry* **2003**, *159* (2), 135–143.

(163) Gu, Y.; Zhao, J.; Johnson, J. A. Polymer Networks: From Plastics and Gels to Porous Frameworks. *Angew Chem Int Ed Engl* **2020**, *59* (13), 5022–5049.

(164) Peyton, S. R.; Chow, L. W.; Finley, S. D.; Versypt, A. N. F.; Hill, R.; Kemp, M. L.; Langer, E. M.; McGuigan, A. P.; Meyer, A. S.; Seidlits, S. K.; Roy, K.; Mumenthaler, S. M. Synthetic Living Materials in Cancer Biology. *Nature Reviews Bioengineering* **2023**, *1* (12), 972–988.

(165) Bagheri, A.; Fellows, C. M.; Boyer, C. Reversible Deactivation Radical Polymerization: From Polymer Network Synthesis to 3d Printing. *Adv Sci (Weinh)* **2021**, *8* (5), 2003701.

(166) Rimmer, S.; Johnson, C.; Zhao, B.; Collier, J.; Gilmore, L.; Sabnis, S.; Wyman, P.; Sammon, C.; Fullwood, N. J.; MacNeil, S. Epithelialization of Hydrogels Achieved by Amine Functionalization and Co-Culture with Stromal Cells. *Biomaterials* **2007**, *28* (35), 5319–5331.

(167) Villani, M.; Deshmukh, Y. S.; Camlibel, C.; Esteves, A. C. C.; With, G. d. Superior Relaxation of Stresses and Self-Healing Behavior of Epoxy-Amine Coatings. *RSC Advances* **2015**, *6* (1), 245–259.

(168) Wang, S.; Shuai, L.; Saha, B.; Vlachos, D. G.; Epps, T. H. From Tree to Tape: Direct Synthesis of Pressure Sensitive Adhesives from Depolymerized Raw Lignocellulosic Biomass. *ACS Central Science* **2018**, *4* (6), 701–708.

(169) Frounchi, M.; Dadbin, S.; Panahinia, F. Comparison between Electron-Beam and Chemical Crosslinking of Silicone Rubber. *Nuclear Instruments and Methods in Physics Research Section B: Beam Interactions with Materials and Atoms* **2006**, *243* (2), 354–358.

(170) Brown, A. E. X.; Litvinov, R. I.; Discher, D. E.; Purohit, P. K.; Weisel, J. W. Multiscale Mechanics of Fibrin Polymer: Gel Stretching with Protein Unfolding and Loss of Water. *Science* **2009**, *325* (5941), 741–744.

(171) Bu, T.; Wang, H.-C. E.; Li, H. Single Molecule Force Spectroscopy Reveals Critical Roles of Hydrophobic Core Packing in Determining the Mechanical Stability of Protein Gb1. *Langmuir* **2012**, *28* (33), 12319–12325.

(172) Smith, M. L.; Gourdon, D.; Little, W. C.; Kubow, K. E.; Eguiluz, R. A.; Luna-Morris, S.; Vogel, V. Force-Induced Unfolding of Fibronectin in the Extracellular Matrix of Living Cells. *PLOS Biology* **2007**, *5* (10), e268.

(173) Oberhauser, A. F.; Badilla-Fernandez, C.; Carrion-Vazquez, M.; Fernandez, J. M. The Mechanical Hierarchies of Fibronectin Observed with Single-Molecule AFM. *Journal of Molecular Biology* **2002**, *319* (2), 433–447.

(174) Kuijpers, M. W. A.; Iedema, P. D.; Kemmere, M. F.; Keurentjes, J. T. F. The Mechanism of Cavitation-Induced Polymer Scission; Experimental and Computational Verification. *Polymer* **2004**, *45* (19), 6461–6467.

(175) Lenhardt, J. M.; Black Ramirez, A. L.; Lee, B.; Kouznetsova, T. B.; Craig, S. L. Mechanistic Insights into the Sonochemical Activation of Multimechanophore Cyclopropanated Polybutadiene Polymers. *Macromolecules* **2015**, *48* (18), 6396–6403.

(176) Yu, X.; Liu, Q.; Wu, J.; Zhang, M.; Cao, X.; Zhang, S.; Wang, Q.; Chen, L.; Yi, T. Sonication-Triggered Instantaneous Gel-to-Gel Transformation. *Chemistry* **2010**, *16* (30), 9099–9106.

(177) Vidil, T.; Tournilhac, F.; Musso, S.; Robisson, A.; Leibler, L. Control of Reactions and Network Structures of Epoxy Thermosets. *Topical Volume on Polymer chemistry* **2016**, *62*, 126–179.

(178) Izunobi, J. U.; Higginbotham, C. L. Polymer Molecular Weight Analysis by #super[1]h NMR Spectroscopy. *Journal of Chemical Education* **2011**, *88* (8), 1098–1104.

(179) Ehlers, J.-E.; Rondan, N. G.; Huynh, L. K.; Pham, H.; Marks, M.; Truong, T. N. Theoretical Study on Mechanisms of the Epoxy–amine Curing Reaction. *Macromolecules* **2007**, *40* (12), 4370–4377.

(180) Gadwal, I.; Stuparu, M. C.; Khan, A. Homopolymer Bifunctionalization Through Sequential Thiol-Epoxy and Esterification Reactions: An Optimization, Quantification, And Structural Elucidation Study. *Polymer Chemistry* **2015**, *6* (8), 1393–1404.

(181) Winter, H. H.; Chambon, F. Analysis of Linear Viscoelasticity of a Crosslinking Polymer at the Gel Point. *Journal of Rheology* **1986**, *30* (2), 367–382.

(182) Chambon, F.; Winter, H. H. Stopping of Crosslinking Reaction in a PDMS Polymer at the Gel Point. *Polymer Bulletin* **1985**, *13* (6).

(183) Chambon, F.; Winter, H. H. Linear Viscoelasticity at the Gel Point of a Crosslinking PDMS with Imbalanced Stoichiometry. *Journal of Rheology* **1987**, *31* (8), 683–697.

(184) Poh, L.; Narimissa, E.; Wagner, M. H.; Winter, H. H. Interactive Shear and Extensional Rheology-25 Years of IRIS Software. *Rheologica Acta* **2022**, *61* (4), 259–269.

(185) Kong, Y.; Hay, J. The Measurement of the Crystallinity of Polymers by DSC. *Polymer* **2002**, *43* (14), 3873–3878.

(186) Dougan, C. E.; Song, Z.; Fu, H.; Crosby, A. J.; Cai, S.; Peyton, S. R. Cavitation Induced Fracture of Intact Brain Tissue. *Biophysical Journal* **2022**, *121* (14), 2721–2729.

(187) Barney, C. W.; Dougan, C. E.; McLeod, K. R.; Kazemi-Moridani, A.; Zheng, Y.; Ye, Z.; Tiwari, S.; Sacligil, I.; Riggleman, R. A.; Cai, S.; Lee, J.-H.; Peyton, S. R.; Tew, G. N.; Crosby, A. J. Cavitation in Soft Matter. *Proceedings of the National Academy of Sciences* **2020**, *117* (17), 9157–9165.

(188) Li, Z.; Tang, M.; Liang, S.; Zhang, M.; Biesold, G. M.; He, Y.; Hao, S.-M.; Choi, W.; Liu, Y.; Peng, J.; Lin, Z. Bottlebrush Polymers: From Controlled Synthesis, Self-Assembly, Properties to Applications. *Progress in Polymer Science* **2021**, *116*, 101387.

(189) T. Nguyen, L.-T.; Talha Gokmen, M.; Prez, F. E. D. Kinetic Comparison of 13 Homogeneous Thiol–X Reactions. *Polymer Chemistry* **2013**, *4* (22), 5527–5536.

(190) Flory, P. J. *Principles of Polymer Chemistry*; Cornell University Press, 1953; p 696.

(191) Ferry, J. D. *Viscoelastic Properties of Polymers*; John Wiley & Sons, 1980; p 676.

(192) Kulicke, W. M.; Nottelmann, H. Structure and Swelling of Some Synthetic, Semisynthetic, And Biopolymer Hydrogels. *Polymers in Aqueous Media*, 1989, 15–44.

(193) Hennrich, F.; Krupke, R.; Arnold, K.; Rojas St√°tz, J. A.; Lebedkin, S.; Koch, T.; Schimmel, T.; Kappes, M. M. The Mechanism of Cavitation-Induced Scission of Single-Walled Carbon Nanotubes. *The Journal of Physical Chemistry B* **2007**, *111* (8), 1932–1937.

(194) Lutz, J.-F.; Hoth, A. Preparation of Ideal PEG Analogues with a Tunable Thermosensitivity by Controlled Radical Copolymerization of 2-(2-Methoxyethoxy)ethyl Methacrylate and Oligo(Ethylene Glycol) Methacrylate. *Macromolecules* **2006**, *39* (2), 893–896.

(195) Daoud, M. Viscoelasticity near the Sol–gel Transition. *Macromolecules* **2000**, *33* (8), 3019–3022.

(196) Winter, H. H. Gel Point. *Encyclopedia of Polymer Science and Technology*, 2016, 1–15.

(197) Wang, K.; Pang, X.; Cui, S. Inherent Stretching Elasticity of a Single Polymer Chain with a Carbon,äìcarbon Backbone. *Langmuir* **2013**, *29* (13), 4315–4319.

(198) Hermes, M.; Boulatov, R. The Entropic and Enthalpic Contributions to Force-Dependent Dissociation Kinetics of the Pyrophosphate Bond. *Journal of the American Chemical Society* **2011**, *133* (50), 20044–20047.

(199) Shi, W.; Zhang, Y.; Liu, C.; Wang, Z.; Zhang, X.; Zhang, Y.; Chen, Y. Toward Understanding the Effect of Substitutes and Solvents on Entropic and Enthalpic Elasticity of Single Dendronized Copolymers. *Polymer* **2006**, *47* (7), 2499–2504.

(200) Cui, S.; Yu, Y.; Lin, Z. Modeling Single Chain Elasticity of Single-Stranded DNA: A Comparison of Three Models. *Polymer* **2009**, *50* (3), 930–935.

(201) Caruso, M. M.; Davis, D. A.; Shen, Q.; Odom, S. A.; Sottos, N. R.; White, S. R.; Moore, J. S. Mechanically-Induced Chemical Changes in Polymeric Materials. *Chemical Reviews* **2009**, *109* (11), 5755–5798.

(202) Beyer, M.; Clausen-Schaumann, H. Mechanochemistry: The Mechanical Activation of Covalent Bonds. *Chem Rev* **2005**, *105* (8), 2921–2948.

(203) Madras, G.; Kumar, S.; Chattopadhyay, S. Continuous Distribution Kinetics for Ultrasonic Degradation of Polymers. *Polymer Degradation and Stability* **2000**, *69* (1), 73–78.

(204) May, P. A.; Munaretto, N. F.; Hamoy, M. B.; Robb, M. J.; Moore, J. S. Is Molecular Weight or Degree of Polymerization a Better Descriptor of Ultrasound-Induced Mechanochemical Transduction?. *ACS Macro Letters* **2016**, *5* (2), 177–180.

(205) Monnier, H.; Wilhelm, A. M.; Delmas, H. Influence of Ultrasound on Mixing on the Molecular Scale for Water and Viscous Liquids. *Ultrasonics Sonochemistry* **1999**, *6* (1), 67–74.

(206) Zimberlin, J.; Sanabria-DeLong, N.; Tew, G.; Crosby, A. Cavitation Rheology for Soft Materials. *Soft Matter* **2007**, *3* (6), 763–767.

(207) Barney, C.; Zheng, Y.; Wu, S.; Cai, S.; Crosby, A. Residual Strain Effects in Needle-Induced Cavitation. *Soft Matter* **2019**, *15* (37), 7390–7397.

(208) Baral, N.; Davies, P.; Baley, C.; Bigourdan, B. Delamination Behaviour of Very High Modulus Carbon/epoxy Marine Composites. *Composites Science and Technology* **2008**, *68* (3), 995–1007.

(209) Mąka, H.; Spychaj, T.; Zenker, M. High Performance Epoxy Composites Cured with Ionic Liquids. *Journal of Industrial and Engineering Chemistry* **2015**, *31*, 192–198.

(210) Takeshita, H.; Sasagawa, G.; Takenaka, K.; Miya, M.; Shiomi, T. Crystallization of Graft Copolymers 1. Graft Chains Miscible with Main Chains. *Polymer Journal* **2010**, *42* (6), 482–488.

(211) Inomata, K.; Nakanishi, E.; Sakane, Y.; Koike, M.; Nose, T. Side-Chain Crystallization Behavior of Graft Copolymers Consisting of Amorphous Main Chain and Crystalline Side Chains: Poly(Methyl Methacrylate)-Graft-Poly(Ethylene Glycol) and Poly(Methyl Acrylate)-Graft-Poly(Ethylene Glycol). *Journal of Polymer Science Part B: Polymer Physics* **2005**, *43* (1), 79–86.

(212) Manson, J. A.; Cragg, L. H. A Study of Graft Copolymers. II. Viscosity and Light-scattering Measurements. *Journal of Polymer Science* **1958**, *33* (126), 193–205.

(213) Jiang, Z.; Wang, R.; Xue, G. Morphology and Phase Diagram of Comb Block Copolymer Am+1(Bc)m. *J Phys Chem B* **2009**, *113* (21), 7462–7467.

(214) Zhang, J.; Li, T.; Mannion, A. M.; Schneiderman, D. K.; Hillmyer, M. A.; Bates, F. S. Tough and Sustainable Graft Block Copolymer Thermoplastics. *ACS Macro Lett* **2016**, *5* (3), 407–412.

(215) Zhu, L.; Zimudzi, T. J.; Li, N.; Pan, J.; Lin, B.; Hickner, M. A. Crosslinking of Comb-Shaped Polymer Anion Exchange Membranes _via_ Thiol–Ene Click Chemistry. *Polymer Chemistry* **2016**, *7* (14), 2464–2475.

(216) Graff, R. W.; Wang, X.; Gao, H. Exploring Self-Condensing Vinyl Polymerization of Inimers in Microemulsion to Regulate the Structures of Hyperbranched Polymers. *Macromolecules* **2015**, *48* (7), 2118–2126.

(217) Parkatzidis, K.; Truong, N. P.; Whitfield, R.; Campi, C. E.; Grimm-Lebsanft, B.; Buchenau, S.; Rübhausen, M. A.; Harrisson, S.; Konkolewicz, D.; Schindler, S.; Anastasaki, A. Oxygen-Enhanced Atom Transfer Radical Polymerization Through the Formation of a Copper Superoxido Complex. *J Am Chem Soc* **2023**, *145* (3), 1906–1915.

(218) Santos, M. R. E.; Ferreira, S. M.; Mendonça, P. V.; De Bon, F.; Serra, A. C.; Coelho, J. F. J. Guanidine as Inexpensive Dual Function Ligand and Reducing Agent for ATRP of Methacrylates. *Polymer Chemistry* **2019**, *10* (36), 4944–4953.

(219) Catalão, F.; Góis, J. R.; Trino, A. S. M.; Serra, A. C.; Coelho, J. F. J. Facile Synthesis of Well-Controlled Poly(Glycidyl Methacrylate) and Its Block Copolymers _via_ SARA ATRP at Room Temperature. *Polymer Chemistry* **2015**, *6* (10), 1875–1882.

(220) Kaya, İ.; İlter, Z.; Şenol, D. Thermodynamic Interactions and Characterisation of Poly[(Glycidyl Methacrylate_-Co-_methyl, Ethyl, Butyl) Methacrylate] by Inverse Gas Chromatography. *Polymer* **2002**, *43* (24), 6455–6463.

(221) Kwak, R. N. Y.; Matyjaszewski, K. Dibromotrithiocarbonate Iniferter for Concurrent ATRP and RAFT Polymerization. Effect of Monomer, Catalyst, And Chain Transfer Agent Structure on the Polymerization Mechanism. *Macromolecules* **2008**, *41* (13), 4585–4596.

(222) Stals, P.; Li, Y.; Burdyńska, J.; Nicolaÿ, R.; Nese, A.; Palmans, A.; Meijer, E.; Matyjaszewski, K.; Sheiko, S. How Far Can We Push Polymer Architectures?. *J Am Chem Soc* **2013**, *135* (31), 11421–11424.

(223) Xu, H.; Casillas, J.; Krishnamoorthy, S.; Xu, C. Effects of Irgacure 2959 and Lithium Phenyl-2,4,6-Trimethylbenzoylphosphinate on Cell Viability, Physical Properties, And Microstructure in 3d Bioprinting of Vascular-Like Constructs. *Biomed Mater* **2020**, *15* (5), 55021.

(224) Cuthbert, J.; Wanasinghe, S. V.; Matyjaszewski, K.; Konkolewicz, D. Are RAFT and ATRP Universally Interchangeable Polymerization Methods in Network Formation?. *Macromolecules* **2021**, *54* (18), 8331–8340.

(225) He, R.; Zhan, X.; Zhang, Q.; Chen, F. Improving the Toughness of Epoxy with a Reactive Tetrablock Copolymer Containing Maleic Anhydride. *Journal of Applied Polymer Science* **2016**, *133* (1), 8.

(226) Johnson, J. A.; Jones, D. W. The Mechanical Properties of PMMA and Its Copolymers with Ethyl Methacrylate and Butyl Methacrylate. *Journal of Materials Science* **1994**, *29* (4), 870–876.

(227) Kim, S. L.; Skibo, M.; Manson, J. A.; Hertzberg, R. W. Fatigue Crack Propagation in Poly(Methyl Methacrylate): Effect of Molecular Weight and Internal Plasticization. *Polymer Engineering & Science* **1977**, *17* (3), 194–203.

(228) Rodriguez-Rivera, G. J.; Post, A.; John, M.; Buchan, S.; Bernard, D.; Razavi, M.; Cosgriff-Hernandez, E. Injectable Hydrogel Electrodes as Conduction Highways to Restore Native Pacing. *Nat Commun* **2024**, *15* (1), 64.

(229) Kolewe, K. W.; Peyton, S. R.; Schiffman, J. D. Fewer Bacteria Adhere to Softer Hydrogels. *ACS Appl Mater Interfaces* **2015**, *7* (35), 19562–19569.

(230) Seidlits, S. K.; Drinnan, C. T.; Petersen, R. R.; Shear, J. B.; Suggs, L. J.; Schmidt, C. E. Fibronectin-Hyaluronic Acid Composite Hydrogels for Three-Dimensional Endothelial Cell Culture. *Acta Biomater* **2011**, *7* (6), 2401–2409.

(231) Parmar, P. A.; Chow, L. W.; St-Pierre, J.-P.; Horejs, C.-M.; Peng, Y. Y.; Werkmeister, J. A.; Ramshaw, J. A. M.; Stevens, M. M. Collagen-Mimetic Peptide-Modifiable Hydrogels for Articular Cartilage Regeneration. *Biomaterials* **2015**, *54*, 213–225.

(232) Herrick, W.; Nguyen, T.; Sleiman, M.; McRae, S.; Emrick, T.; Peyton, S. PEG-Phosphorylcholine Hydrogels as Tunable and Versatile Platforms for Mechanobiology. *Biomacromolecules* **2013**, *14* (7), 2294–2304.

(233) Peyton, S. R.; Ghajar, C. M.; Khatiwala, C. B.; Putnam, A. J. The Emergence of ECM Mechanics and Cytoskeletal Tension as Important Regulators of Cell Function. *Cell Biochem Biophys* **2007**, *47* (2), 300–320.

(234) Temenoff, J. S.; Shin, H.; Conway, D. E.; Engel, P. S.; Mikos, A. G. In Vitro Cytotoxicity of Redox Radical Initiators for Cross-Linking of Oligo(Poly(Ethylene Glycol) Fumarate) Macromers. *Biomacromolecules* **2003**, *4* (6), 1605–1613.

(235) Masuma, R.; Kashima, S.; Kurasaki, M.; Okuno, T. Effects of UV Wavelength on Cell Damages Caused by UV Irradiation in Pc12 Cells. *J Photochem Photobiol B* **2013**, *125*, 202–208.

(236) Niu, J.; Lunn, D.; Pusuluri, A.; Yoo, J.; O'Malley, M.; Mitragotri, S.; Soh, H.; Hawker, C. Engineering Live Cell Surfaces with Functional Polymers _via_ Cytocompatible Controlled Radical Polymerization. *Nat Chem* **2017**, *9* (6), 537–545.

(237) Pissuwan, D.; Boyer, C.; Gunasekaran, K.; Davis, T. P.; Bulmus, V. In Vitro Cytotoxicity of RAFT Polymers. *Biomacromolecules* **2010**, *11* (2), 412–420.

(238) Wanasinghe, S. V.; Sun, M.; Yehl, K.; Cuthbert, J.; Matyjaszewski, K.; Konkolewicz, D. PET-RAFT Increases Uniformity in Polymer Networks. *ACS Macro Letters* **2022**, *11* (9), 1156–1161.

(239) Thang, S. H.; Chong, (.; Mayadunne, R. T.; Moad, G.; Rizzardo, E. A Novel Synthesis of Functional Dithioesters, Dithiocarbamates, Xanthates and Trithiocarbonates. *Tetrahedron Letters* **1999**, *40* (12), 2435–2438.

(240) Cortez-Lemus, N. A.; Hermosillo-Ochoa, E.; Licea-Claverie, Á. Effective End-Group Modification of Star-Shaped PNVCL from Xanthate to Trithiocarbonate Avoiding Chemical Crosslinking. *Polymers (Basel)* **2021**, *13* (21), 3677.

(241) Lehnen, A.-C.; Gurke, J.; Bapolisi, A. M.; Reifarth, M.; Bekir, M.; Hartlieb, M. Xanthate-Supported Photo-Iniferter (XPI)-RAFT Polymerization: Facile and Rapid Access to Complex Macromolecules. *Chemical Science* **2023**, *14* (3), 593–603.

(242) Bhanu, V. A.; Kishore, K. Role of Oxygen in Polymerization Reactions. *Chemical Reviews* **1991**, *91* (2), 99–117.

(243) Nomeir, B.; Fabre, O.; Ferji, K. Effect of Tertiary Amines on the Photoinduced Electron Transfer-Reversible Addition–Fragmentation Chain Transfer (PET-RAFT) Polymerization. *Macromolecules* **2019**, *52* (18), 6898–6903.

(244) Lehnen, A.-C.; Kurki, J. A. M.; Hartlieb, M. The Difference between Photo-Iniferter and Conventional RAFT Polymerization: High Livingness Enables the

Straightforward Synthesis of Multiblock Copolymers. *Polymer Chemistry* **2022**, *13* (11), 1537–1546.

(245) Otsu, T. Iniferter Concept and Living Radical Polymerization. *Journal of Polymer Science Part A: Polymer Chemistry* **2000**, *38* (12), 2121–2136.

(246) Zhao, B.; Li, J.; Xiu, Y.; Pan, X.; Zhang, Z.; Zhu, J. Xanthate-Based Photoiniferter RAFT Polymerization toward Oxygen-Tolerant and Rapid Living 3d Printing. *Macromolecules* **2022**, *55* (5), 1620–1628.

(247) Beres, M. A.; Rho, J. Y.; Kerr, A.; Smith, T.; Perrier, S. Photoiniferter-RAFT Polymerization Mediated by Bis(Trithiocarbonate) Disulfides. *Polymer Chemistry* **2024**, *15* (6), 522–533.

(248) Kerr, A.; Moriceau, G.; Przybyla, M. A.; Smith, T.; Perrier, S. Bis(Trithiocarbonate) Disulfides: From Chain Transfer Agent Precursors to Iniferter Control Agents in RAFT Polymerization. *Macromolecules* **2021**, *54* (14), 6649–6661.

(249) Huang, F.; Wang, F.; Han, S.; Zhang, W. Xanthate Disulfide-Mediated RAFT Polymerization toward Oxygen Tolerance. *Macromol Rapid Commun* **2024**, e2400697.

(250) Surya Prakash, G. K.; Mathew, T. Sodium Trifluoroacetate. **2010**, 1.

(251) Bowman, J. I.; Eades, C. B.; Vratsanos, M. A.; Gianneschi, N. C.; Sumerlin, B. S. Ultrafast Xanthate-Mediated Photoiniferter Polymerization-Induced Self-Assembly (PISA). *Angew Chem Int Ed Engl* **2023**, *62* (48), e202309951.

(252) Li, J.; Ding, C.; Zhang, Z.; Pan, X.; Li, N.; Zhu, J.; Zhu, X. Visible Light-Induced Living Radical Polymerization of Butyl Acrylate: Photocatalyst-Free, Ultrafast, And Oxygen Tolerance. *Macromol Rapid Commun* **2017**, *38* (13).

(253) Li, J.; Pan, X.; Li, N.; Zhu, J.; Zhu, X. Photoinduced Controlled Radical Polymerization of Methyl Acrylate and Vinyl Acetate by Xanthate. *Polymer Chemistry* **2018**, *9* (21), 2897–2904.

(254) Thomas, D. B.; Convertine, A. J.; Hester, R. D.; Lowe, A. B.; McCormick, C. L. Hydrolytic Susceptibility of Dithioester Chain Transfer Agents and Implications in Aqueous RAFT Polymerizations. *Macromolecules* **2004**, *37* (5), 1735–1741.

(255) Nwoko, T.; Zhang, B.; Vargo, T.; Junkers, T.; Konkolewicz, D. Temperature Effects in Conventional and RAFT Photopolymerization. *Macromolecules* **2025**, *58* (1), 488–494.

(256) Zoller, A.; B. Kockler, K.; Rollet, M.; Lefay, C.; Gigmes, D.; Barner-Kowollik, C.; Guillaneuf, Y. A Complete Kinetic Study of a Versatile Functional Monomer: Acetoacetoxyethyl Methacrylate (AAEMA). *Polymer Chemistry* **2016**, *7* (35), 5518–5525.

(257) Denissen, W.; Rivero, G.; Nicolaÿ, R.; Leibler, L.; Winne, J. M.; Du Prez, F. E. Vinylogous Urethane Vitrimers. *Advanced Functional Materials* **2015**, *25* (16), 2451–2457.

(258) Schlaad, H.; Krasia, T.; Antonietti, M. Superhelices of Poly[2-(Acetoacetoxy)ethyl Methacrylate]. *Journal of the American Chemical Society* **2004**, *126* (36), 11307–11310.

(259) Mandal, P.; Banerjee, S. L.; Bhattacharya, K.; Singha, N. K. A Superparamagnetic Metallopolymer Using Tailor-Made Poly[2-(Acetoacetoxy)ethyl Methacrylate] Bearing Pendant B-Keto Ester Functionality. *European Polymer Journal* **2018**, *103*, 31–39.

(260) Nese, A.; Sheiko, S. S.; Matyjaszewski, K. Effect of Residual Copper on Stability of Molecular Brushes Prepared by Atom Transfer Radical Polymerization. *European Polymer Journal* **2011**, *47* (5), 1198–1202.

(261) Montarnal, D.; Capelot, M.; Tournilhac, F.; Leibler, L. Silica-Like Malleable Materials from Permanent Organic Networks. *Science* **2011**, *334* (6058), 965–968.

(262) Meng, F.; Saed, M.; Terentjev, E. Rheology of Vitrimers. *Nat Commun* **2022**, *13* (1), 5753.

(263) Stouten, J.; Roy, M. de; Bernaerts, K. Synthesis and Characterization of Water-Borne Vanillin Derived Copolymers Containing Dynamic Imine Cross-Links. *Materials Today Sustainability* **2023**, *22*, 100396.

(264) Teo, Y. C.; Xia, Y. Facile Synthesis of Macromonomers _via_ ATRP–Nitroxide Radical Coupling and Well-Controlled Brush Block Copolymers. *Macromolecules* **2019**, *52* (1), 81–87.

(265) Foyer, G.; Barriol, M.; Negrell, C.; Caillol, S.; David, G.; Boutevin, B. Aldehyde Functional Monomer as Efficient Cross-Linkable Comonomer with Biobased Phenols in Acrylic Coatings. *Progress in Organic Coatings* **2015**, *84*, 1–8.

(266) Sun, G.; Cheng, C.; Wooley, K. L. Reversible Addition Fragmentation Chain Transfer (RAFT) Polymerization of 4-Vinylbenzaldehyde. *Macromolecules* **2007**, *40* (4), 793–795.

(267) Neugebauer, D. Two Decades of Molecular Brushes by ATRP. *Polymer* **2015**, *72*, 413–421.

(268) Xie, G.; Martinez, M. R.; Daniel, W. F. M.; Keith, A. N.; Ribelli, T. G.; Fantin, M.; Sheiko, S. S.; Matyjaszewski, K. Benefits of Catalyzed Radical Termination: High-Yield Synthesis of Polyacrylate Molecular Bottlebrushes Without Gelation. *Macromolecules* **2018**, *51* (16), 6218–6225.

(269) Li, Y.; Niu, Z.; Burdy≈Ñska, J.; Nese, A.; Zhou, Y.; Kean, Z. S.; Dobrynin, A. V.; Matyjaszewski, K.; Craig, S. L.; Sheiko, S. S. Sonication-Induced Scission of Molecular Bottlebrushes: Implications of the ‚äúhairy‚äù Architecture. *Polymer* **2016**, *84*, 178–184.

(270) Peterson, G. I.; Lee, J.; Choi, T.-L. Multimechanophore Graft Polymers: Mechanochemical Reactions at Backbone‚äìarm Junctions. *Macromolecules* **2019**, *52* (24), 9561–9568.

(271) Pauly, C.; Schlichter, L.; Ravoo, B. J.; Studer, A. Sonochemical Nitroxide-Mediated Polymerization: Harnessing Sonochemistry for Polymer Synthesis. *Macromol Rapid Commun* **2025**, *46* (3), e2400732.

(272) Jing, Y.; Mardyukov, A.; Bergander, K.; Daniliuc, C. G.; Studer, A. Synthesis of Bulky Nitroxides, Characterization, And Their Application in Controlled Radical Polymerization. *Macromolecules* **2014**, *47* (11), 3595–3602.

(273) Hirao, A.; Loykulnant, S.; Ishizone, T. Recent Advance in Living Anionic Polymerization of Functionalized Styrene Derivatives. *Progress in Polymer Science* **2002**, *27* (8), 1399–1471.

(274) Satoh, K.; Mori, Y.; Kamigaito, M. Direct Through Anionic, Cationic, And Radical Active Species: Terminal Carbon–Halogen Bond for ``controlled''/living Polymerizations of Styrene. *Journal of Polymer Science Part A: Polymer Chemistry* **2019**, *57* (3), 465–473.

(275) Yoshioka, H.; Yamaguchi, K.; Kobayashi, M. Deviant Polymerization Behavior of 4-Acetoxystyrene Found Through a Detailed Study on the ATRP of Para-Substituted Styrenes. *Polymer Journal* **2019**, *51* (7), 627–636.

(276) Rebelo, A.; Liu, Y.; Liu, C.; Schäfer, K.-H.; Saumer, M.; Yang, G. Poly(4-Vinylaniline)/polyaniline Bilayer Functionalized Bacterial Cellulose Membranes as Bioelectronics Interfaces. *Carbohydr Polym* **2019**, *204*, 190–201.

(277) Sutthasupa, S.; Shiotsuki, M.; Sanda, F. Recent Advances in Ring-Opening Metathesis Polymerization, And Application to Synthesis of Functional Materials. *Polymer Journal* **2010**, *42* (12), 905–915.

(278) Suzuki, K.; Yamaguchi, K.; Hirao, A.; Nakahama, S. Protection and Polymerization of Functional Monomers. 12. Synthesis of Well-Defined Poly(4-Aminostyrene) by Means of Anionic Living Polymerization of 4-(N,N-Bis(Trimethylsilyl)amino)styrene. *Macromolecules* **1989**, *22* (6), 2607–2611.

(279) Destarac, M.; Bzducha, W.; Taton, D.; Gauthier-Gillaizeau, I.; Zard, S. Z. Xanthates as Chain-transfer Agents in Controlled Radical Polymerization (MADIX): Structural Effect of the O-alkyl Group. *Macromolecular Rapid Communications* **2002**, *23* (17), 1049–1054.

(280) Moad, G.; Rizzardo, E.; Thang, S. H. Living Radical Polymerization by the RAFT Process. *Australian Journal of Chemistry* **2005**, *58* (6), 379.

(281) Stenzel, M. H.; Cummins, L.; Roberts, G. E.; Davis, T. P.; Vana, P.; Barner-Kowollik, C. Xanthate Mediated Living Polymerization of Vinyl Acetate: A Systematic Variation in MADIX/RAFT Agent Structure. *Macromolecular Chemistry and Physics* **2003**, *204* (9), 1160–1168.

(282) Coote, M. L.; Radom, L. Ab Initio Evidence for Slow Fragmentation in RAFT Polymerization. *J Am Chem Soc* **2003**, *125* (6), 1490–1491.

(283) Edson, C. B.; Liu, M.; Totsingan, F.; O'Berg, E.; Salvucci, J.; Dao, U.; Khare, S. D.; Gross, R. A. Monomer Choice Influences n-Acryloyl Amino Acid Grafter Conversion _via_ Protease Catalysis. *Biomacromolecules* **2023**, *24* (4), 1798–1809.

(284) Bentolila, A.; Vlodavsky, I.; Ishai-Michaeli, R.; Kovalchuk, O.; Haloun, C.; Domb, A. J. Poly(N-Acryl Amino Acids): A New Class of Biologically Active Polyanions. *J Med Chem* **2000**, *43* (13), 2591–2600.

(285) Li, G.; Feng, W.; Corrigan, N.; Boyer, C.; Wang, X.; Xu, J. Precise Synthesis of Poly(N-Acryloyl Amino Acid) Through Photoinduced Living Polymerization. *Polymer Chemistry* **2018**, *9* (20), 2733–2745.